University College
of Southeast Norway

FMH606 Master's Thesis 2017
Process technology

Lithium-ion battery safety

Jonathan Johnsplass

Faculty of Technology, Natural sciences and Maritime Sciences

Campus Porsgrunn

University College of Southeast Norway

Course: FMH606 Master's Thesis, 2017

Title: Li-ion battery safety

Number of pages: 101

Keywords: Li-ion batteries, thermal runaway, laminar burning velocity, deflagration index, Gulder coefficients, flame speed, NASA polynomials, LMFIT, Cantera 2.3.0, OpenFOAM and XiFoam.

Student:	Jonathan Johnsplass
Supervisor:	Dag Bjerketvedt, Knut Vågsæther and Joachim Lundberg
External partner:	MoZEES (FFI and Grenland Energy)
Availability:	Open

Approved for archiving: _____

(supervisor signature)

Abstract:

The aim of this thesis was two folded: Numerically compute the combustion properties of the discharge materials from lithium-ion batteries, and experimentally measure the properties, at a test rig, by overheating lithium-ion batteries and igniting the vented mixture, and using a high-speed camera, pressure sensor and temperature senor to capture, and measure the flame propagation.

The combustion properties targeted to determine were: The laminar burning velocity, the flame speed, the deflagration index, the volumetric expansion ratio at constant pressure combustion and the overpressure at constant volume combustion.

Additionally, to numerically compute the combustion properties, the aim was to determine the input properties: the NASA polynomials and the Gulder coefficients of the vented gas mixture to enable CFD studies in OpenFOAM with the premixed turbulent solver XiFoam of the vented mixture from overheated lithium-ion batteries, and to validate the input values in XiFoam by a simple case study of a flame propagation.

The computations of the laminar-combustion properties, i.e. deflagration index, laminar burning velocity, the volumetric expansion ratio at constant pressure combustion and the overpressure at constant volume combustion were programmed in the open source chemical kinetics software Cantera 2.3.0. The computations have been based primarily on two chemical mechanisms: GRI-Mech 3.0 and the DMC-Mech. The composition of the discharge materials was based on the Golubkov et al. study *Thermal-runaway experiments on consumer Li-ion batteries with metal-oxide and olivine-type cathodes.* The study analysed the vented mixture from three 18650 overheated lithium batteries named after their cathode-chemistry: a lithium cobalt oxide battery, a lithium iron phosphate battery and a lithium nickel manganese cobalt oxide battery.

To determine the XiFoam input values the NASA polynomials, and the Gulder coefficients it was necessary to compute the laminar burning velocity as a function of initial temperature, pressure and equivalence ratio, and the thermodynamical data enthalpy, entropy, and heat capacity for the premixed fuel-air mixture in Cantera 2.3.0 and to curve fit the computed datasets, in Cantera, with the optimization software LMFIT to the NASA function, and Gulder function.

The experimental measurements were based on two overheated lithium manganese dioxide batteries, and a methane-air mixture. The flame speed was determined by tracking the flame front position with respect to time, and curve fit the position data to a sextic polynomial expression with the LMFIT software. The sextic polynomial was then derivated with respect to time. The derivative expression, i.e. the quintic polynomial was due to this method an approximate for the flame speed. This method was based on the statistical technique referred to as smoothing.

The numerically computations of the laminar-combustion properties indicated that the vented lithium-ion battery gas have similar combustion properties as the two common hazardous gases methane and propane. The electrolyte solvent component dimethyl carbonate had an equal deflagration index as the vented battery gas from the lithium cobalt oxide battery, which was higher than the deflagration index of the lithium iron phosphate battery and the lithium nickel manganese cobalt oxide battery.

The Gulder coefficients and the NASA polynomials were implemented, and tested in OpenFOAM with XiFoam. The test indicated that additional tests are necessary to determine if the NASA coefficients and Gulder coefficients needs to be further adjusted.

The experimental measurement from the test rig of the lithium manganese dioxide battery indicated that the vented gas propagates approximately with the same flame speed as methane, however further tests are necessary to validate this.

Preface

This work is the final part of obtaining a Master degree in the Faculty of Technology, Natural Sciences and Maritime Sciences at the University College of Southeast Norway. This report presents and demonstrates the work of my thesis study performed under the supervision of Dag Bjerketvedt.
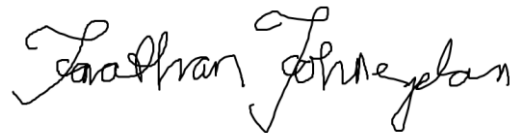
This thesis was initiated by the process safety, combustion and explosion research group of USN to determine and evaluate the combustion properties of the materials which are discarded from overheated lithium-ion. The objectives were to determine these properties numerically with the an open-source chemical kinetics software Cantera 2.3.0, and the CFD software OpenFOAM with the premixed turbulent solver XiFoam, and experimentally, i.e. using the laboratory test rig to measure the combustion properties in discharge products from run-a-way Li-ion batteries with a high-speed camera, pressure sensors and temperature sensors.
It was planned to do an extensive literature review of the flame propagation in hybrid gas, mist, and dust-air mixtures related to batteries, but since there is almost no information in open literature related to batteries this part of the thesis was drastically reduced.

I wish to thank my supervisor Dag Bjerketvedt for discussions and inputs, and Carlos Pfeiffer for advice regarding optimization.

Jonathan Johnsplass

Porsgrunn, 15.05.2017

Nomenclature

Abbreviations:

LCO: Lithium Cobalt Oxide

LNMCO: Lithium Nickel Manganese Cobalt Dioxide

LFP: Lithium Ferric Phosphate

LMO: Lithium Manganese dioxide

Anode: Negative Electrode

Cathode: Positive Electrode

18650: Dimension of a cylindrical battery [Ø=18mm, L=65mm]

SOC: State of Charge [%]

Li-ion: Lithium-ion

CFD: Computational Fluid Dynamics

Greek symbols

γ: Heat capacity ratio i.e. (c_p/c_v)

Roman Symbols

K_G: Deflagration index. Characteristic value according to the cubic law from the rate of pressure rise, in a 1 m^3 vessel. ($K_G = (dP/dT)_{max} * V^{1/3}$) [Bar m/s].

S_l: Laminar burning velocity [m/s].

U: Flame speed [m/s]

P_m: Overpressure due to constant volume combustion [Bar]

V/V_0: Volume expansion ratio due to constant pressure combustion [-]

Subscripts

m: Maximum

b: Burning

u: Unburned

G: Gas

Contents

1 Introduction

In the recent years, there have been a rapid increase in the use of Lithium-ion batteries in the transport sector. This growth is expected to continue in future transport applications on road, rail, and sea. The advantage of lithium-ion batteries is the relatively high energy density. However, the high-energy density also represents a hazard. If a battery is overheated it can vent a hybrid gas mixture which can release a significant amount of energy in the form of heat. The mixture is flammable, and might be toxic. If this mixture is ignited in a confined space, the mixture can cause severe damage to the surrounding equipment and people.

To develop qualitatively risk assessments and consequence analysis it is necessary to determine, and quantify the combustion properties of the mixtures which are involved.

This thesis is part of a task on safety in the MoZEES project, a Norwegian national centre for environment friendly energy research (NFR-FME) with focus on battery and hydrogen technology for transport applications.

1.1 Objectives

The objective of the present work is to provide an overview of combustion properties of the mixture which are vented from overheated lithium-ion batteries based on two separate techniques:

> A. numerically computations
> B. experimentally measurements

The objectives are somewhat preliminary since it is an initial step towards modelling the released mixture from Li-ion batteries in with the premixed turbulent solver XiFoam in the open source toolbox OpenFOAM since the input data necessary have not been published. Two of these input data; the NASA polynomials and the burning velocity function denoted the Gulder coefficients will be developed for three different overheated Li-ion 18650 vented gases, in addition to the electrolyte component dimethyl carbonate.

These two-input data; the NASA polynomial and Gulder coefficients, are highly demanded in the OpenFOAM community since these inputs are currently only available for methane, propane and iso octane. The application of the codes written to approximate these values are broader than the scope of the thesis, and can easily be used to expand the current limitations, i.e. the amount of fuel types.

Additionally, to numerically compute these two inputs for OpenFOAM, the following laminar combustion properties for the Li-ion battery vented gas will be approximated, numerically in the kinetic software Cantera 2.3.0, for the vented Li-ion battery gas:

> A. Numerical laminar combustion properties:
>> a. The laminar burning velocity
>> b. The volume expansion ratio at constant pressure combustion
>> c. The pressure generated from constant volume combustion
>> d. The deflagration index

The computed properties, in Cantera 2.3.0 will be compared to known hazardous flammable gases, as hydrogen, methane and propane.

The objectives related to the experimentally measurements, i.e. listed as objective B, is to test, and verify if the rig, and the diagnostic equipment (i.e. high-speed camera, pressure sensor and temperature sensor) at Porsgrunn Campus at USN can provide qualitatively data, to approximate the flame speed and the vent-temperature of the battery, i.e. the temperature the gas vents from the battery.

The literature review section of the thesis has been drastically reduced due to the limit of relevant published information with respect to the discharge material from overheat lithium-ion batteries.[1]

1.2 Structure of this Report

Chapter 2 summarizes the limited literature of flame propagation in discharge material from lithium-ion batteries.

Chapter 3 presents a brief overview of the solvers, method and software which have been used to numerically estimate the OpenFOAM input data, and the laminar combustion properties. The key properties of the batteries, gas composition and the electrolyte component dimethyl carbonate is presented briefly. Then the results, and methods from the computations of the vented gas is listed successively. The results are discussed in the respective subchapters. At the end of the chapter a simulation of a specific gas mixture vented from an overheated battery is briefly described to determine whether the input values are properly computed.

Chapter 4 gives an overview of the batteries used, and the experimental setup of the rig and equipment. The results are categorized based on the equipment used to measure and derive the measured entity, i.e. flame speed, and vent-temperature.

To linearize the report a considerable amount of numerically computated combustion properties have been left out, to make the report more readable and easier to comprehend. Part of these computations are implemented in the appendixes[2].

---

[1] The current material analysis which have been conducted on discharge lithium-ion battery materials have only confirmed that there is gas present, hence it is, from the authors opinion, questionable how relevant reviewing the general aspects of flame propagation of dust, mist and hybrid mixtures since it has not been adequately validated whether these phases or mixtures is actual present from the released material of lithium-ion batteries. It is highly likely that the mixture contains mist and dust, but it has not been confirmed or proven in a published paper in open literature to the authors knowledge.

[2] A considerable amount has been left out, e.g. heat of combustion approximations of electrolytes in 18650 Li-ion batteries based on the papers [11] and [9], and heat of combustion approximations of the solids, i.e. graphite, aluminum and copper based on [11] and LEL and UEL of the batteries depicted in chapter 3 (LCO, LMNCO, LFP).

2 Review of flame propagation in hybrid gas, mist and dust mixtures

2.1 Introduction

The scope of the chapter is to review the literature of flame propagation in hybrid gas, mist and dust-air mixtures related to lithium-ion batteries. The literature reviewed for this thesis generally fit into one or more of two key areas: Flame propagation in hybrid gas, mist and dust-air mixtures in general, and flame propagation specifically related to discharge materials from Li-ion batteries.

Flames can, independent of phase or fuel type, in general propagates as either:

- Homogeneous or heterogeneous
- Turbulent or laminar
- Diffusion or premixed

2.1.1 Hybrid mixtures

To adequately compare either dust propagation to hybrid gas propagation the conditions needs to be approximately similar. E.g., comparison of a propagating turbulent mixture of dust compared to a propagating laminar gas mixture will present a biased, and inconclusive conclusion. This matter has been the primarily issue with studying flame propagation of hybrid mixtures of dust, aerosols, and gases, which have caused the consensus of the field to change. Sanchirico et al. in [1]. claimed based on their nicotinic acid/methane study that the explosion severity of gas is more severe than hybrid mixtures, and pure dust mixtures. Contradicting reports have been published e.g. by Denkevits in [2], where Denkovits have reported that hybrid explosions of graphite-hydrogen mixture are higher than those observed with pure hydrogen.

2.1.2 Dust mixtures

Leuschke [3] [4] reported that dust clouds propagate with a thicker reaction zone, approximately 10-100 mm, than premixed gas-air mixtures, independent of the dust combustion type. The Nusselt type, i.e. combustion of Anthracite-coal dust, had a thicker flame zone due to slow rate of molecular diffusion. The second type, i.e. volatile dust combustion, i.e. starch-dust combustion, has an enlarged preheat zone, where the volatiles are vaporized and gasified from the solid particles.

Garol studied in [5] the effect of inert particles in lean methane-air mixtures, and reported that the particles enhanced the turbulence, and velocity of the upwards propagating flame, i.e. the flame speed. Garol reported that the flame speed had a positive depends of the increased grain size. [4]

Gao et al. reported that the damkohler number is a significant parameter for controlling the combustion behaviour of dust combustion. Gao et al. reported that a Damkohler number below 1, suggested that the dust burned relative equal to premixed gas-vapor mixture. [6]

2.1.3 Mist

Mist is a term used to describe airborne suspension of droplets, aerosols are frequently used as a synonym. Flame propagation of mist is highly depending on the size of the droplets. Cohen reported in [7] that mist with droplet smaller than 10 μm propagates as a vapour-air mixture. In the same article [7] Cohen reports that droplets larger than 40 μm have a complete different combustion behaviour from the 10 μm in the sense that each droplet burns as an independent diffusion flame, and not behave as a homogenous gas mixture. [8]

2.2 Flame propagation of discharged materials from lithium-ion batteries

Studies related to the vented hybrid, dust, or mist mixture from overheated lithium-ion batteries remain scarce.

Harris et al. studied the impact from the carbonate solvents used in Li-ion batteries in [9]. Harris et al. reported that flames of carbonate solvents are less energetic than hydrocarbons as propane. The authors claim that the electrolytes are released through the vent mechanism combined with gas in aerosol droplets. Further on the author suggest that due to the phase of the discharged electrolyte the mist released will be harder to combust since the aerosols must evaporate before they can react with air and combust. It seems that the author assumes that the droplet size is above 20 μm. However, the author doesn't relate the claim to any reference, and this is the only source found during the literature study mentioning the release of aerosol droplets of electrolyte.

Most lithium-ion studies are primarily focused on the gases vented from the batteries, the other phases are neglected. The study [10] by Ponchaut et al. studied two combustion properties, the deflagration index and the overpressure at constant volume combustion of the vented gases from two lithium-ion pouch batteries. The study discussed the Table 2-1, and concludes that the gases vented from the li-ion pouch battery are comparable to the hydrocarbons methane, and propane, but that vented gas have a broader combustion range, due to the presence of hydrogen, and carbon monoxide. The vented gas contained approximately 30 % hydrogen, 30 % carbon dioxide, 20 % carbon monoxide and 20 % hydrocarbons. The chromatograph was not calibrated for electrolyte components, i.e. carbonate species, or salts.

Table 2-1: Combustion characteristics of vented gases released during a thermal failure of 7.7 Wh cells. From the study [19]

Gas	LFL	UFL	Pressure at constant volume combustion [barg]	Deflagration index [m*bar/s]
Li-ion Vent gas (100 % SOC)	3.8 %	38 %	7.1	65
Li-ion Vent gas (150 % SOC)	6 %	40 %	7.7	90

Golubkov et al. studied thermal runaway of consumer Li-ion batteries in [11]. Based on the gas chromatography results of the vented gaseous mixture from the overheated consumer Li-ion batteries the gases contained approximately 30 % hydrogen, 35 % carbon dioxide, 15 % carbon monoxide and 20 % hydrocarbons. This is an average composition of the three consumer batteries. The result is relatively consistent with the composition measured by Ponchaut in [10].

Research related to the released particles, i.e. dust from overheated lithium-ion batteries is non-existing. Whether dust particles from graphite, aluminium foil from cathode, or copper foil from anode is fragmented and released, through the batteries vent mechanism is currently unknown, and if this is the case, i.e. dust particles is released, the particle size distribution of these fragments are not known. This information is vital to determine if these fragmented particles are combustible, since dust combustion is very sensitive to the particle size.

3 Numeric

3.1 Introduction

The scope of the chapter is two folded. 1. Generate the data necessary to simulate a CFD, i.e. Computational Fluid Dynamics, case of premixed turbulent combustion of the discharged materials from Li-ion batteries. Then based on the preliminary work make a simple OpenFOAM simulation with the premixed turbulent combustion solver XiFoam [12] and test if the newly derived functions are working.

2. Compute the deflagration index, i.e. measurement of the explosibility, of the discharged material from the batteries. Then based on the result compare the vented Li-ion gas [11] with common hazardous gases such as methane, propane and hydrogen. The known gases have already an established safety mitigating routine, and these routines for comparable hazardous gases can be adopted for the batteries.
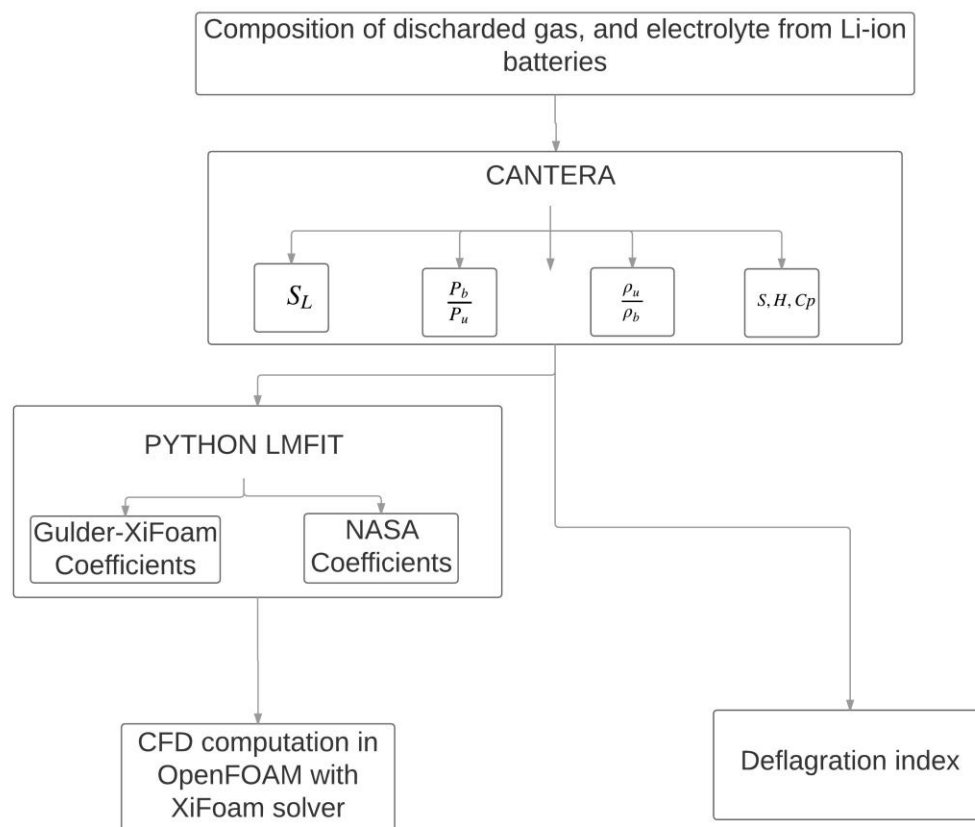

Figure 3-1: Structure of Chapter 3

To resolve the 1. objective a rather complex computational routine was necessary to conduct, where several combustion properties needed to be computed. These combustion properties were computed in the chemical kinetics software Cantera 2.3.0 [13]. The combustion properties generated in Cantera was then curve fitted, with the LMFIT optimization interphase for Python [14], for two functions; the NASA polynomials, i.e. polynomials approximation of the thermodynamical data [15], and the Gulder coefficients, i.e. a non-linear function curve fitted to the burning velocity correlation between initial temperature, equivalence ratio, and initial pressure of the unburned fuel-air mixture [16].

Initially, the goal of the thesis was to simulate a propagating vented gas mist from 18650 batteries, in XiFoam. Since XiFoam requires at a minimum the Gulder coefficients, and NASA polynomials for the gas mixture, and the only composition which is imbedded in XiFoam by default are propane-air, methane-air and iso-octane-air, it was necessary to approximate these two functions [15] [16]. To generate these two parameters a relative complex algorithm was necessary to follow, as seen in Figure 3-1.

To resolve the 2. objective, i.e. compute the deflagration index, the burning velocity at standard conditions, and the pressure at constant volume combustion was implemented in a function.

The discharge material composition is based on a Li-ion study of three consumer batteries, by Golubkov et al. [11]. The study was commented in Chapter 2. The gas composition, and some material, and functional properties are given in the next subchapter.

Due to suggestion from Harris et al.in [9], the numerical combustion property computation will be additional to the gas vented from the three consumer batteries [11] include the electrolyte component dimethyl. The numerical computations will treat the electrolyte separately from the vented gases, since it is not known whether the gas and electrolyte will vent simultaneously, or what the relation between the concentration, i.e. whether it is a binary relation, in the sense that an increased amount of the partially reacted gases will cause an equal mass reduction of the electrolyte. Hence, it is assumed that the electrolyte and the gases represent two extrema. The actual content vented will most likely contain both gases as methane, hydrogen but also electrolyte components as dimethyl carbonate. Which phase the electrolytes will be in is currently unknown. It is assumed in this thesis that it is either vapor, or aerosol particles with diameters smaller than 10 µm, i.e. that the electrolyte mist will propagate as a vapour-air mixture.

3.2 Material characteristics of the batteries, gases, and components which are deployed in the chapter 3 numeric.

This subchapter list the properties of the three different 18650 lithium-ion batteries used to approximate the burning velocity, explosion pressure, deflagration index, NASA polynomial, and Gulder coefficients in chapter 2 "Numeric". The subchapter is structured into separate sub subchapter; one for the material composition analysis of the batteries at operation conditions, and the secondary sub subchapter is describing the gases vented from the three-overheated lithium-ion batteries, the tertiary is regarding the electrolyte component dimethyl carbonate.

All the information related to the batteries are retrieved from the Golubkov et al. study [11].

The respective three batteries are in the Golubkov et al. study [11] referred to as Li-ion LFP, LNMCO and LCO batteries. This notation reflects their respective cathode material. The following figure depicts the cells mechanical properties:

Table 3-1: The material properties of the three lithium-ions batteries LFP, LNMCO, and LCO, data from [11].

Property	Variable	LCO	LNMCO	LFP
Cell mass	g	44.3	43.0	38.8
Capacity	Ah	2.6	1.5	1.1
Minimum voltage	V	3.0	3.0	2.5
Maximum voltage	V	4.2	4.1	3.5
Electrolyte solvents		DMC:EMC:EC (6:2:1)[3]	DMC:EMC:EC:PC (7:1:1: 1)	DMC:EMC:EC:PC (4:2:3:1)
Cathode material		$LiCoO_2$: $Li(Ni_{0.5}Mn_{0.25}Co_{0.25})O_2$ (2:1)	$Li(Ni_{0.5}Mn_{0.25}Co_{0.10})O_2$	$LiFePO_4$
Anode material		Graphite	Graphite	Graphite

3.2.1 Gas composition

The compositions of the sampled gases in the Golubkov et a. study [11] were analysed using a gas chromatograph. A thermal conductivity detector was used to detect permanent gases. The GC was calibrated for H_2, O_2, N_2, CO, CO_2, CH_4, C_2H_2, C_2H_4 and C_2H_6. Ar and He were used as carrier gases.

The chromatograph was not calibrated for the electrolyte components, i.e. dimethyl carbonate, ethylene carbonate, propylene carbonate or ethyl methyl carbonate. Hence, unreacted electrolyte could have been present, but have not been detected.

---

[3] DMC: Dimethyl Carbonate, EMC: Ethyl Methyl Carbonate, EC: Ethylene Carbonate and PC: Propylene Carbonate.
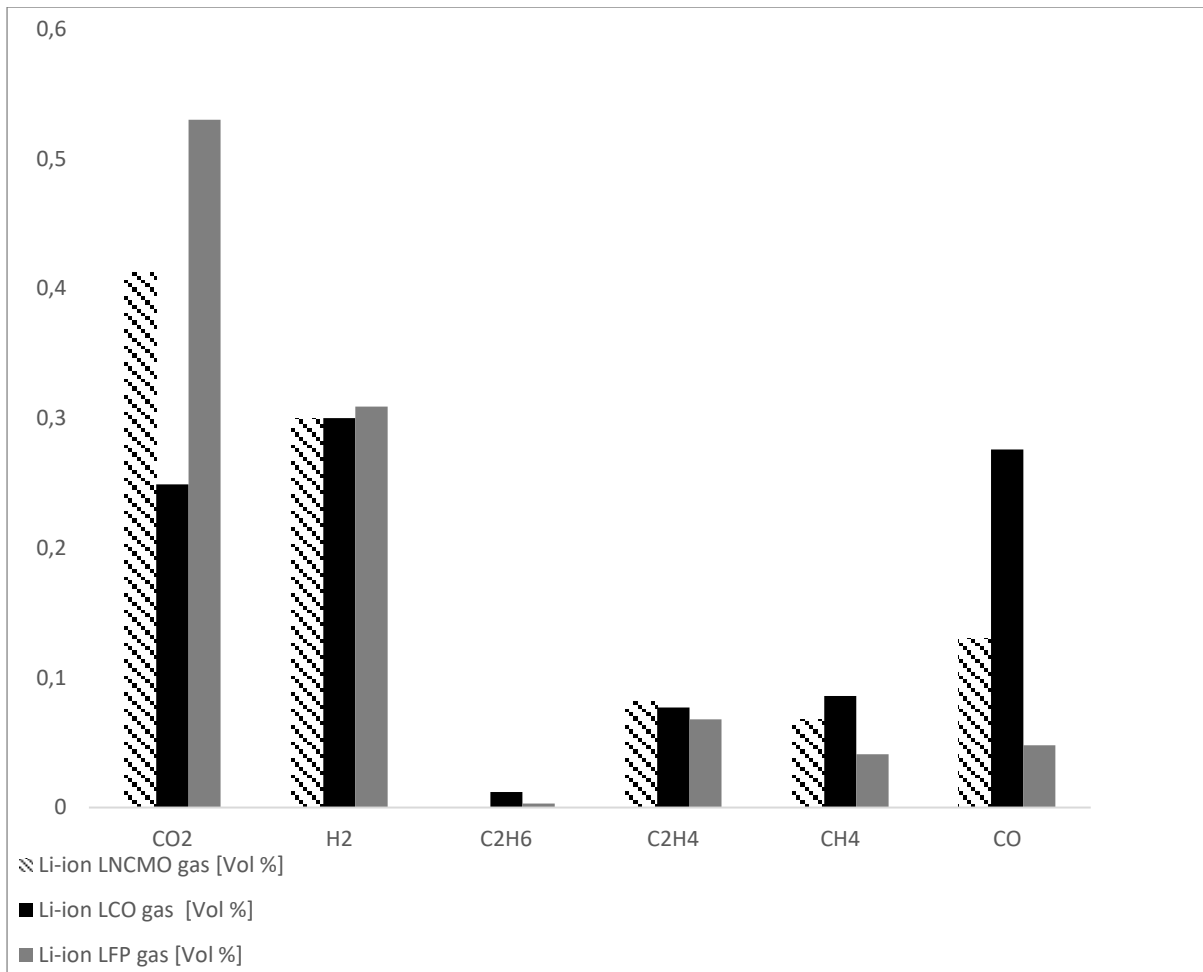
Figure 3-2: The volumetric fractions of species from gas vented off a variety of Lithium-ion batteries which are denoted in the graph. Composition retrieved from [11].

For the rest of the chapter, and thesis Li-ion LCO gas, Li-ion LNCMO gas and Li-ion LFP are denotations of the gas mixtures in Figure 3-2.

3.2.2 Electrolyte dimethyl carbonate component

The electrolyte component dimethyl carbonate is used as a solvent in all the three batteries, as seen in Table 3-1. Since there is currently only one reaction mechanism for carbonate species [17], and it is only valid for the dimethyl carbonate of the carbonates in Table 3-1, dimethyl carbonate will through the rest of the chapter, and thesis represent the electrolyte. [17] [18] [4]

---

[4] A method to approximate the burning velocity of ethylene carbonate, propylene carbonate and ethyl-methyl carbonate has been developed, and can be seen in Appendix D.

3.3 Cantera

3.3.1 Introduction

Cantera is an open-source chemical kinetics software used to solve chemically reacting laminar flows. It is equal to the commercial chemical kinetics software CHEMKIN. Cantera is a third-party program and is dependent on a programming language. All the Cantera codes have been written in Python 2.7. The version of Cantera was the 2.3.0.

[13]

Cantera has been used extensively in this chapter, to compute all the laminar combustion properties, i.e. burning velocity, pressure at constant volume combustion, volume expansion ratio at constant pressure combustion, and the thermodynamical-properties enthalpy, entropy and heat capacity of the components described in the subchapter above. These properties were necessary to determine to compute the deflagration index, and the thermodynamical, and burning velocity functions NASA Polynomial, and Gulder coefficients.
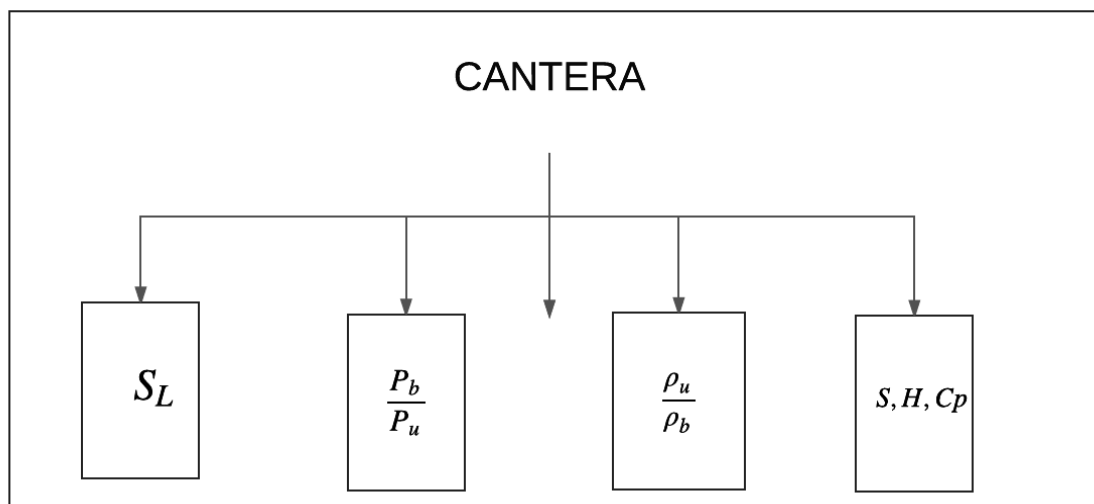

Figure 3-3: The combustion properties computed with Cantera 2.3.0 [13].

3.3.2 Reaction mechanism

Cantera uses reaction mechanism files, in the formats. cti, and .xml. These files are databases of the thermodynamical data, e.g. enthalpy, entropy and heat capacity, kinetic mechanisms data e.g. the reaction rates of elementary reactions, and the transport data. Cantera has some default reaction mechanism files included in the installation package.

However, the only reaction mechanism which includes the relevant species from the Li-ion vented gas, in the Cantera-folder **data** is the reaction mechanism denoted GRI-Mech 3.0. GRI-Mech 3.0 is optimized for natural gas combustion, i.e. CH_4, but includes several other species, e.g. H_2, CO, C_2H_4 and C_2H_6. [19]

It is important to note that GRI-Mech 3.0 mechanism is not designed especially for the gas mixture vented from the batteries in Figure 3-2 and that mechanisms, in general, provide consistent results for some species in the Figure 3 2, but not necessarily for all of them.

To test the relevance of the GRI-Mech 3.0 mechanism three relevant mechanism have been selected to approximate the combustion property *burning velocity* of the Li-ion LCO vented gas mixture as seen in Figure 3-2. It is out of the scope of this thesis to thoroughly analyse all the mechanisms in detail. This comparison does not provide enough data to conclude whether the GRI-Mech 3 mechanism is over- or underestimating the laminar burning velocity, but emphasise the inaccuracy of the results. The mechanisms used for this purpose are in the Table 3-2 , below.

Table 3-2: Key parameters of the chemical mechansims used to compute the burning velocity in Figure 3-4.

| Name of mechanism:	Number of species:	Number of chemical reaction	Validated for burning velocity by the authors for:	Utilized in the thesis for:	Source:
DMC-Mech	102	805	$C_3H_6O_3$-air	Electrolyte-component dimethyl carbonate	[17]
GRI-Mech 3.0	53	325	CH_4-air, CO-air, C_2H_6-air, CO-H_2-air	Pseudo reacted gaseous mixture	[19]
UCSD-Mech	57	268	H_2-air, CH4-air	Pseudo reacted gaseous mixture	[20]
WANG-Mech	99	533	C2H6-air	Pseudo reacted gaseous mixture	[21]
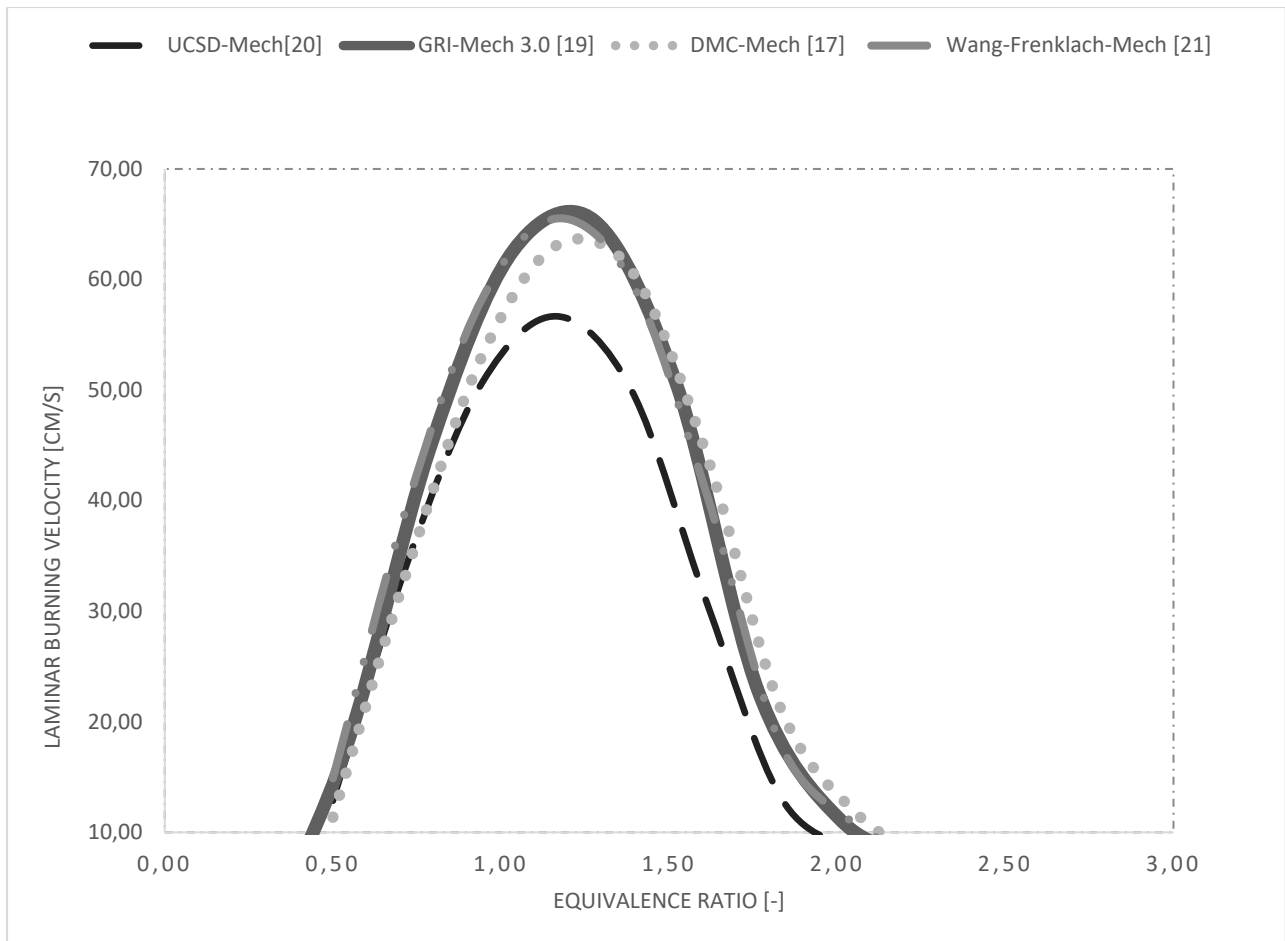
Figure 3-4: Comparison of the chemical reaction mechanism impacting the laminar burning velocity of the discharged gas emitted from an Li-ion LCO-battery-premixed with air, at initial conditions of 1 atm, and 298.15 K, were the burning velocity is a function of equivalence ratio. All the data are estimated with the mechanisms denoted in the graph, estimated on Cantera 2.3.0. See Appendix B Sublevel B.1 for source code.

Even though the mechanisms, as seen in Figure 3-4, are used for a variety of species, the deviation between the results are within the limits of most experimental measured laminar burning velocity techniques e.g. Bunsen and Slot burner measurements. [22] [5]

Since the GRI-MECH 3.0 mechanism is the most available of the mechanisms in Table 3-2, it was used extensively in the report to compute the combustion properties: laminar burning velocity, pressure at constant volume combustion, volume expansion at constant pressure combustion and the deflagration index.

However, to compute the laminar burning velocity, volume expansion at constant pressure combustion, pressure at constant volume combustion, and the deflagration index of the electrolyte component dimethyl carbonate it was necessary to use the DMC-Mech mechanism [17].

[5] It is important to note that the variance between the mechanisms tend to increase at the extrema values, i.e. maximum and minimum. This is especially evident from the figures 5-1, 5-2, 5-3, 5-6 and 5-7 in Appendix A.

This mechanism was only accessible in the "CK FORMAT", which is the input format developed for the Chemkin-II software package. The CK format was converted in the Cantera friendly CTI-format with the converting utility program *ck2cti*. It was necessary to debug some issues with the CK-code before it was possible to run the converting utility program *ck2cti*. [13]

3.4 Adiabatic-laminar burning velocity

The laminar burning velocity is a measurement of the rate at which the unburned gaseous mixture, i.e. reactants, is moving into the flame zone in a direction normal to the flame at laminar condition, with no heat loss to the environment i.e. adiabatic. The laminar burning velocity is a combustion property which implements the thermal, and mass diffusive properties of the fuel mixture and is a good measurement to relate how an actual fuel-type mixture will propagate relative to other fuel-types. The goal of this subchapter is to document how the initial temperature, pressure and equivalence ratio of the unburned gaseous mixture impacts the laminar burning velocity. These results are necessary to relate the vented gas, and electrolyte component from the LCO, LNCMO and LFP batteries to other known flammable fuel types.

[23]

3.4.1 Equivalence ratio

This subchapter documents the Cantera results from computing the burning velocity as a function of the equivalence ratio.

The equivalence ratio, φ – is the ratio of the fuel-to-oxidizer ratio to the stoichiometric fuel-to-oxidizer ratio. For an equivalence ratio, $\varphi < 1$, the fuel-oxidizer mixture is denoted lean with respect to the fuel, i.e. excess oxidizer. At $\varphi > 1$, the mixture is denoted rich with respect to the fuel. [24]

Figure 3-5: Comparison of the laminar burning velocity of the discharged gas emitted from an LCO, LNCM, and an LFP battery premixed with air, dimethyl carbonate-air and methane-air at initial conditions of 1 atm, and 298.15 K, were the burning velocity is a function of equivalence ratio. All data are estimated with the GRI-MECH 3.0 mechanism, except the dimethyl carbonate-air, where the DMC-Mech was used on Cantera 2.3.0, the transport model was "Multi".
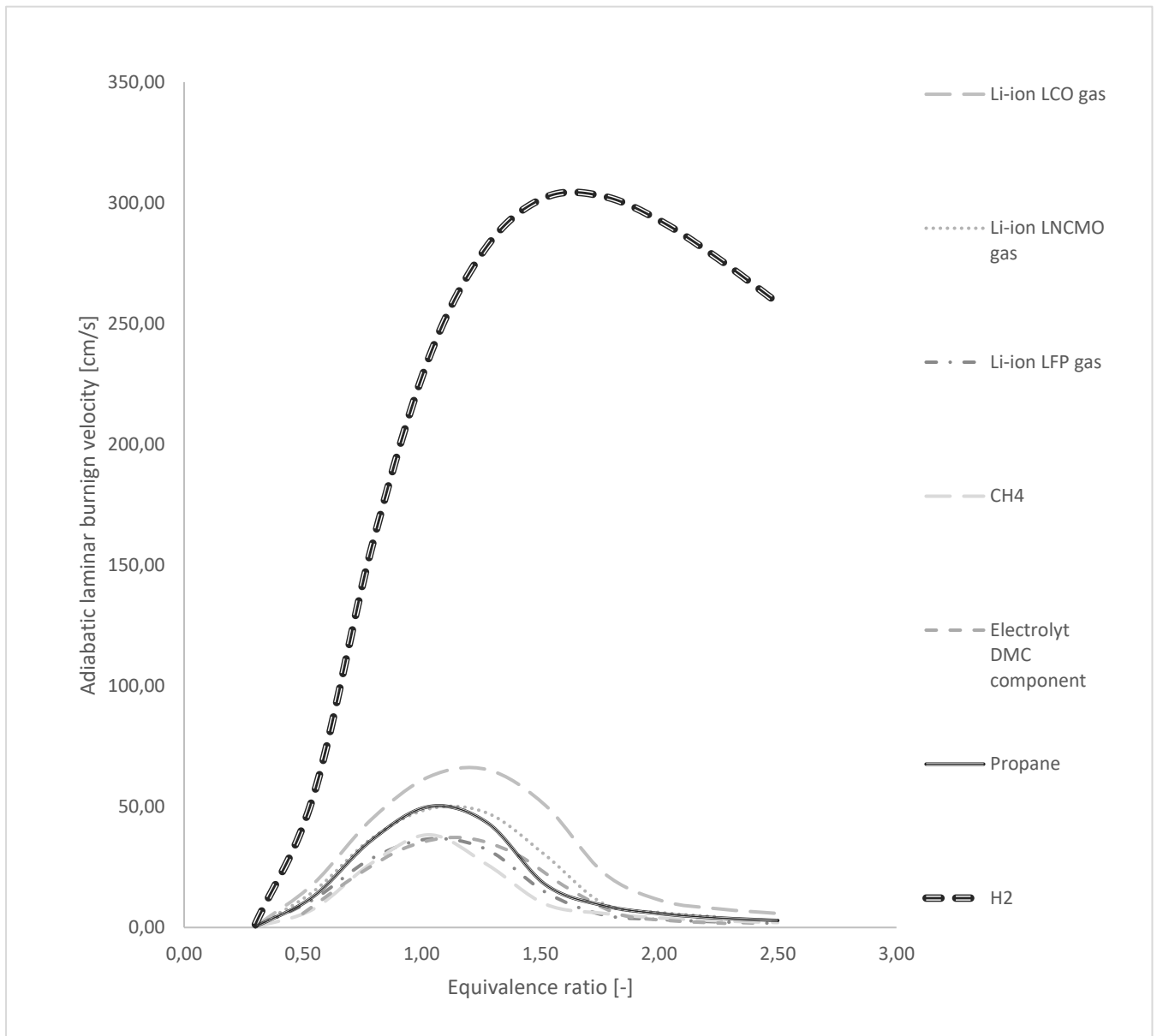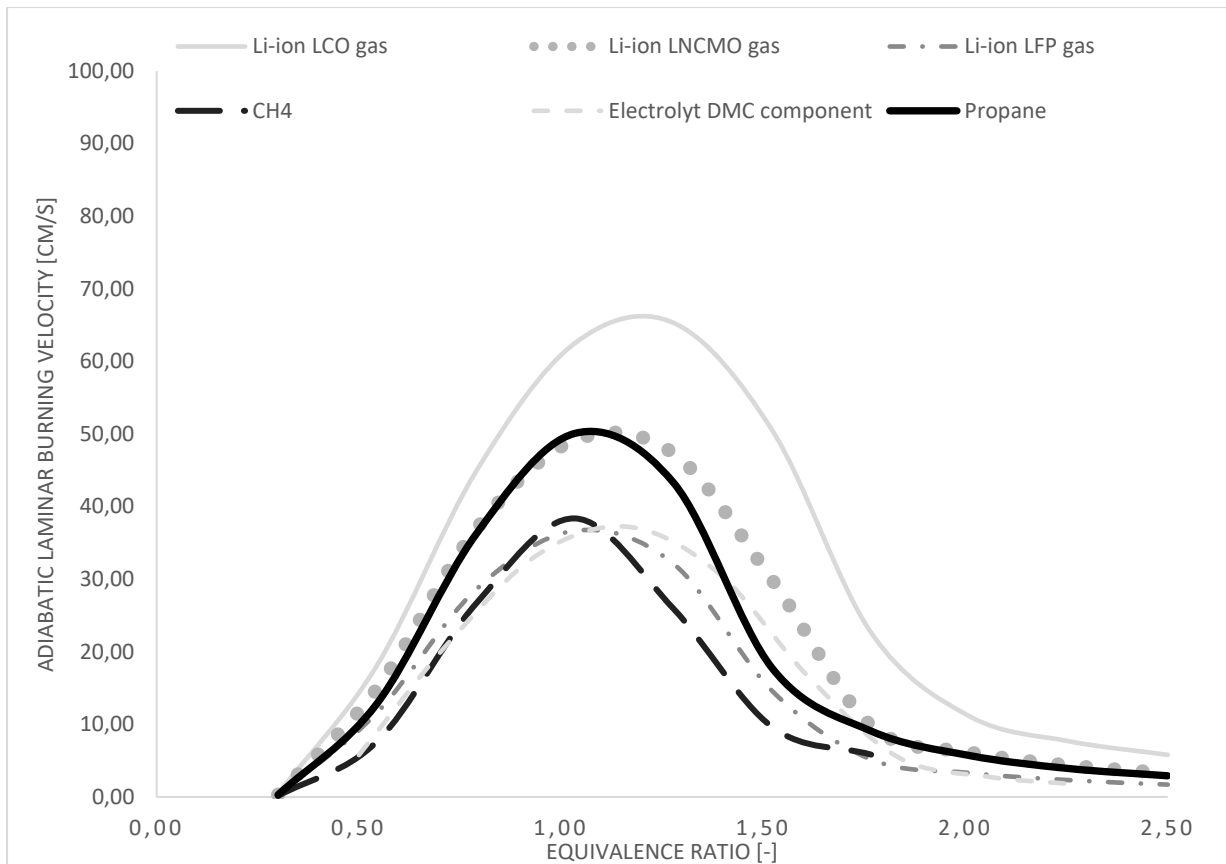
Figure 3-6: Comparison of the laminar burning velocity of the discharged gas emitted from an LCO, LNCM, and an LFP battery premixed with air, electrolyte component dimethyl carbonate-air and methane-air at initial conditions of 1 atm, and 298.15 K, were the burning velocity is a function of equivalence ratio. All the data are estimated with the GRI-MECH 3.0 [19], except the dimethyl carbonate-air, where the DMC-Mech [17], mechanism was used in Cantera 2.3.0, the transport model was "Multi".

Figure 3-6 indicates that Li-ion LNCMO gas propagates at the same burning velocity as propane. The Li-ion LFP gas, the electrolyte component dimethyl carbonate and methane are approximately equivalent. The Li-ion LCO gas diverges from the other gases, and has a maximum burning velocity at 65 cm/s at equivalence ratio at 1.28, which is the fastest mixture in Figure 3-6. The most reasonable variable causing this, is that the Li-ion LCO gas has the lowest CO_2 concentrations, and the highest CO concentrations of the three-vented gas mixture. This can be seen in Figure 3-2.

However, if the Li-ion LCO gas is compared to the flame speed of hydrogen in Figure 3-5, the Li-ion LCO gas is roughly equivalent to hydrocarbons.

It is evident from Figure 3-5 and Figure 3-6 that the maximum burning velocity peaks slightly on the rich side, i.e. when $\phi > 1$. The degree of rich side peak is not uniformly through all the composition, but varies and is mostly due to the differences in the recombination and chain-branching reaction mechanism between the chemical compositions. The laminar burning velocity is a strong function of the adiabatic flame temperature, due the Arrhenius term, and it is not coincidently that the laminar burning velocity peaks approximately at the same equivalence ratio as the adiabatic flame temperature, i.e. at approximately $1.1 \leq \phi \leq 1.3$.

The reason that the peak is not exactly at stoichiometric fuel air mixture is because additional fuel is necessary to compensate for the effect of dissociation at higher temperature. At lean side, i.e. when the equivalence ratio is less than 1, the heat the oxidizer is in excess with respect to the combustion stoichiometry. The excess oxidizer will act as an inert gas in the combustion process, and will "consume" some of the heat which will reduce the overall adiabatic temperature. For an equivalence ratio, larger than one, there will not be enough oxygen available to oxidize all the fuel, hence the same effect as for lean, i.e. that the excess fuel will act as an inert which will dissipate some of the heat.

[24] [25]

3.4.2 Pressure

This subchapter documents the Cantera results from computing the burning velocity as a function of the pressure of the reactants in the preheat zone.

.

Figure 3-7: Comparison of the laminar burning velocity of the discharged gas emitted from an LCO, LNCM, and an LFP battery premixed with air, dimethyl carbonate-air and methane-air at initial conditions of 298.15 K, were the burning velocity is a function of the initial pressure in bar. All the data are estimated with the GRI-MECH 3.0 [19], except the DMC, where the DMC-Mech [17], was used in Cantera 2.3.0, the corresponding transport model was "Multi".

It is evident from Figure 3-7 that the burning velocity, in general, decreases with the pressure rise for all the mixtures, at least beyond 10 bar a. However, specifically the pressure dependency of the burning velocity for hydrogen, in Figure 3-7, peaks at 2.25 bara, i.e.

increases from vacuum to 2.25 bar a, and decreases from 2.25 bara and beyond. Similar results for pressure dependency of the burning velocity for hydrogen is reported in [26].

Even though the gas from the Li-ion LCO, LNCMO and LFP batteries constitutes approximately of 30 % hydrogen this does not seem to cause the pressure dependency for the burning velocity of the gaseous mixtures to behave as pure hydrogen-air mixture.

The pressure dependency for the burning velocity are equal among the Li-ion battery gases, and the electrolyte component dimethyl carbonate

The conclusion for Figure 3-7 is that the electrolyte component dimethyl carbonate and the Li-ion battery gases will propagate slower in a pressurized confined space. [6]

---

[6] It is noteworthy to mention that the pressure dependency of the burning velocity is not independent of the equivalence ratio or the reaction mechanism. This can be seen in the figures 5-1 and 5-2 in Appendix A. The burning velocity, in figure 5-1, of the lean mixture, i.e. $\phi = 0.5$ is significantly less dependent of pressure than the rich mixture, $\phi = 2.6$, and the stoichiometric mixture, $\phi = 1.0$. The reaction mechanisms spread increase for elevated pressure. The reaction mechanism is usually not tested for high ranges of pressure, but are curve fitted from a small pressure range segment, hence, whether Cantera estimates these dependencies correctly, for high pressures, is in general for the reaction mechanisms not experimentally verified. [26]

3.4.3 Temperature

This subchapter documents the Cantera results from computing the burning velocity as a function of the initial temperature of the reactants in the preheat zone.
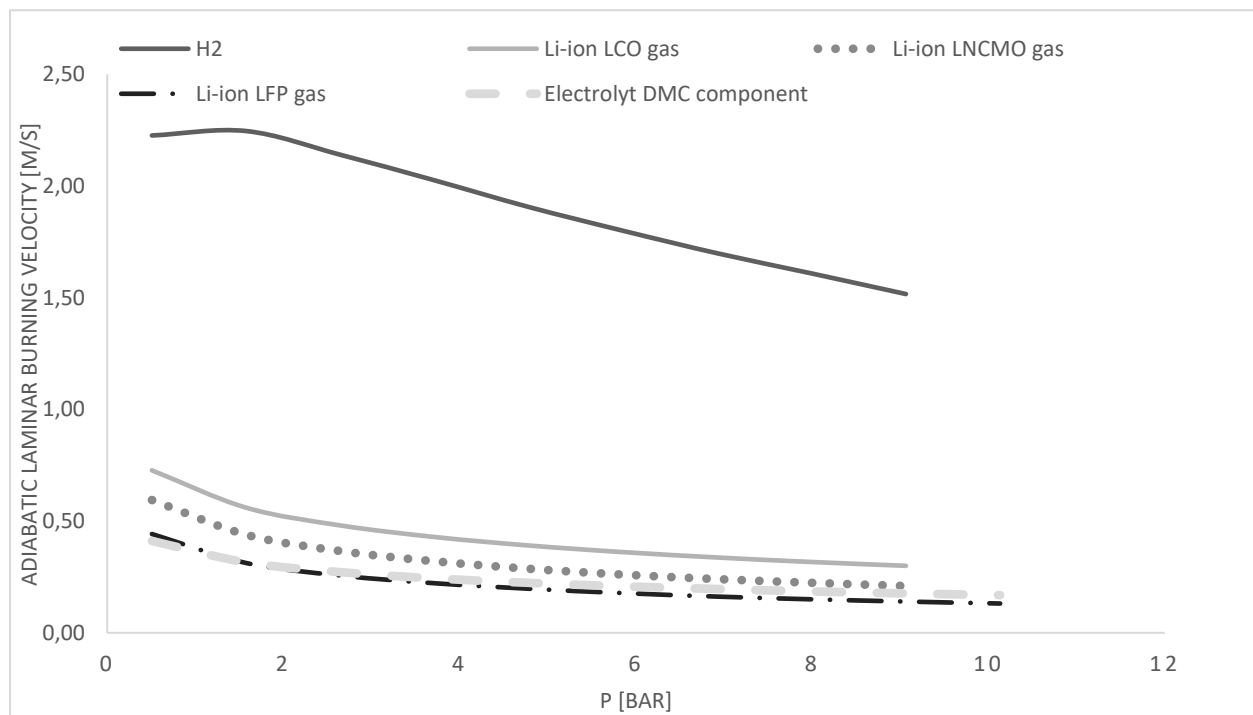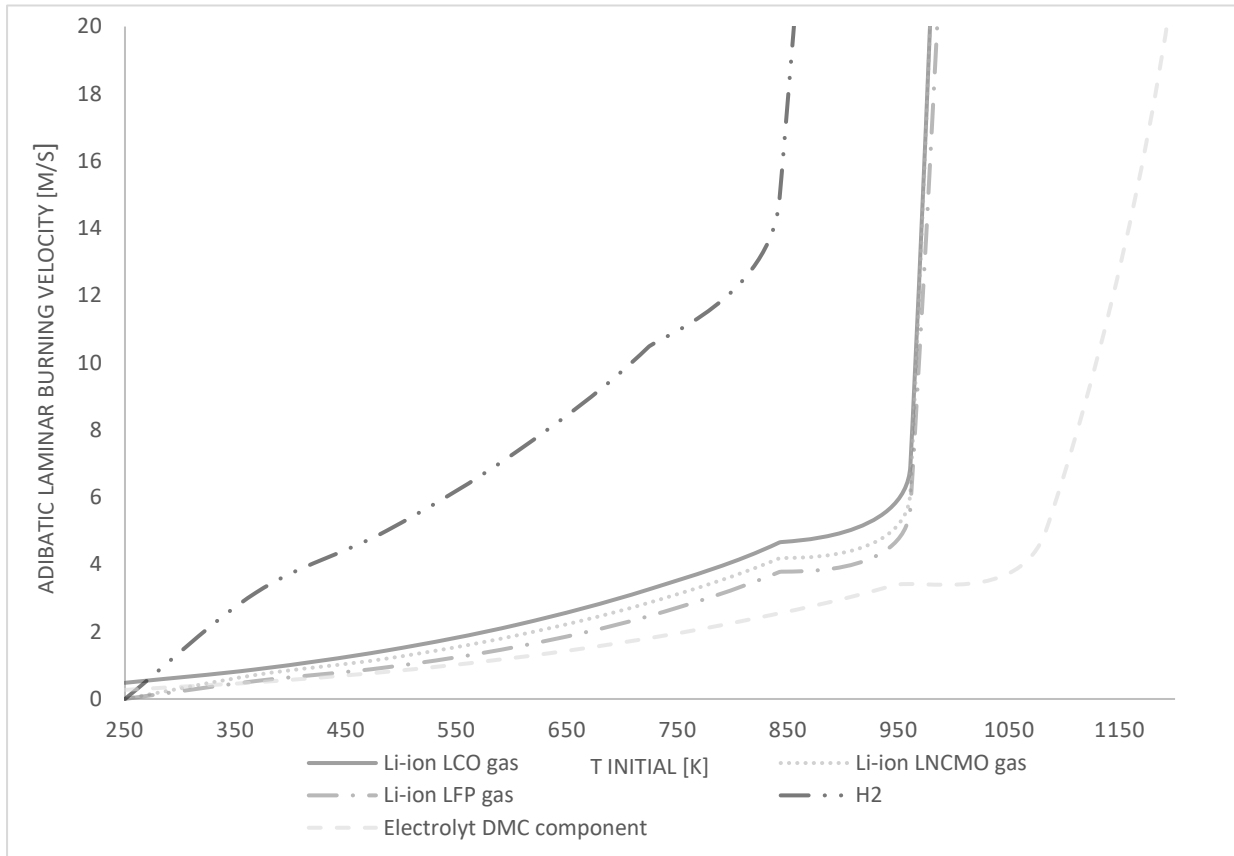

Figure 3-8: Comparison of the laminar burning velocity of the discharged gas emitted from an LCO, LNCM, and an LFP battery premixed with air, and methane-air at initial conditions of 1 atm, were the burning velocity is a function of the initial temperature in Kelvin.

It is clear from Figure 3-8 that the burning velocity is a strong function of initial temperature of the reactants. The li-ion batteries gases are behaving uniformly; the velocity is elevated linearly from 250≤T≤950 and increases exponentially from T ≥ 950 K. The electrolyte component dimethyl carbonate is less sensitive to temperature compared to the vented gases from the Li-ion batteries.

As a conclusion, the burning velocity is decreasing for elevated initial pressure and is increased for elevated temperature.

3.5 Constant Volume combustion

Constant volume combustion will cause the pressure within the confined space to increase. This relation can be seen in the ideal gas law, based on the premise that the number of moles remain constant before and after the reaction:

$$\frac{P_b}{P_u} \approx \frac{T_b}{T_u} \qquad\qquad (3\text{-}1)$$

The pressure rise estimated in this subchapter is not the overall maximum pressure that can be obtained. It is the pressure developed at laminar condition, i.e. slow burning rate. A real, or simulated gas propagating will generate higher local pressure due to dynamics as pre-compression. [23]

As seen in [23] the pressure ratio, P/P_0, developed in laminar flow regime due to constant volume combustion is approximately 8, for most fuel-air mixtures. [7]
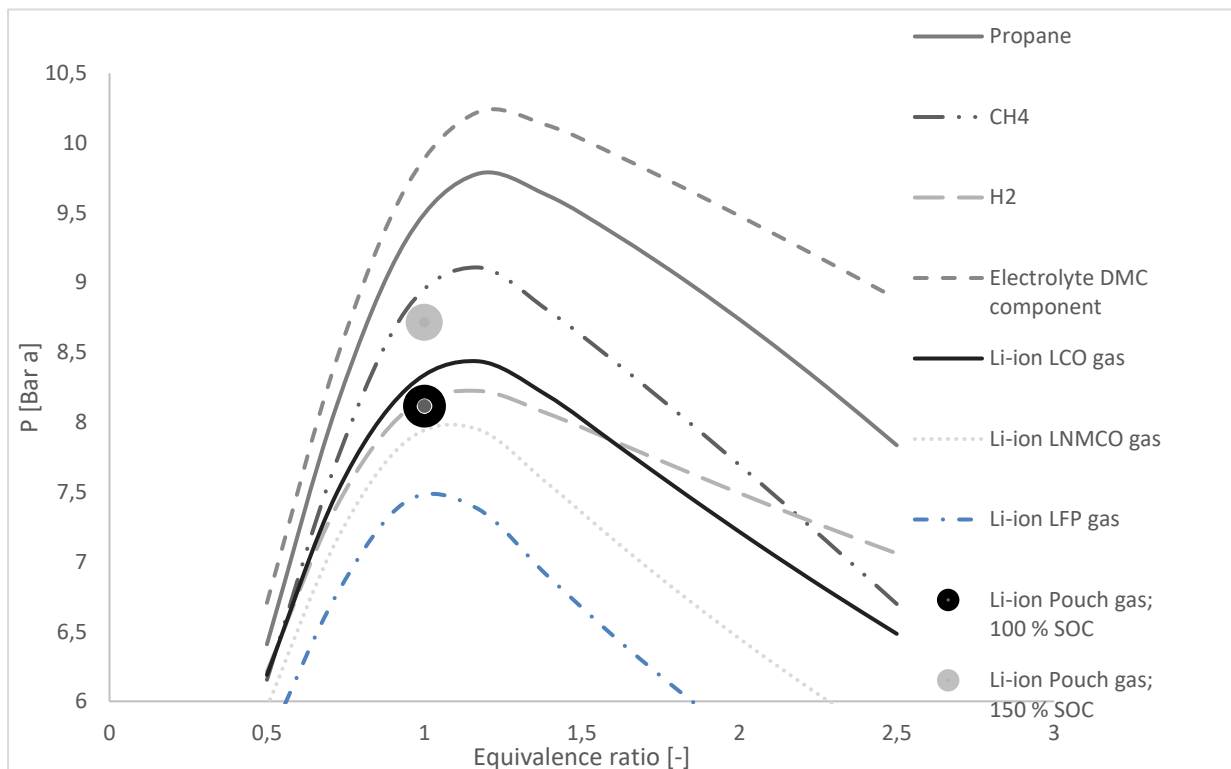
Figure 3-9: The maximum pressure developed in a contained deflagration as a function of the equivalence ratio. The initial temperature was 298.15 K, and the fuel-air ratio was stoichiometric. All the data are approximated in Cantera 2.3.0., except the two dots; they are pressure measurements from the study [10]. The pressure lines are approximated with GRI-MECH 3.0 [10], and DMC-Mech [17].

The electrolyte dimethyl carbonate generates the highest explosion pressure, in Figure 3-9, i.e. 10.1 bar a at φ = 1.4. The Li-ion LCO gas generates the highest explosion pressure of the three Li-ion battery vented gases. The LFP has the lowest pressure of the three at 7.3 Bar A, for φ = 1.2. The pressure estimated for the Li-ion LNCMO is in full agreement with the pressure for the Li-ion Pouch gas measured in [10]. These batteries have the approximately

---

[7] The code used to generate the Figure 3-9 in this subchapter is given in Appendix B, sublevel B.2.

the same capacity, i.e. LNCMO ≈ 2.5 ah, and Pouch ≈ 2.1 ah. Which might suggest that the pressure of the battery gases might be depending on the capacity.

3.6 Constant pressure combustion

The temperature effects the volume for constant pressure combustion approximately the same way pressure is affected at constant volume combustion. The volume will expand, causing a reduction of the density. This cause and effect relation can be deduced from the ideal gas law, as seen in formula (3-2), assuming constant pressure, and that the number of moles remain constant before and after the reaction:

$$\frac{\rho_u}{\rho_b} = \frac{T_b}{T_u}$$

(3-2)
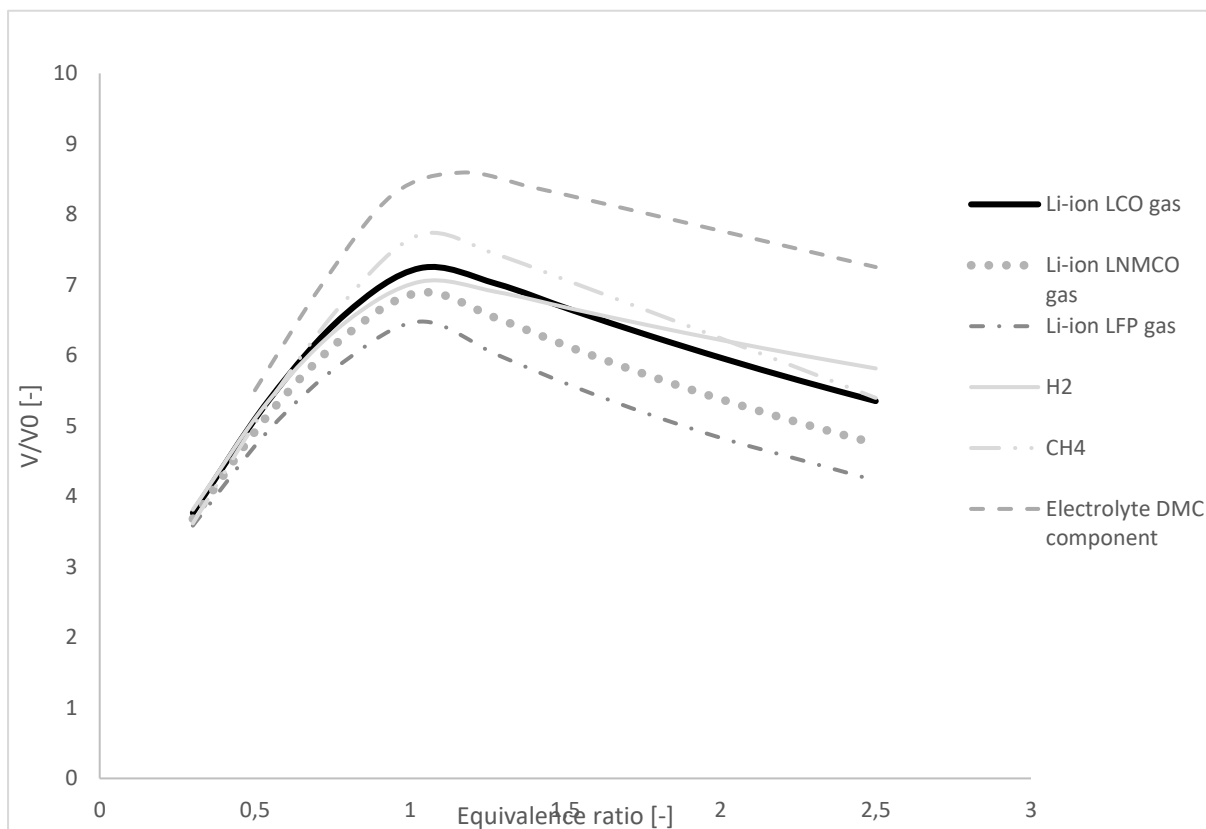
Figure 3-10: The volume expansion ratio as a function of the equivalence ratio, at 1 bar, and 298.15 K. The volume expansion lines are approximated in Cantera 2.3.0, GRI-MECH 3.0 [10], and DMC-Mech [17]. [89]

---

[8] The Cantera-Python code used to compute the volume expansion ratio is seen in Appendix B, B.3.

[9] The volume expansion, as seen in Figure 3-10, at isobaric condition is used to approximate the laminar flame speed in Figure 5-5 in Appendix A.

It is evident from Figure 3-2 that all the mixtures, and species peaks at a stoichiometric mixture of fuel-air, except the electrolyte component dimethyl carbonate, which is at φ≈1.17, i.e. rich fuel air mixture. The results of the methane, and hydrogen gas are comparable to the volume expansions ratio given in [23].

3.7 Deflagration index

The deflagration index is measurement of how fast a dust, gas and hybrid explosion can propagate in a confine space. It is a product of the maximum pressure rise, and the cube root of the volume of the space. It is often used in a design phase to validate the design of protection systems, i.e. explosion containment and suppression units. The index is primarily acquired through empirical tests in a 20 L sphere, however the size may vary. [28] [29]

However, there have been formulated some theoretical models which tries to represent these empirical measurements. The formula which has been applied in this thesis are known as "the thin-flame model" and is derived by Dahoe et al, in [16], and was originally intended for dust explosions, but has been used, i.e. [29] for gases. This formula is normalized with respect to the vessel volume, hence, the term $(36\pi)^{\frac{1}{3}}$ is not directly representing the V term.

$$K_G = (\frac{dP}{dt})_{max} V^{\frac{1}{3}} \approx (36\pi)^{\frac{1}{3}}(P_{max} - P_0)(\frac{P_{max}}{P_0})^{\frac{1}{\gamma u}} S_L \quad\quad (3\text{-}3)$$

Formula (3-3) is a model developed by Dahoe in [28]. The model is referred in [28] as *the thin-flame model*. See [28] for the full derivation.[10]

The gamma term, γ, is heat capacity ratio. This quantity is not depicted in this thesis, but is integrated in the code, seen in Appendix B, B.4. [11]

---

[10] According to Dahoe et al.in [31]. the model has the following assumptions:

"The unburnt as well as the burnt mixture are treated as ideal gases.
The specific heats of both the unburnt and the burnt mixture are the same and remain constant during the explosion.
⁻ The transition of the unburnt into burnt mixture occurs through a single-step, irreversible chemical reaction which can be described by a global reaction rate expression.
⁻ The temperature of the unburnt mixture, Tu, continually increases as'a consequence of the compression, which is assumed to be adiabatic.
⁻ The burning velocity remains constant during the explosion (i.e., it does not depend on the pressure, temperature, dust concentration and state of turbulence during the explosion).

⁻ Point ignition at the centre of the dust cloud occurs with a negligible energy input."

[11] The Python-Cantera code used to compute Figure 3-11 and Figure 3-12 is categorized in Appendix B, B.4
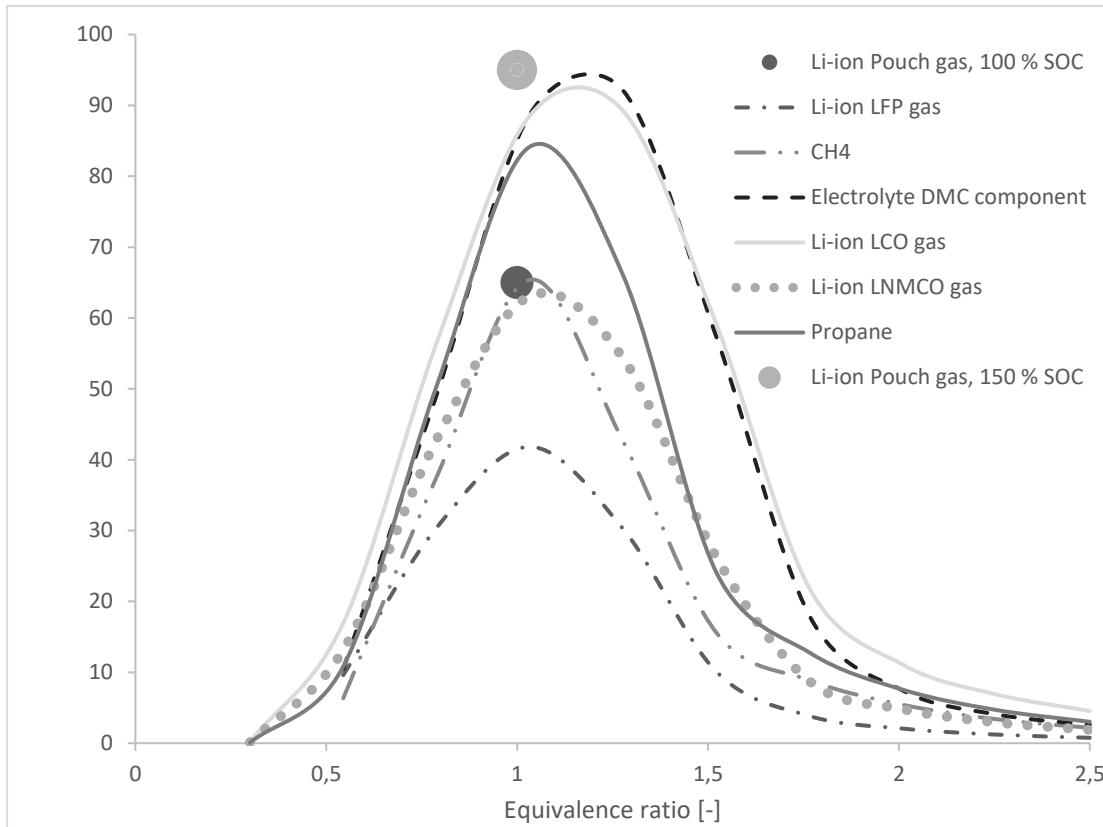
Figure 3-11 : The deflagration index as a function of the equivalence ratio. The initial conditions were 1 atm and 293.15 K. All the lines are approximated on Cantera. The deflagration index lines are approximated with GRI-MECH 3.0 [10], and DMC-Mech [17]. The two dots are result from [19]

Figure 3-12: The deflagration index as a function of the equivalence ratio, with hydrogen. The initial conditions were 1 atm and 293.15 K. All the data are approximated on Cantera. The deflagration index lines are approximated with GRI-MECH 3.0 [10], and DMC-Mech [17].

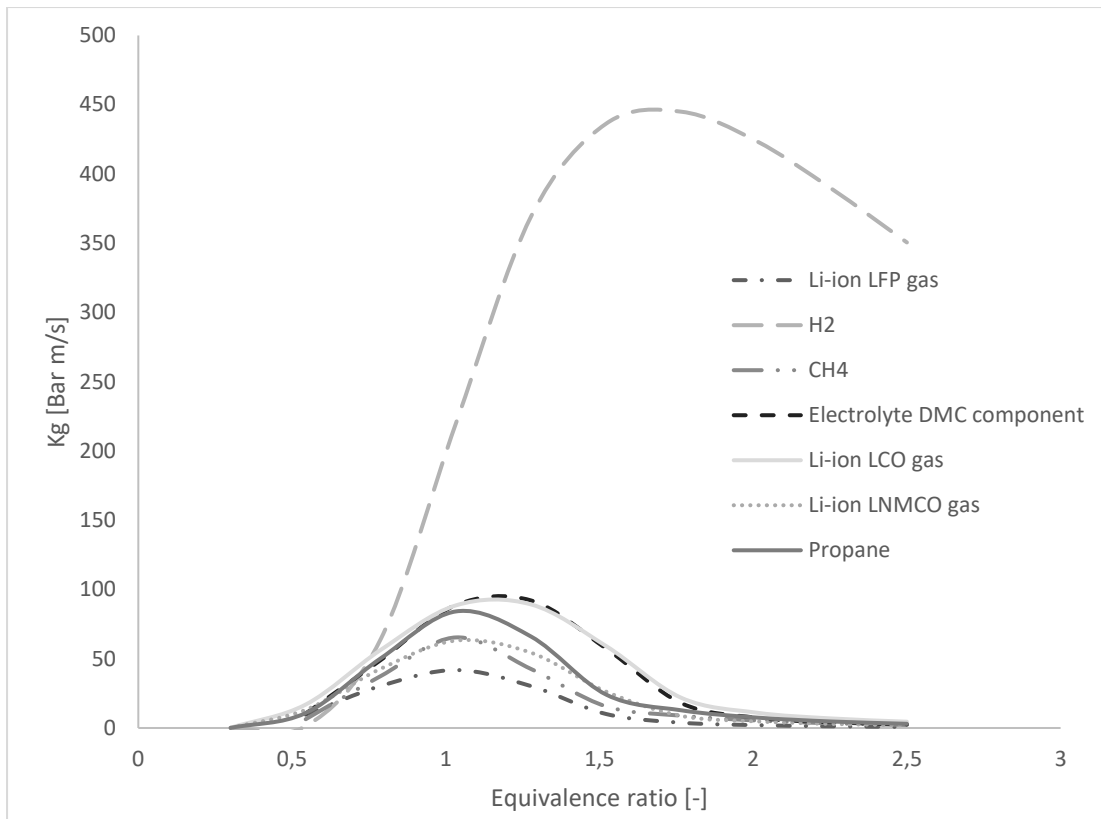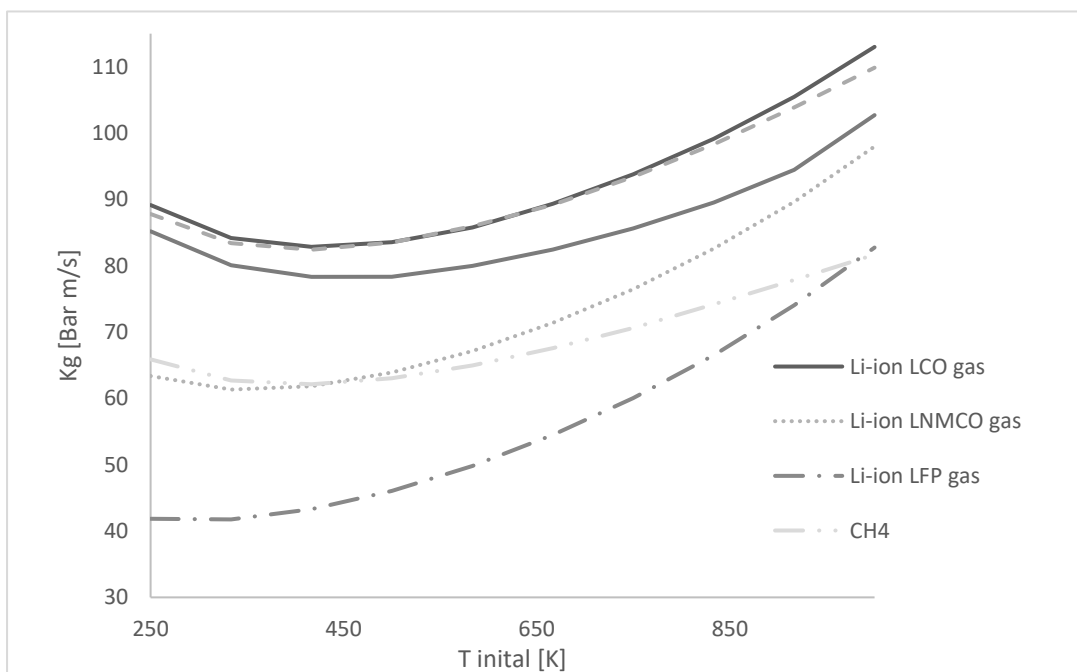

Figure 3-13: The deflagration index as a function of the initial preheat temperature. The initial conditions were 1 atm and the mixture was stoichiometric.

It is evident from Figure 3-11 that the gas from the Li-ion LCO battery has the highest deflagration index of the three vented gas mixtures. This is relative to the results from Figure 3-7 and Figure 3-9 not surprising, since the gas from Li-ion LCO battery have the highest burning velocity and explosion pressure at normal conditions, due to it lower concentration of carbon dioxide, and increased amount of carbon monoxide, relative to the other gases.

The results, in Figure 3-11, for the Li-ion LCO gas, Li-ion LFP gas and Li-ion LNMCO gas are completely in agreement with the deflagration index of the Li-ion Pouch gas measured in a 20-l combustion chamber by Ponchaut and al in [10].

The deflagration index of the electrolyte component dimethyl carbonate is equal in magnitude to the Li-ion LCO gas mixture which indicates that the severity of a confine explosion of the batteries content is in some situations independent of the reactivity of the cathode, i.e. that the electrolyte reacts and forms the gas components, e.g. hydrogen, carbon monoxide and methane. However, such situations are depending on the amount of energy which are caused by the abusive condition, it is necessary that the electrolyte is vaporized, and vented. Relevant situations include batteries exposed to external heat source due to sun exposure. It is important to note the Figure 3-12 text, that the dimethyl carbonate was approximated with a different reaction mechanism than the other components.

[29]

Another observation which can be derived from Figure 3-12, is that the content of the electrolyte, at least the component dimethyl carbonate, is more severe than the gas mixture in the Li-ion LNCMO battery and Li-ion LFP battery. However, whether the magnitude of the deflagration index of the remaining components in the electrolyte, i.e. ethylene carbonate, polypropylene carbonate and diethyl carbonate are equal to dimethyl carbonate is currently unknown. [12]

From Figure 3-13 the severity of the mixture is to some degree affected by the initial temperature. It seems that the severity of the explosion is higher for cold conditions compared to normal temperature conditions. It seems like a stretch, but it can be in relative terms be stated that a battery undergoing thermal runaway is safer in the summer season compared to the cold season. However, this dependency is for the most part neglectable, approximately a reduction of 5 % of the severity from cold to normal condition, i.e. 298.15 K.

3.8 Python LMFIT

LMFIT was used to curve fit the burning velocity, and thermodynamical data from Cantera to the Gulder coefficients, and the NASA polynomials.

---

[12] It seems from Appendix D that the other respective carbonates would generate at least a lower burning velocity, which in turn would indicate a lower deflagration index. But, since neither the actual burning velocity or the deflagration pressure of these carbonate species can be currently estimated this suggestion is inconclusive. However, inconclusive is not equivalent to insignificant. It is highly important to further study at least the burning velocity and explosion pressure of the electrolytes.

LMFIT is a Python based interface build to solve non-linear optimization and curve fitting problems. It is an extension of the optimization methods of *scipy.optimize*. The lmfit package is a free software, using an Open Source license, and is used in the thesis since it does not require a time dependent license. Additionally, since the Cantera interface is run in Python it was convenient to program the entire code in the same programming language. [13]

[14]

3.9 Gulder coefficients

The Gulder coefficients are the model parameters the laminar burning velocity dataset in subchapter 3.4 are fitted to through nonlinear regression. The premixed turbulent combustion solver XiFoam uses a specific formulation of the Gulder function which is denoted as GuldersEGRCoeffs [30]. The XiFoam version of the Gulder function is a nonlinear combination of the model parameters W, η, ξ, α and β and the three independent variables equivalence ratio, initial pressure and initial temperature of the unburned fuel-oxidizer mixture. [31]

$$S_L(\varphi, P, T) = W\varphi^\eta e^{-\xi(\varphi-1.075)^2}(\frac{T}{T_0})^\alpha(\frac{P}{P_0})^\beta \qquad (3\text{-}4)$$

Formula (3-4 is the product of three regression based functions,$S_L(\varphi) = W\varphi^\eta e^{-\xi(\varphi-1.075)^2}$, $S_L(T) = S_{L,0}(\frac{T}{T_0})^\alpha$ and $S_L(P) = S_{L,0}(\frac{P}{P_0})^\beta$.

3.9.1 W, η and ξ - coefficients

The first function is a nonlinear combination of the model parameters W, η and ξ and the independent variable equivalence ratio, φ. The first function is evaluated at constant pressure, 101325 Pa, and initial temperature at 298.15 K. The dataset includes 10 points of corresponding burning velocity and equivalence ratio values. The burning velocity values are covering the equivalence range between, $0.3 \leq \Phi \leq 2.5$.

The model parameters where determined with the Non-Linear Least-Squares Minimization and Curve-Fitting for Python regression solver, evaluating these parameters with least-squares function approximation. [31]

---

[13] The Gulder coefficients, and NASA polynomials was initially estimated in the Excel non-linear optimization tool GRG.

However, since it is difficult to document Excel code, the curve fitting method was switched from Excel GRG to Python LMFIT.

Table 3-3: Gulder coefficients, which is seen in formula (3-4), for the discharged gas emitted from an LCO, LNCM, and an LFP battery premixed with air, and methane-air at initial conditions of 1 atm, and 298.15 K. The burning velocity, for Li-ion LCO, LMC, LFP, H2 is estimated with the GRI-MECH 3.0, except for the electrolyte component dimethyl carbonate, where the DMC-Mech was used in Cantera 2.3.0, the parameters have been fitted with the Python based numerical optimization solver LMFIT.[14]

Fuel	W [m/s]	η [-]	ξ [-]	R^2 [-][15]	Φ [-]
Li-ion LCO gas	0.612	0.758	2.555	0.98	[0.3; 2.5]
Li-ion LMNCO gas	0.490	0.413	3.338	0.98	[0.3; 2.5]
Li-ion LFP gas	0.381	0.013	4.192	0.98	[0.3; 2.5]
H2	2.094	1.068	0.424	0.97	[0.3; 2.5]
CH4	0.395	-0.53	6.372	0.98	[0.3; 2.5]
Electrolyte DMC component	0.364	0.510	3.592	0.98	[0.5; 2.5]

3.9.2 A and β – coefficients

The secondary function, $S_L(T) = S_{L,0}(\frac{T}{T_0})^\alpha$, and tertiary, $S_L(P) = S_{L,0}(\frac{P}{P_0})^\beta$. , is unlike the first function, $S_L(\varphi) = W\varphi^\eta e^{-\xi(\varphi-1.075)^2}$, harder to evaluate since the model parameters α, and β are highly sensitive to the independent variable range of temperature and pressure, which the model variables α, and β are fitted to respectively. While the $W\varphi^\eta e^{-\xi(\varphi-1.075)^2}$-function has a somewhat case insensible ϕ-range at 0.3 ≤ ϕ ≤ 2.5, which is approximately the corresponding lower and upper flammability limits of the fuel, the α and β are highly case dependent, e.g. in a pressurized vessel the initial pressure can be significantly higher than 1 atmosphere. The temperature of the unburned gaseous mixture can vary as the ambient temperature, especially in Norway ranges from 221.75 K ≤T ≤ 308.75 K, and during a thermal runaway process the battery vents the gaseous mixture at approximately 473.15 K ± 50 K. Hence, the model parameters α, and β needs to be evaluated to the specific case.

---

[14] The code used to program the coefficients in Table 3-3 is categorized in Appendix B, sublevel B.5.1.
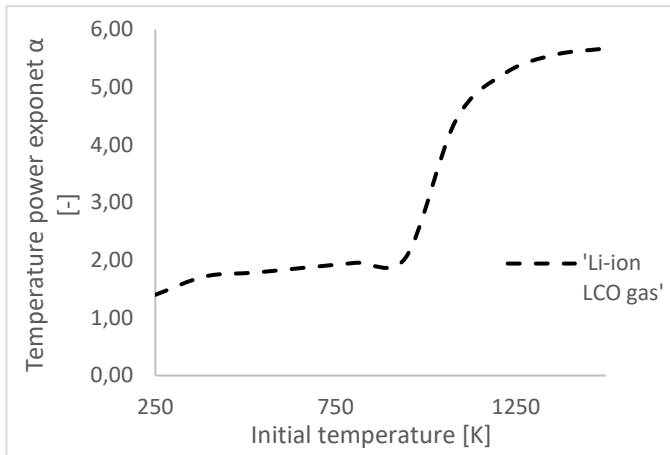
Figure 3-14: Power exponent coefficient, α, in formula (3-4 for the discharged gas emitted from an LCO battery premixed with air. The initial conditions where 1 atm, the fuel air mixture was stoichiometric. The power exponent, α, is estimated with the GRI-MECH 3.0 on Cantera 2.3.0, the parameters have been fitted with the Python numerical optimization solver LMFIT.
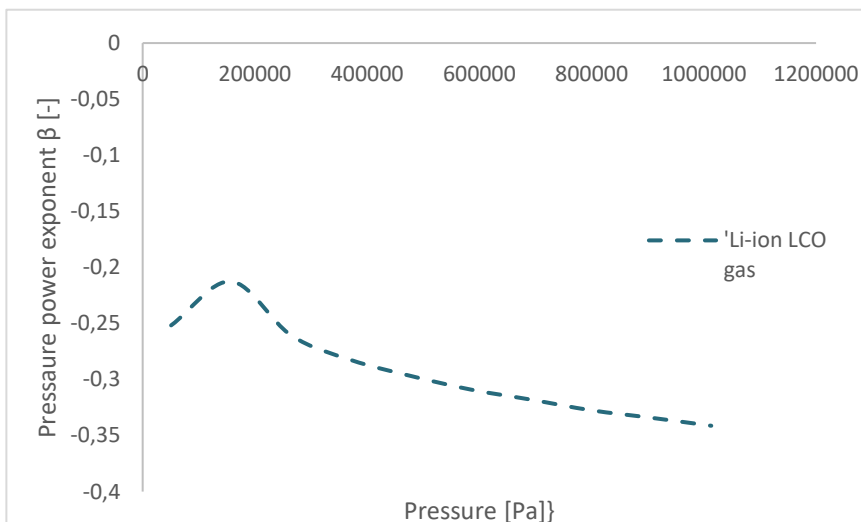
Figure 3-15: Power exponent coefficient, β, in (3-4, for the discharged gas emitted from an Li-ion LCO battery premixed with air. The Li-ion LCO gas was premixed at stoichiometric fuel ratio, and the initial pressure was 1 atm. The power exponent, β, is estimated with the GRI-MECH 3.0 on Cantera 2.3.0, the parameters have been fitted with the Python numerical optimization solver LMFIT.

The Figure 3-14 indicates that within the range of approximately $250K \leq T \leq 900$ K, an average alpha constant value can be relative accurate. However, beyond the threshold value T≈1000, the alpha constant increases almost exponentially within the temperature $1000 K \leq T \leq 1500$ K. From T≈1500 K the alpha value as a function of temperature flattens out for increasing temperature comparable to the temperature interval between $250K \leq T \leq 900$ K.

Figure 3-15 shows that the beta power exponent coefficient increases for 0.5 atm $\leq P \leq$ 1.5 atm. From P $\approx$ 1.5 atm the beta power exponent coefficient decreases, at increasing pressure, almost linearly.

Table 3-4: Gulder coefficients α and β at two specific intervals, where the correlation is approximated.[16]

Fuel	α [-]	R^2 α [-]	T [-]	β [-]	R^2 β [-]	P [-]
Li-ion LCO gas	1.99	0.98	[250 K; 961 K]	-0.24	0.99	[0.5 atm; 10 atm]
Li-ion LMNCO gas	2.11	0.99	[250 K; 961 K]	-0.28	0.99	[0.5 atm; 10 atm]
Li-ion LFP gas	2.29	0.99	[250 K; 961 K]	-0.32	0.99	[0.5 atm; 10 atm]
H2	2.9	0.71	[250 K; 961 K]	-0.04	0.78	[0.5 atm; 10 atm]
Electrolyte DMC component	2.05	0.99	[250 K; 1083 K]	-0.25	0.99	[0.5 atm; 10 atm]

The α and β power exponent coefficients, in Table 3-4, where estimated for cases covering normal conditions, i.e. temperature interval between 250 K to 1000 K, and pressure ranges between 0.5 atm to 10 atm. The correlation of alpha, and beta values for hydrogen is smaller than the other mixes, since the alpha coefficient for hydrogen increases exponentially at an earlier point at T≈840 K. This can also be seen in Figure 3-8. The beta power exponent correlation is relative the alpha coefficient correlation higher, but is still smaller, i.e. more inaccurate than the other beta coefficient correlation.

The correlation depicts relation between the $S_{L,0}(\frac{P}{P_0})^{\beta}$ with the curve fitted beta coefficient with the computed burning velocity at the same respective conditions. The same is the case for the alpha correlation, i.e. the relation between the $S_{L,0}(\frac{T}{T_0})^{\alpha}$ with the curve fitted alpha constant, and the computed burning velocity for the same temperature condition.

---

[16] The code used to program the coefficients in Table 3-4 is categorized in Appendix B, sublevel B.5.2.and B. 5.3.

3.10 NASA polynomial approximation of thermodynamical properties

The NASA polynomials are polynomial approximations of the thermodynamic properties enthalpy, entropy and the heat capacity. The function consists of seven coefficients that is curve fitted based on the least-square method to represent these thermodynamical properties over a wide temperature range, at a specific pressure. The NASA polynomial are used in both Cantera and OpenFOAM as functions for the thermodynamical properties for all gaseous species.

[15] [32]

The thermodynamical properties have the form:

$$\frac{C_p}{R} = a_2 T^1 + a_3 T^2 + a_4 T^2 + a_5 T^3 + a_1$$

$$\frac{H}{RT} = a_1 + \frac{a_2 T^1}{2} \frac{a_3 T^2}{3} + \frac{a_4 T^3}{4} + \frac{a_5 T^4}{5} + \frac{a_6 T^5}{6}$$

$$\frac{S}{R} = a_1 lnT + a_2 T^1 + \frac{a_3 T^2}{2} + \frac{a_4 T^3}{3} + \frac{a_5 T^4}{4} + a_7$$

$$\left. \begin{cases} T_i \leq T \leq T_c \end{cases} \right.$$

$$\frac{C_p}{R} = a_9 T^1 + a_{10} T^2 + a_{11} T^2 + a_{12} T^3 + a_8$$

(3-5)

$$\frac{H}{RT} = a_8 + \frac{a_9 T^1}{2} \frac{a_{10} T^2}{3} + \frac{a_{11} T^3}{4} + \frac{a_{12} T^4}{5} + \frac{a_{13} T^5}{6}$$

$$\frac{S}{R} = a_8 lnT + a_9 T^1 + \frac{a_{10} T^2}{2} + \frac{a_{11} T^3}{3} + \frac{a_{12} T^4}{4} + a_{14}$$

$$\left. \begin{cases} T_c \geq T \leq T_m \end{cases} \right.$$

The polynomials are representing the thermodynamical data in both Cantera and XiFoam for two temperature ranges; a lower, and a higher temperature range. The end temperature for the low temperature interval equals the initial temperature for the high temperature interval. This temperature is referred in OpenFOAM as "TC", or common temperature. Hence, the "7 "term polynomials includes 14 constants. 7 for the lower range, and 7 for the upper range.

The first five coefficients $a_1 \ldots a_5$, for lower range, and $a_8 \ldots a_{12}$ for the upper range are curve fitted to the heat capacity data sets, for the respective temperature intervals, with the constraint of minimizing the deviation at the start and endpoint of the temperature interval. The coefficients a_6 and a_{13} are least square fitted to minimize the deviation between the enthalpy for the two temperature intervals at the common temperature. Likewise, the coefficients a_7 and a_{14} are square fitted to minimize the deviation between the entropy value for the two temperature intervals at the common temperature.

Unlike the NASA polynomial representation of the thermodynamical data in Cantera where the coefficients only represent a specific gaseous specie, the NASA polynomial in OpenFOAM represents the fuel and oxidizer as a specific mixture, or i.e. as one specie. Additionally, it is necessary to have 15 coefficients for the fuel-oxidizer mixture before the combustion reaction, and 15 coefficients for the combustion products. It is then, necessary to optimize 30 coefficients to represent the thermodynamical properties for the heat capacity,

enthalpy and entropy to enable a feasible simulation of a specific fuel-oxidizer mixture. This is only valid for a specific equivalence ratio, and initial pressure.

Due to this rather complicated routine, the 30 coefficients necessary to represent the thermodynamical data for a specific fuel-oxidizer, have been made only for the Li-ion LCO gas, the electrolyte dimethyl carbonate component-air, and hydrogen-air all at stoichiometric condition.

The optimization method necessary to generate the NASA polynomials consisted of the following routine:

1. The specific enthalpy, entropy and heat capacity by mass for a gas mixture of oxidizer and fuel, were computed over a temperature range, in Cantera, limited by the temperature range of the specimens in the mixture.
2. The dataset computed in Cantera is then divided into two approximately equal sized sets, based on the temperature; One dataset for the lower temperature range, and the other for the high temperature range.
3. The 15 coefficients are curve fitted to the computed datasets, with the Python non-linear least-squares minimization and curve-fitting optimization tool LMFIT.
4. This routine is reiterated for the combustion products.[17]

[33]

Table 3-5: NASA polynomial approximation of the thermodynamical properties of the LCO-LNCO [2:1] vented gas premixed with air, at stoichiometric fuel-air condition.

	a_1	a_2	a_3	a_4	a_5	a_6	a_7	T -interval [K]
Reactants	3.26	1.10e-3	-2.8e-11	0	0	-4.42e3	5.43	$200 \leq T \leq 1000$
Reactants	3.28	1.00e-3	0	0	0	-4.43e3	5.31	$1000 \leq T \leq 5000$
Products	4.69	2.0e-4	-6.96e-10	-2.99e-13	0	-1.52e4	-3.28	$200 \leq T \leq 1000$
Products	3.41	1.00-3	-2.7e-10	-5.92e-13	0	-1.44e4	4.56	$1000 \leq T \leq 5000$

---

[17] The Table 3-5, Table 3-6 and Table 3-7 are computed from a code similar to the one in Appendix B, sublevel B.6. The code shows how the $a_1 \ldots a_7$ coefficients are determined.

Table 3-6: NASA polynomial approximation of the termodynical properties of the dimethyl carbonate premixed with air, at stoichiometric fuel-air condition.

	a_1	a_2	a_3	a_4	a_5	a_6	a_7	T -interval [K]
Reactants	5.39	4.71e-10	3.76e-11	0	0	-6.50e3	-6.26	$300 \leq T \leq 1000$
Reactants	5.39	-4.71e-10	-3.76e-11	0	0	-6.50e3	-6.26	$1000 \leq T \leq 5000$
Products	4.57	4.71e-10	3.76e-11	0	0	-1.49e4	-2.29	$300 \leq T \leq 1000$
Products	4.57	-4.72e-10	-3.76e-11	0	0	-1.49e4	-2.29	$1000 \leq T \leq 5000$

Table 3-7: NASA polynomial approximation of the thermodynamical properties of the hydrogen premixed with air, at stoichiometric fuel-air condition.

	a_1	a_2	a_3	a_4	a_5	a_6	a_7	T -interval [K]
Reactants	3.89	4.72e-10	3.76e-11	0	0	-1.31e3	-3.76e-1	$300 \leq T \leq 1000$
Reactants	3.89	-4.72e-10	-3.76e-11	0	0	-1.31e3	-3.76e-1	$1000 \leq T \leq 5000$
Products	4.3	4.71e-10	3.76e-11	0	0	-1.16e4	-1.42	$300 \leq T \leq 1000$
Products	4.3	-4.71e-10	-3.76e-11	0	0	-1.16e4	-1.42	$1000 \leq T \leq 5000$

3.11 CFD simulation in OpenFOAM with the turbulent premixed combustion solver XiFoam

3.11.1   Introduction

The scope of the subchapter is to document that the computed Gulder Coefficients, and the NASA polynomials for the li-ion LCO gas are operative in in OpenFOAM with the premixed turbulent solver XiFoam. The subchapter gives a brief overview of the OpenFOAM toolbox used to test the NASA, and Gulder input parameters, and of the simulated test case.

OpenFOAM is a toolbox for CFD applications used to create executables, known as applications. These applications are either solvers, or utilities. Solvers are used to solve a specific problem in continuum mechanics. Utilities are involved to perform data manipulations. OpenFOAM contains numerous solvers and utilities enabling the user to solve fluid flows with chemical reactions and turbulence. XiFoam is a solver designated to solve turbulent premixed combustion flows. It is used extensively for CFD explosion modelling.

[12] [30]

The following sub subchapters depicts the simulated case of the Li-ion LCO gas which includes a brief overview of the mesh, initial conditions, turbulence model, and screenshots of the simulations from paraView which is the the main post-processing tool in OpenFOAM

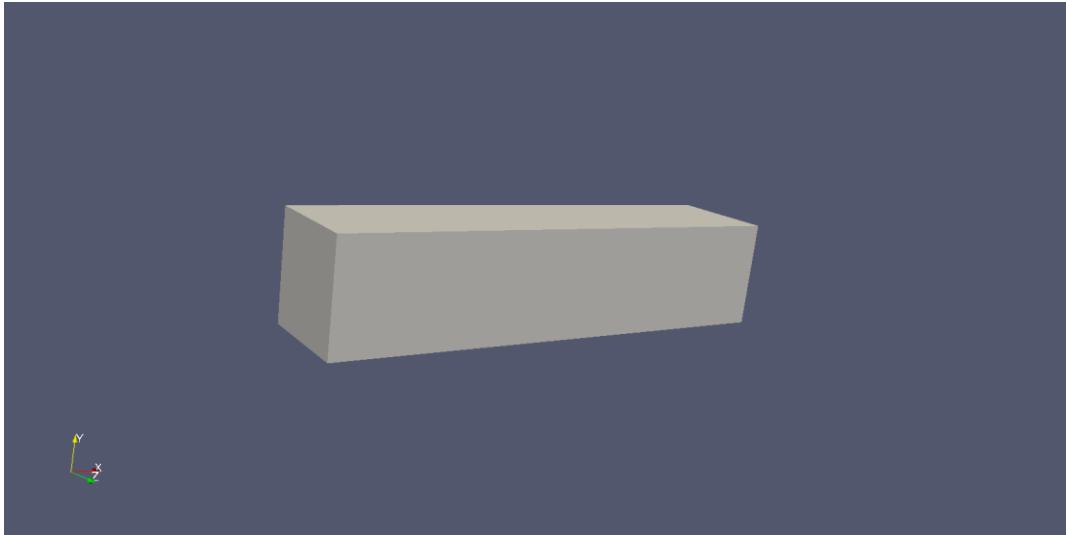### 3.11.2 Mesh, initial conditions and turbulence model[18]

Figure 3-16: Screenshot from the post-processing tool paraView of the mesh.

The mesh has approximately the same geometry and dimensions as the rig in chapter 4. The geometry of the object is a cuboid, as seen in Figure 3-16, with the length 45 cm, height 10 cm, and width 10 cm. The ignition point is 3.5 cm from the entry point. The cell number for the mesh was (180 40 1).[19]

The selected turbulence model was LES, i.e. Large Eddy Simulation.

The initial conditions remained mostly unadjusted from the default values in the 0-folder from the tutorial example pitzDaily in the XiFoam folder. The only adjustment was made in the U-directory where inlet reference field was changed from 13 to 0 in the x-direction. The selected turbulence model was LES (Large Eddies Simulation).

The rest of the settings remained unchanged, except the implementation of the Gulder coefficients, and the NASA polynomials in the dictionaries: combustionProperties and thermophysicalProperties[20].

---

[18] The following case is heavily based, and influenced by the tutorial seen in [31].

[19] The mesh dictionary is given in Appendix C, sublevel C.1.

[20] The combustionProperties, and thermophysicalProperties directories can be seen in Appendix C, sublevel C.2 and C.3

3.11.3   Results and discussion

Figure 3-17:Density of premixed Li-ion LCO gas-air, at time step: 0.01.

Figure 3-18: Density of premixed Li-ion LCO gas-air, at time step: 0.03.
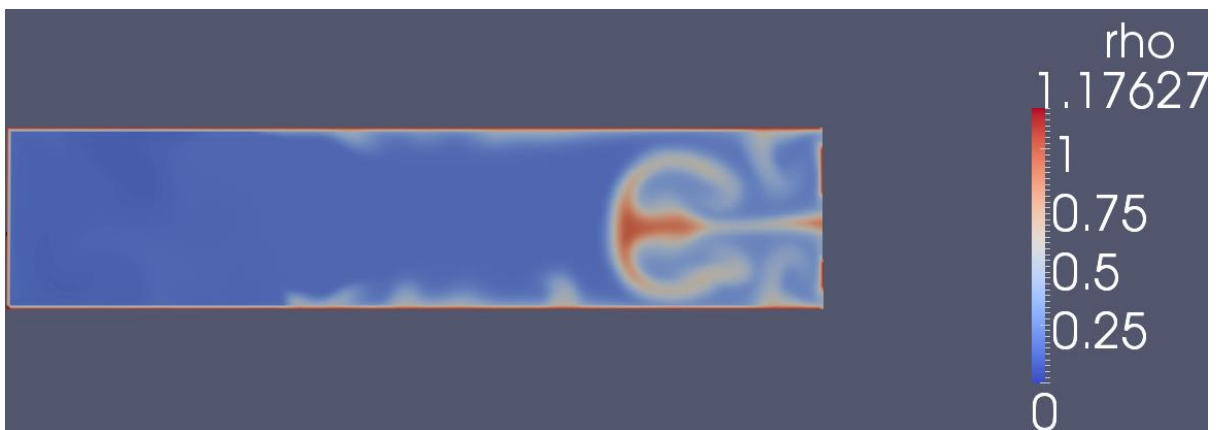
Figure 3-19:: Density of premixed Li-ion LCO gas-air, at time step: 0.05.

Figure 3-20: Temperature of premixed Li-ion LCO gas-air, at time step: 0.01
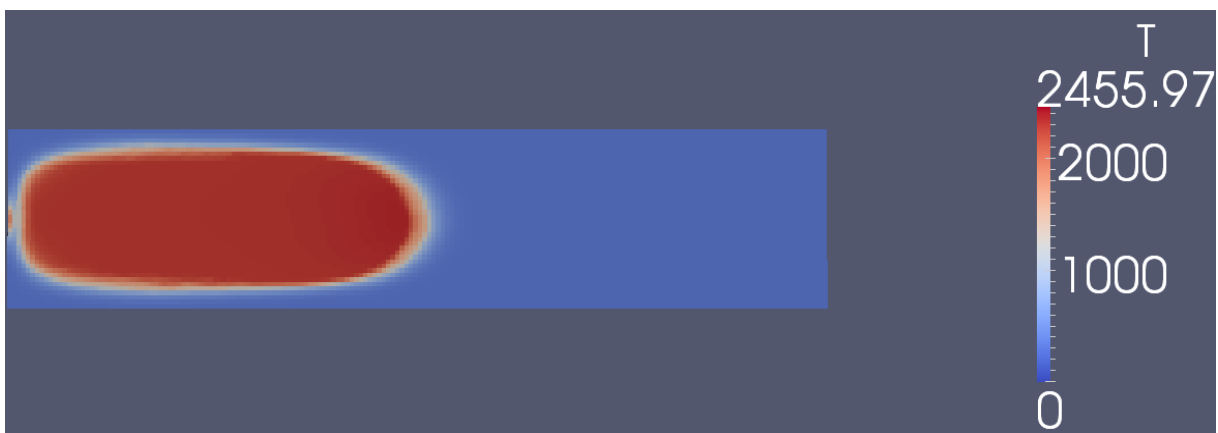
Figure 3-21: Temperature of premixed Li-ion LCO gas-air, at time step: 0.03.
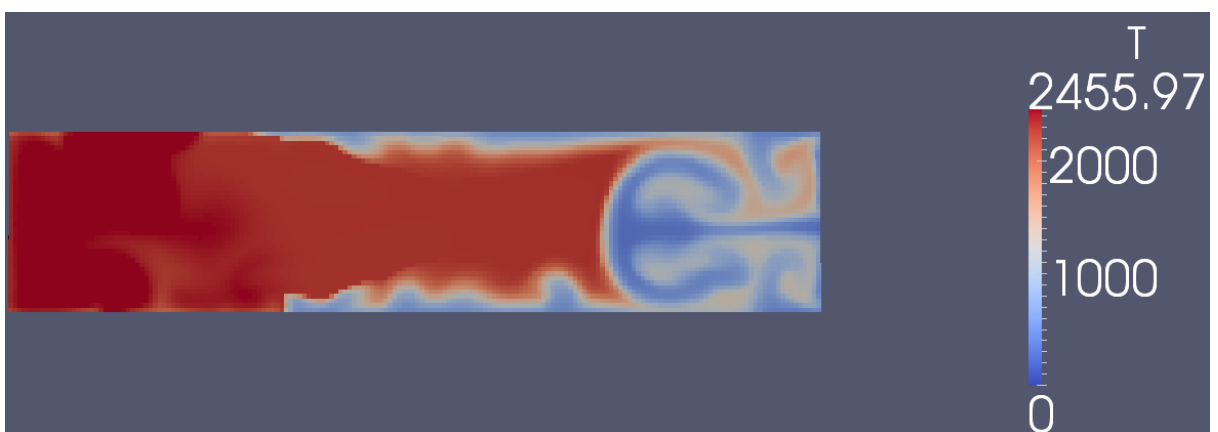
Figure 3-22: Temperature of premixed Li-ion LCO gas-air, at time step: 0.05.
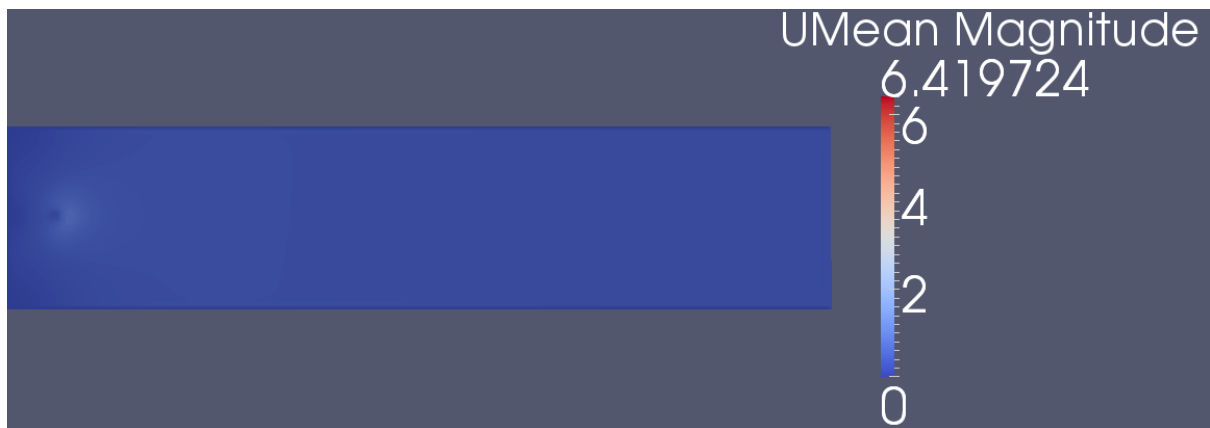
Figure 3-23: Average flame speed of premixed Li-ion LCO gas-air, at time step: 0.01.

Figure 3-24: Average flame speed of premixed Li-ion LCO gas-air, at time step: 0.03.
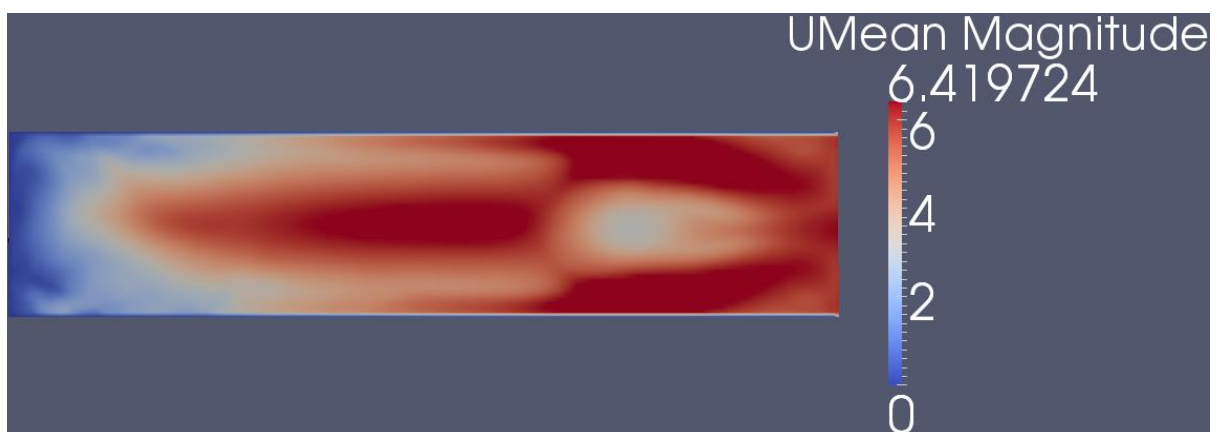
Figure 3-25: Average flame speed of premixed Li-ion LCO gas-air, at time step: 0.05.

It is important to notice that it was necessary to adjust the courant number and the time step of the simulation, denoted deltaT, in the controlDict dictionary for the XiFoam-solver to converge. In several of the attempts the solver XiFoam gave unphysical temperatures below 250 K, causing the simulation to crash. Whether this is caused by the computed NASA polynomials implemented in the thermophysicalProperties-directory, or if it is due to the

setup of the case, the boundary conditions, the numerical schemes or mesh has not been resolved.

The temperature seen in Figure 3-20, Figure 3-21 and Figure 3-22 is higher than the adiabatic flame temperature at constant pressure and enthalpy, i.e. 2227.39 K, but below the adiabatic flame temperature at constant volume and internal energy, i.e. 2565.58 K. It is currently unknown if this is due to a quasi-constant volume mesh, or if it is due to the computed NASA polynomials. To resolve this more testing is necessary.[21]

The density simulated in Figure 3-17, Figure 3-18 and Figure 3-19 are in relative agreement with an inverse version of the Canter 2.3.0 computed Figure 3-10.

The mean velocity, as seen in Figure 3-23, Figure 3-24 and Figure 3-25, are in relative compliance with the Cantera-computed laminar flame speed, as seen in Appendix A, sublevel A.3, which was 4.6 m/s at φ=1.3. The difference is as stated in [30]: "*The effect of turbulence is that it wrinkles and stretches the propagating laminar flame sheet, increasing the sheet area and, in turn, the effective flame speed.*".

Due to time limitations, the case was not compared with e.g. propane, which could have been beneficial to evaluate the NASA, and Gulder inputs, and is a great place to begin for further evaluation of the input values.

3.12 Summary of chapter 3.

The combustion properties for Li-ion LCO, LMNCO, and LFP gases, and the electrolyte component dimethyl carbonate was computed in Cantera 2.3.0, and the code for these computations are listed in Appendix B.

As an overall summary, the combustion properties of the Li-ion batteries vented gas and electrolyte component dimethyl carbonate are equal to methane and propane.

The burning velocity of the vented Li-ion gases, as depicted in Figure 3-2, are approximately within the range of 34 cm/s $\leq S_l \leq$ 70 cm/s at normal conditions, i.e. 1 atm, and 298 K, which resembles the burning velocity range of hydrocarbons.

The pressure at constant volume for the lithium-ion batteries LCO, LFP, and LMNCO agree with the result from [10], and resembles hydrocarbons. The electrolyte dimethyl carbonate component generated the highest pressure of the mixtures in Figure 3-9, at 10.1 bar a.

Due to the high pressure of the dimethyl carbonate the deflagration index of this electrolyte component was higher than the gas from the LFP, and LNCMO overheated battery, but equal to the Li-ion LCO gas, i.e. 95 Bar m/s. The computed deflagration index are in agreement to the deflagration index of the Li-ion Pouch cells in [10].

The NASA, and Gulder inputs for OpenFOAM was computed, but needs further tests to determine the validity of them.

---

[21] The adiabatic- flame temperatures are estimated in computed Cantera with the thermos-functions equilibrate('HP') and equilibrate('UV').

4 Experiment

4.1 Introduction

The scope of the chapter is to document the experimental setup, and the test results of two overheated 18650 lithium manganese oxide, $LMnO_2$, batteries. The objective is to capture the flame front, and approximate the flame speed[22] of the premixed vented gas-air mixture, and determine the corresponding temperature at which the batteries starts to vent. The motivation is to test the diagnostics tools, i.e. a high-speed camera, pressure and temperature sensor on the batteries, and determine if the current equipment and setup can be used for further battery experiments. The amount of batteries will be limited to two batteries, hence some of the observable correlations is not necessarily causal, and the conclusions derived from these observations might be inconclusive.

---

[22] The "flame speed" experimentally measured in this chapter is not the same quantity as the measurement denoted as burning velocity. Flame speed S, is defined as the velocity of the flame relative to a stationary observer. The relation between these two measurements, i.e. the one-dimensional adiabatic laminar burning velocity and the one-dimensional adiabatic laminar flame speed, are as following:

$$U = \frac{\rho_0}{\rho_{flame}} S_L \tag{4-0}$$

The symbol denoted S_{LB} is representing the flame speed, and the symbol S_L is the burning velocity, ρ_0 is the density of the premixed fuel-oxidizer mixture, and the ρ_{flame} is the density in the flame. Formula (4-0) is derived from the conservation of mass. [23]

4.2 Experimental setup

Figure 4-1: Picture of the experimental setup at Kjølnes Campus, HSN.

The rig at University College of Southeast Norway in the Porsgrunn campus consist of a semi open channel, where the back, top, bottom, and sides of the channel are enclosed.

The height, length, and width of the channel are respectively 10.0 cm, 44.5 cm and 10.4 cm. The material of the sides of the channel are made of PMMA (Poly (methyl 2-methylpropenoate). The back, top and bottom material are made of steel. An electrical spark plug was mounted 3.5 cm from the backplate on the top of the channel. A hole was drilled through the middle of the backplate where a detachable brass holster designed to hold an 18650-battery was mounted during the battery setup.

Figure 4-2: Picture of the battery-holster being mounted on the channel.

To heat up the batteries, a Omegalux heat wire was twisted around the brass holster. The heat wire was connected to an autotransformer, i.e. a power supply, with an adjustable voltage knob. Two thermocouples were used during the experiment, one on top, and the other one inside the battery holster to record the temperature effect of the heat wires, and to record the onset temperature of the battery system, i.e. the temperature the batteries starts to vent. The thermocouples were connected to the *Hioki 8430-20- Memory Hilogger*.

During the methane, and hydrogen setup, the battery holster was replaced with a detachable hose which was connected from the pressurized gas tank to the backplate of the channel.

The experiment was filmed with the high-speed camera "Photron APX-RS monochrome camera and the film where edited and analysed with the software Photron FASTCAM Viewer. The camera is depicted in Figure 4-1.

4.3 Material characteristics of the batteries which are used in the experiment.

The experimental specimens were two LMO, lithium manganese-dioxide, 18650 batteries, a pre-mixed methane-air mixture where the batteries had the following material properties:

Table 4-1: Properties for the LMO-batteries

Property		Variable	LMO
Cell mass		g	42.5
Capacity		Ah	1.5
Minimum voltage		V	3.0
Maximum voltage		V	4.2
Electrolyte weight			≤ 4.4 g
Cathode material			$LiMn_2O_4$
Anode material			Graphite

4.4 Results and discussion

4.4.1 Results from the temperature sensors
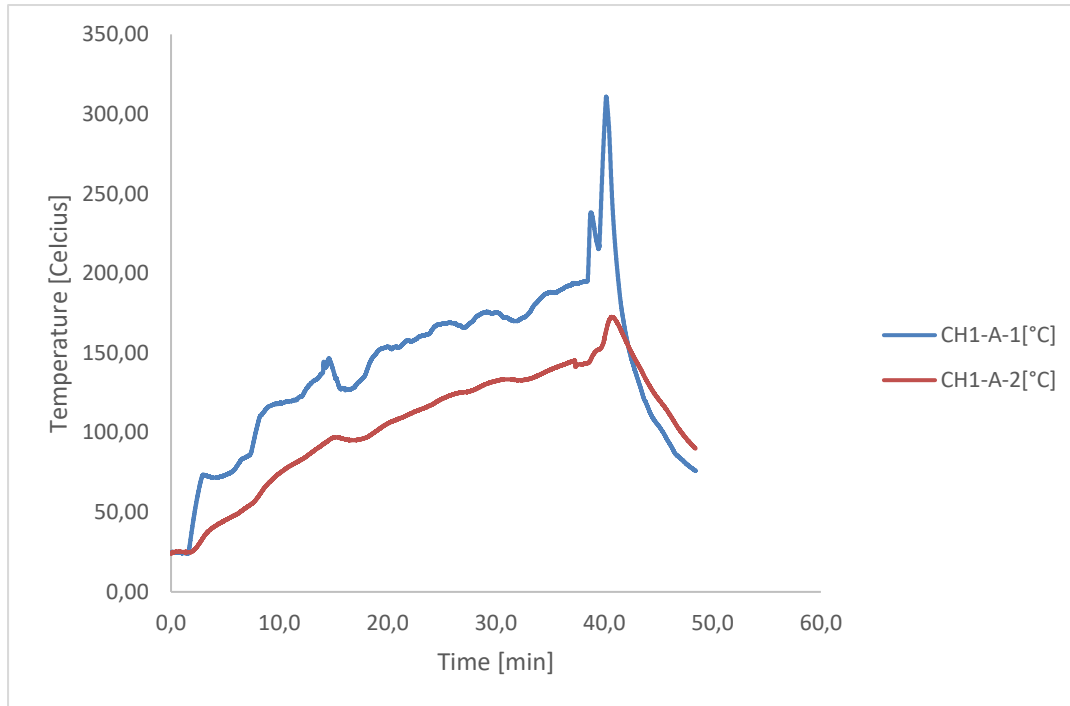
Figure 4-3: Graph of the surface-temperature of the F37 battery as a function of time. The Ch1-A-1 legend depicts the thermocouple on the outside of the heat wire, and the CH1-A-2 legend depicts the thermocouple on the inside of the heat wire.
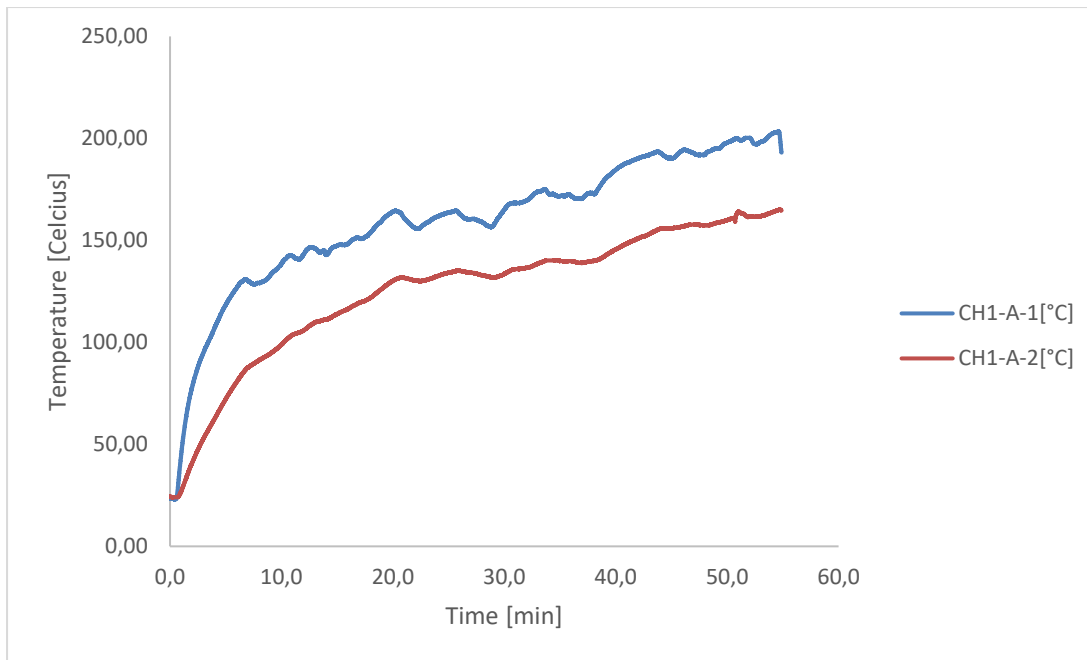
Figure 4-4: Graph of the surface-temperature of the F39 battery as a function of time. The Ch1-A-1 legend depicts the thermocouple on the outside of the heat wire, and the CH1-A-2 legend depicts the thermocouple on the inside of the heat wire.

Table 4-2: Measured key temperatures, based on Figure 4-3 and Figure 4-4

Specimen	Total amount of time before the battery started to vent. [min]	Surface-temperature of the battery at which the gas vented. [°C]	Surface-temperature drop, during gas venting [°C]	SOC [%]	Experiment name
Methane	N/A	N/A	N/A	N/A	F25
LMO-18650 battery	36	145±3	3.2±1	30±1	F37
LMO-18650 battery	50	161±3	1.9±1	100±1	F39

The surface-temperature at which the battery vented was 20 Celsius degrees lower for the Li-ion LMO battery with a SOC at 30 %, i.e. F37 compared to the battery with SOC at 100 %, F39. This suggest that the battery with an SOC at 100 % is more resistant to heat than the battery with a lower SOC.

The time it took to reach the vent surface-temperature was higher for F39 which had a SOC at 100 %, compared to the F37 battery which had a SOC at 30. This trend is contradicting what's observed in [20], where the heating time became shortened with ascending SOC.

The vent surface-temperatures registered for the batteries, F37 and F39, as seen in Table 4-2, are equal to the temperatures reported in [11] and [34].

So, to conclude the equipment test during the Li-ion battery experiments; the Hioki 8430-20-Memory Hilogger logger with the experimental setup as described in chapter 4.2 Experimental setup, where able to determine the vent temperature, and temperature drop at which the gas vented, and expanded. However, with the setup in chapter 4.2 Experimental setup the temperature of the quasi-premixed vented-gas and air mixture before it was ignited was not registered. This should be included in successive experiments on the rig.

4.4.2 Results derived from the high-speed camera

s

Figure 4-5: Premixed methane-air mixture, presumably lean. Flame front approximately 9.5 cm from backplate.

Figure 4-6: Premixed methane-air mixture, presumably lean. Printscreen of the flame front 0.0475 s from the position in Figure 4-5.

Figure 4-7: Premixed Li-ion LMO-air mixture, with SOC at 100 %. The flame front was approximately 9.5 cm from backplate. The battery is referred to as F39.

Figure 4-8: Premixed Li-ion LMO-air mixture, with SOC at 100 %. Printscreen of the flame front 0.0475 s from the position in Figure 4-7. The battery is referred to as F39.
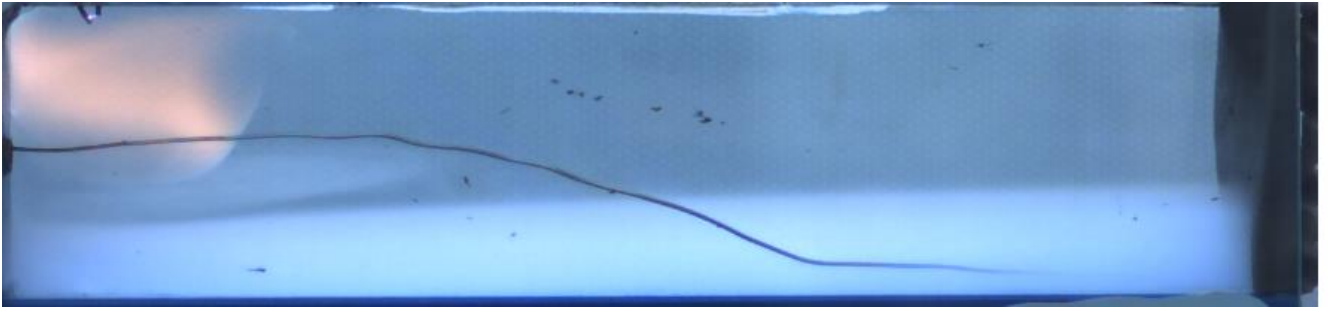

Figure 4-9: Premixed Li-ion LMO-air mixture, with SOC at 30 %. Flame front approximately 9.5 cm from backplate. The battery is referred to as F37.
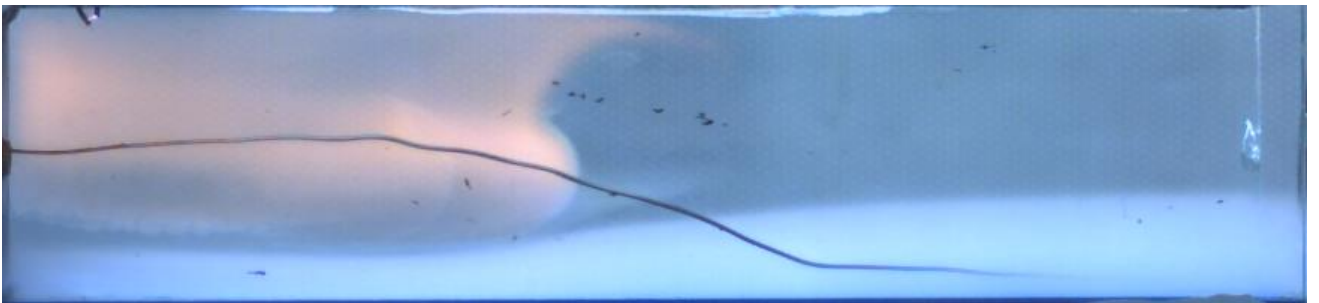

Figure 4-10: Premixed Li-ion LMO-air mixture, with SOC at 30 %. Printscreen of the flame front 0.0475 s from the position in Figure 4-9. The battery is referred to as F37.

The Figure 4-5, Figure 4-6, Figure 4-7, Figure 4-8, Figure 4-9 and Figure 4-10 are screenshots from the Photron APX-RS monochrome camera of the ignited premix gaseous mixture from the two Li-ion LMO batteries, and a premixed methane-air mixture function.
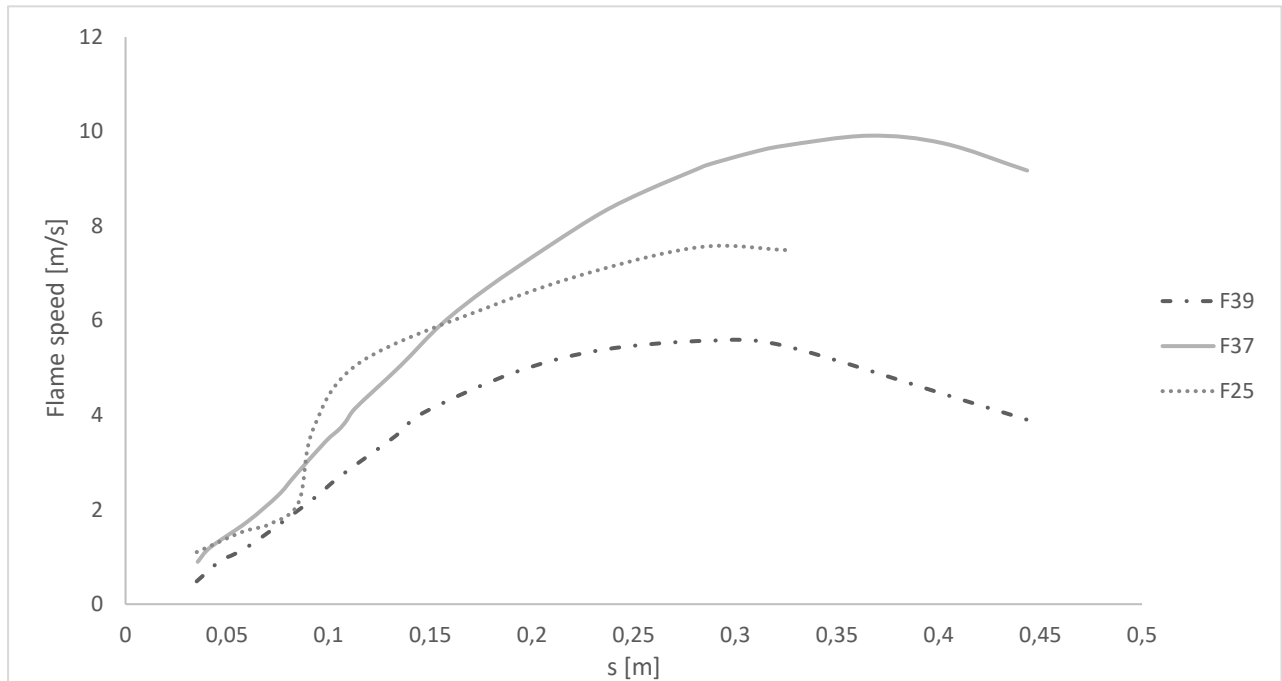
Figure 4-11: Flame speed of the two LMO-batteries, and the premixed hydrogen-air mixture as a function of the length of the channel in x-direction

The flame speed, as seen in Figure 4-11, was derived by measuring the flame front position as a function of time with the scale calibration functionality in the software Photron FASTCAM Viewer. The flame front position, with respect to time. was fitted to a sextic polynomial, i.e. a polynomial of degree six. This was an attempt to smooth the data set, i.e. capture the important pattern in the data, while leaving out noise. The sextic function was then derivated with respect to time, giving the flame speed as a quantic function. This curve fitting procedure was coded in Python, with the interphase LMFIT. [23]

The flame speed of the premixed Li-ion LMO gas-air mixtures, and the methane-air mixture in Figure 4-11 are in line with the Figure 4-5, Figure 4-6, Figure 4-7, Figure 4-8, Figure 4-9 and Figure 4-10. I.e. that the Li-ion LMO battery with SOC at 30 % propagates faster than the Li-ion LMO battery with SOC at 100 %, and the methane-air mixture.

It might be reasonable to conclude that a lower SOC corresponds to the highest flame speed, but since it is just two batteries this correlation might not be causal.

As seen in Table 4-2 the LMO battery denoted F37 vented the gas-mixture at 145 °C, and the battery denoted F39 vented at 161 °C. Since flame speed is enhanced by increased temperature, see Appendix A figure 5-5, this should cause the Li-ion LMO gas F39 to propagate faster than the Li-ion LMO gas F37, but this was not the case. Due to many uncontrollable, undeterminable and unknown factors influencing the velocity and the

---

[23] Since the flame front did not propagate uniformly in the vertical axis it was difficult to determine the average flame front position. Hence, it was necessary to smooth the function to account for this behavior.

measurement technique it is necessary to test more batteries to determine the causality of the upper observation. [24]

Even though some of the observations and results from the experiment might be inconclusive, i.e. effect of SOC, it is evident that the Li-ion LMO gas propagates equal to methane, i.e. an averaged value for the two batteries is approximately equal in magnitude to the premixed methane-air mixture.

4.4.3 Additional results and remarks

The pressure generated by the propagating vented gas mixture was so low that it was cancelled out by disturbance and noise. Hence, the pressure sensors did not work for the specific setup, or experiment.

Table 4-3: Mass loss due to combustion of vented gas

Specimen	Mass loss [g]	SOC [%]	Experiment name
LMO-18650 battery	2.5±1	30±1	F37
LMO-18650 battery	2.5±1	100±1	F39

The mass loss as seen in Table 4-3 is relative to what is measured in [34] low. In the study [34] by Jhu et al. the four lithium-ion batteries lost in average 9.8 grams. However, whether it includes the plastic cover or not, is not mentioned in the report. Since the uncertainties of the Weighing scale was relatively high, it should be replaced for successive experiments with a high precise laboratory weight.

---

[24] The laminar flame speed has been estimated for the Li-ion LCO, LMNCO and LFP gases, and the electrolyte component dimethyl carbonate based on the laminar burning velocity, and the volume expansion at constant pressure combustion and can be seen in figure 5-5 Appendix A. The flame speed measured experimentally in Figure 4-11 is propagating faster than any of the laminar flame speed of the battery gases, and electrolyte component dimethyl carbonate. This suggest that either the temperature of the unburned mixture was significantly higher than 298 K, or that the flow was effected by turbulence. Additionally, the vented gas from the batteries was inhomogeneous, and the laminar flame speed computed in Cantera 2.3.0 is homogenous, this fact can also have a significant effect on the flow.
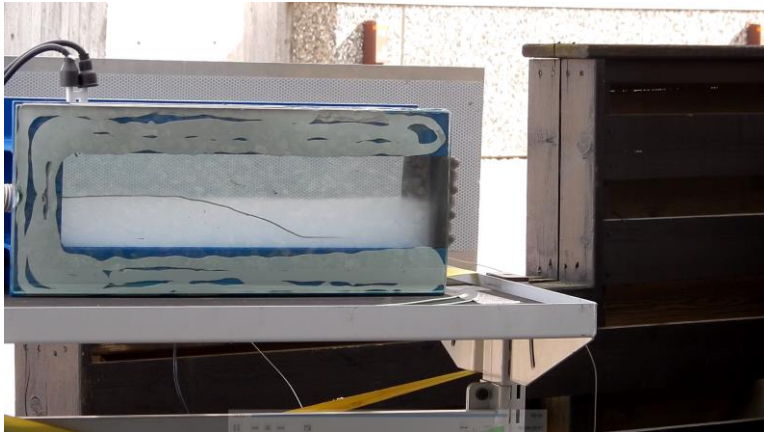
Figure 4-12: Printscreen of the Li-ion LMO F39 gas preignited.

The vented gas mixture from the batteries was observable dense. This is can be seen in Figure 4-12. Since it was relative difficult to ignite the mixture from the batteries this indicates that the concentration of hydrogen must have been rather low, and that the mixture might have consisted of electrolyte vapour and aerosol droplets. As mentioned by Harris et al. [9].

4.5 Summary of chapter 4.

The experimental rig and setup was tested out with two Li-ion LMO batteries. The flame speed of the vented Li-ion LMO gases was in close agreement with the numerical results, i.e. that the vented gases from the Li-ion batteries propagates approximately as fast as methane. However, further research is necessary to validate this, since the uncertainties are large. The vent temperature of the LMO batteries, of the surface of the battery, agreed with the temperatures reported in [11] and [34]. However, the method of determining the flame speed needs to be improved, i.e. implementation of an automatic technique to evaluate the averaged flame front position at each time step (e.g. integration each flame front pixel, and divide on the total number of flame front pixels). Additional thermocouples, needs to be installed inside the channel to evaluate the temperature of the vented gas and air mixture before and during ignition and propagation.

Conclusion and Recommendations

The objectives of the thesis were two folded:

A. Compute the data necessary for simulating the vented gas mixture from lithium-ion batteries in turbulent conditions and compute the combustion properties of the vented gas at laminar conditions.
B. Test the rig equipment on lithium-ion batteries, to verify if it can measure the flame speed, and to detect the vent temperature of the battery. Compare the flame speed with a common hazardous gas such as methane.

4.6 Conclusion

A. Numerical computations of the XiFoam inputs, and laminar combustion properties:

    a. The Gulder Coefficients where computed for the vented gases from the lithium-ion batteries LCO, LMNCO and LFP, electrolyte component dimethyl carbonate and hydrogen. The coefficient of determination, r^2, was approximately 0.98 which indicates that the regression, i.e. Gulder coefficients fitted the data perfectly.

    b. The NASA polynomials were computed for the Li-ion LCO battery gas, the electrolyte dimethyl carbonate component and hydrogen, with un unknown coefficient of determination, r^2.

    c. A XiFoam-case was tested in OpenFOAM with the NASA polynomials and Gulder Coefficients for the Li-ion LCO gas, some issues where discovered which indicated that further testing is necessary for validating the inputs.

    d. The laminar combustion properties of the Li-ion batteries, and electrolyte component dimethyl carbonate were computed for the burning velocity, deflagration index, volume expansion ratio at constant pressure and overpressure at constant volume expansion. The battery gases had properties equal to methane and propane.

    e. The gas from Li-ion LCO battery had the highest burning velocity, pressure, volume expansion and deflagration index of the three batteries LCO, LNCMO and LFP.

f. The electrolyte component dimethyl carbonate was more severe, i.e. had higher deflagration index, than the vented gas from the LNCMO and LFP lithium-ion batteries. Suggesting that a "safer" cathode, e.g. a LFP-battery can release a mixture more severe than e.g. a. LMNCO-battery. However, dimethyl carbonate is just one component of multiple in the electrolyte, and to give a firm conclusion requires that the rest of the components in the electrolytes need to be considered. However, there are currently no reaction mechanism which includes these components, ssi.e. ethylene carbonate, propane carbonate, ethyl methyl carbonate or the salts e.g. Lithium hexafluorophosphate, Lithium tetrafluoroborate or Lithium perchlorate.

B. Test of rig, and diagnostic equipment with the lithium-ion batteries: lithium manganese oxide:

a. The rig, and the diagnostic equipment, i.e. high-speed camera, at current setup where able to capture the flame speed of vented lithium-ion battery gas.

b. The present tests of the vented non-well-defined inhomogeneous mixture from the two lithium manganese oxide batteries indicates that the mixtures propagated at velocities similar to methane-air. However, since the sample size was limited to only two batteries and that the results are associated with multiple unknown factors, i.e. the unknown preignition temperature of the vented gas-air mixture, the ignition time, the degree of gas-air homogeneity the results are unable to provide a clear overall conclusion of the experimental measured vented gas. Further experimental research is necessary to enable that.

c. Additionally, the lithium-ion battery LMO with SOC at 30 % propagated as a factor of 2 times faster than the LMO battery with SOC at 100 %. However, the sample size is too small, and the uncertainties are too large to generalize this correlation, and state that a lower SOC corresponds to a higher flame speed. As with the methane comparison; more research is necessary.

d. The vent surface-temperature of the batteries was measured at 145 ^{0}C and 161 ^{0}C, which is equal to the temperatures reported in [8] and [27].

4.7 Recommendations

This section lists the further developments required to simulate the vented gas from overheated lithium-ion batteries in OpenFOAM with the turbulent premixed solver XiFoam, and to improve the lithium-ion battery test rig.

A. OpenFOAM CFD simulation in XiFoam
   a. Compare the Li-ion LCO gas-air mixture with e.g. a premixed propane-air and methane-air mixture.
   b. Include obstructions in the mesh.
   c. Simulate a case with the electrolyte component dimethyl carbonate-air.

B. Experimental test rig:

   a. Include different Cathode, and Anode chemistry based batteries.
   b. Vary the SOC of the batteries.
   c. Perform gas chromatograph composition analysis of the vented battery gas, where the electrolyte species are calibrated for.
   d. Included additional thermocouple for instalment within the channel, to record the vented gas-air mixture before ignition.

References

[1]   Sanchirico, R., Di Benedetto, A., Garcia-Agreda, A., & Russo, P. (2011). Study of the severity of hybrid mixture explosions and comparison to pure dust–air and vapour–air explosions. Journal of loss prevention in the process industries, 24(5), 648-655.

[2]   Denkevits, A. (2007). Explosibility of hydrogen–graphite dust hybrid mixtures. Journal of loss prevention in the process industries, 20(4), 698-707.

[3]   Leuschke, G. (1965). Beiträge zur Erforschung des Mechanismus der Flammenausbreitung in Staubwolken.

[4]   Eckhoff, R. K. (2003). Dust explosions in the process industries: identification, assessment and control of dust hazards. Gulf professional publishing.

[5]   Goral, P., Klemens, R., & Wolanski, P. (1988). Mechanism of gas flame acceleration in the presence of neutral particles. Dynamics of reactive systems. Part 1: Flames, 325-335.

[6]   Gao, W., Mogi, T., Yu, J., Yan, X., Sun, J., & Dobashi, R. (2015). Flame propagation mechanisms in dust explosions. Journal of Loss Prevention in the Process Industries, 36, 186-194.

[7]   Burgoyne, J. H. and Cohen, L., 1954, The effect of drop size on flame propagation in liquid aerosols. Proc. Roy. Soc., A225: 375–392.

[8]   Gant, S., Bettis, R., Santon, R., Buckland, I., Bowen, P., & Kay, P. (2013). Generation of flammable mists from high flashpoint fluids: literature review. Health and Safety Executive, Research Report RR980.

[9]   Harris, S. J., Timmons, A., & Pitz, W. J. (2009). A combustion chemistry analysis of carbonate solvents used in Li-ion batteries. Journal of Power Sources, 193(2), 855-858.

[10]   Horn, Q., & Engineer, P. P. Thermal Runaway and Safety of Large Lithium-Ion Battery Systems. 0.00, 2, 5-00. [19]

[11]   Golubkov, A. W., Fuchs, D., Wagner, J., Wiltsche, H., Stangl, C., Fauler, G., ... & Hacker, V. (2014). Thermal-runaway experiments on consumer Li-ion batteries with metal-oxide and olivin-type cathodes. RSC Advances, 4(7), 3633-3642. [11]

[12]   H.G. Weller, G. Tabor, A.D. Gosman and C. Fureby, 'Application of a Flame-Wrinkling LES Combustion Model to a Turbulent Mixing Layer', 27th Symp. (Intl.) on Combust., The Combustion Institute, pp. 899-907 (1998)

[13]   David G. Goodwin, Harry K. Moffat, and Raymond L. Speth. Cantera: An object-oriented software toolkit for chemical kinetics, thermodynamics, and transport processes. http://www.cantera.org, 2017. Version 2.3.0. doi:10.5281/zenodo.170284

[14]   Newville, M., Stensitzki, T., Allen, D. B., & Ingargiola, A. (2014). LMFIT: Non-Linear Least-Square Minimization and Curve-Fitting for Python¶ [Data set]. Zenodo. http://doi.org/10.5281/zenodo.11813

[15]   Allison, D. O. (1972). Polynomial approximations of thermodynamic properties of arbitrary gas mixtures over wide pressure and density ranges.

[16]   Yasari, E., Runsten, J., & Andricss, J. (2010). Tutorial XiFoam.

[17]   Glaude, P. A., W. J. Pitz, and M. J. Thomson, "Chemical Kinetic Modeling of Dimethyl Carbonate in an Opposed-Flow Diffusion Flame," Proceedings of the Combustion Institute 30, pp. 1095-1102 (2004); Lawrence Livermore National Laboratory, Livermore, CA, UCRL-JC-201358.

[18]   Huang, P., Wang, Q., Li, K., Ping, P., & Sun, J. (2015). The combustion behavior of large scale lithium titanate battery. Scientific reports, 5, 7788.

[19]   Gregory P. Smith, David M. Golden, Michael Frenklach, Nigel W. Moriarty, Boris Eiteneer, Mikhail Goldenberg, C. Thomas Bowman, Ronald K. Hanson, Soonho Song, William C. Gardiner, Jr., Vitali V. Lissianski, and Zhiwei Qin http://www.me.berkeley.edu/gri_mech

[20]   Chemical-Kinetic Mechanisms for Combustion Applications", http://web.eng.ucsd.edu/mae/groups/combustion/mechanism.html , Mechanical and Aerospace Engineering (Combustion Research), University of California at San Diego (http://combustion.ucsd.edu).

[21]   Joerg Appel, Henning Bockhorn, and Michael Frenklach, 'Kinetic Modeling of Soot Formation with Detailed Chemistry and Physics: Laminar Premixed Flames of C2 Hydrocarbons,' Combust. Flame 121:122 (2000).

[22]   Buffam, J. (2008). Measurement of Laminar Burning Velocity of Methane-Air Mixtures Using a Slot and Bunsen Burner (Doctoral dissertation, Worcester Polytechnic Institute).

[23]   Bjerketvedt, D., Bakke, J. R., & Van Wingerden, K. (1997). Gas explosion handbook. Journal of hazardous materials, 52(1), 1-150.

[24]   Glassman, I., Yetter, R. A., & Glumac, N. G. (2014). Combustion. Academic press.

[25]   C. K. Law, A. Makino, and T. F. Lu, "On the off-stoichiometric peaking of adiabatic f lame temperature," Combustion and Flame, vol. 145, pp. 808-819, 6// 2006.

[26]   Konnov, A. A. (2015). The temperature and pressure dependences of the laminar burning velocity: experiments and modeling. In Proc. 7th European Combustion Meeting, Budapest, Hungary, March 30-April 2.

[27]   Huzayyin, A. S., Moneib, H. A., Shehatta, M. S., & Attia, A. M. A. (2008). Laminar burning velocity and explosion index of LPG–air and propane–air mixtures. *Fuel*, *87*(1), 39-57.

[28]   Dahoe, A. E., Zevenbergen, J. F., Lemkowitz, S. M., & Scarlett, B. (1996). Dust explosions in spherical vessels: the role of flame thickness in the validity of the 'cube-root law'. *Journal of Loss Prevention in the Process Industries*, *9*(1), 33-44

[29]   Huang, P., Wang, Q., Li, K., Ping, P., & Sun, J. (2015). The combustion behavior of large scale lithium titanate battery. Scientific reports, 5, 7788.

[30]   Yasari, E., Runsten, J., & Andric, J. (2010). Tutorial XiFoam.'

[31]   Edgar, Thomas F. , Himmelblau, David M. and Lasdon, Leon S. (2001) Optimization of Chemical Processes 2nd ed. Boston Mc Graw Hill. 2nd edition out of print.

[32]   Burcat, A., & McBride, B. (1993). Technion Report# TAE 697. Technion, Haifa.

[33]   Boettcher, P., Ziegler, J., Thomas, V., Mevel, R., Damazo, J., & Shepherd, J. (2012). Refitting Thermodynamic Data.

[34]   Jhu, C. Y., Wang, Y. W., Shu, C. M., Chang, J. C., & Wu, H. C. (2011). Thermal explosion hazards on 18650 lithium-ion batteries with a VSP2 adiabatic calorimeter. Journal of hazardous materials, 192(1), 99-107.

Appendixes

Appendix A Additional Figures

Appendix B Python Code

Appendix C OpenFOAM documentation

Appendix D Burning velocity computational scheme for carbonate-species

Appendix A
Additional figures

A.1 Additional Laminar Burning Velocity Figures
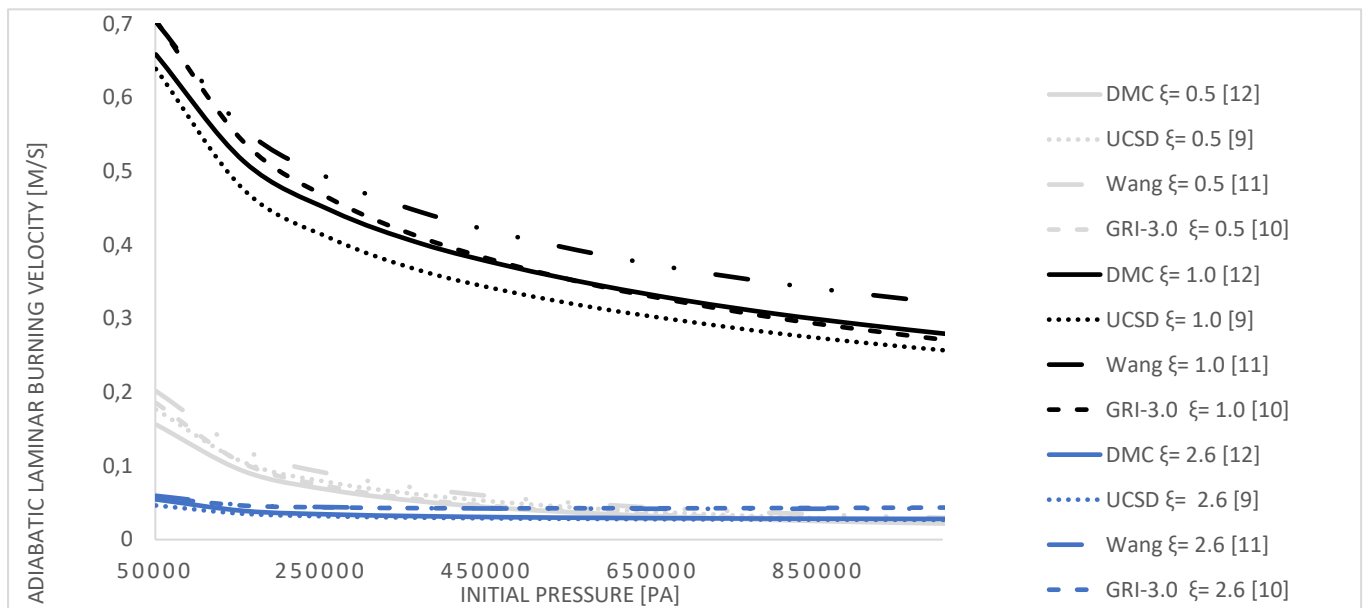
Figure 5-1: Comparison of the chemical reaction mechanism impacting the laminar burning velocity of the discharged gas emitted from an LCO-battery-premixed with air, at initial conditions of 298.15 K, were the burning velocity is a function of the initial pressure in pascals. All the data are estimated with the mechanisms denoted in the graph, estimated on Cantera 2.3.0, and the transport models for all the mechanisms was "Multi".
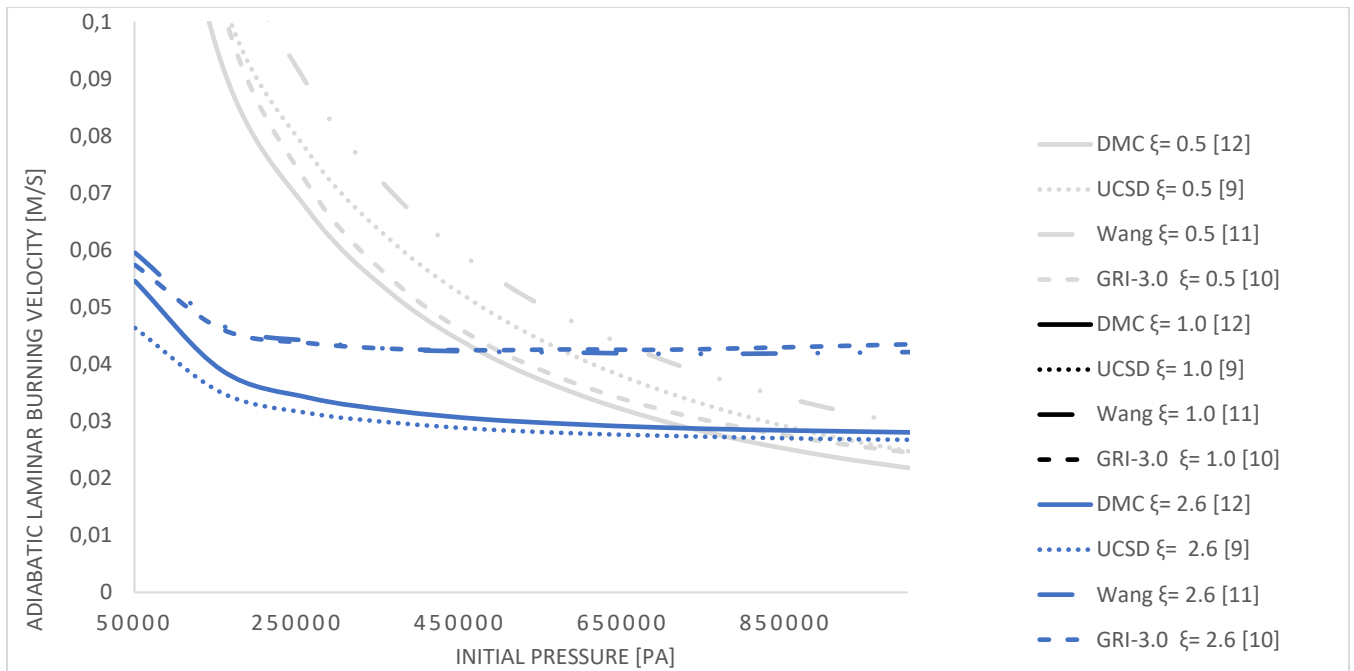
Figure 5-2: Comparison of the chemical reaction mechanism impacting the laminar burning velocity of the discharged gas emitted from an LCO-battery-premixed with air, at initial conditions of 298.15 K, were the burning velocity is a function of the initial pressure
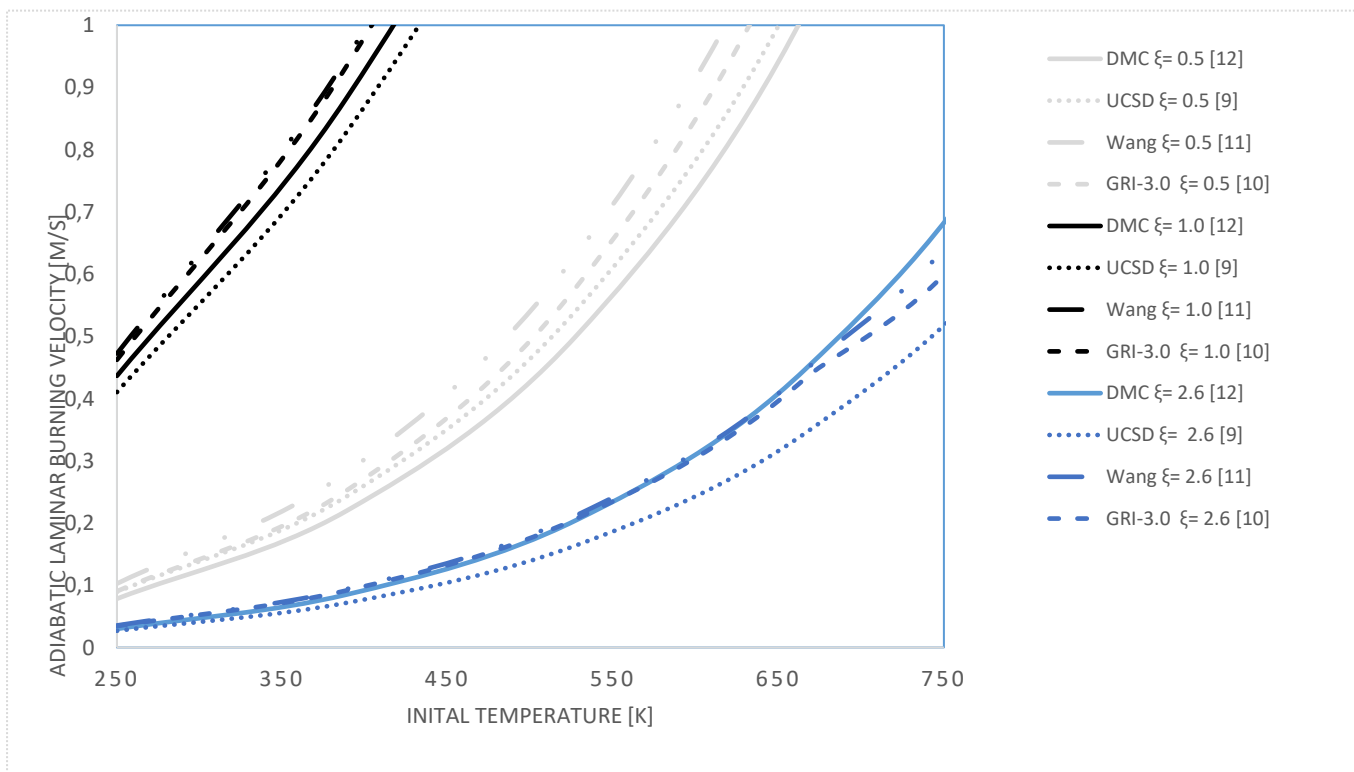
Figure 5-3: Comparison of the chemical reaction mechanism impacting the laminar burning velocity of the discharged gas emitted from an LCO-battery-premixed with air, at initial conditions of 1 atm, were the burning velocity is a function of the initial temperature in Kelvin. All the data are estimated with the mechanisms denoted in the graph, estimated on Cantera 2.3.0, and the transport models for all the mechanisms was "Multi"

A.2 Additional Volume Constant Combustion Figure
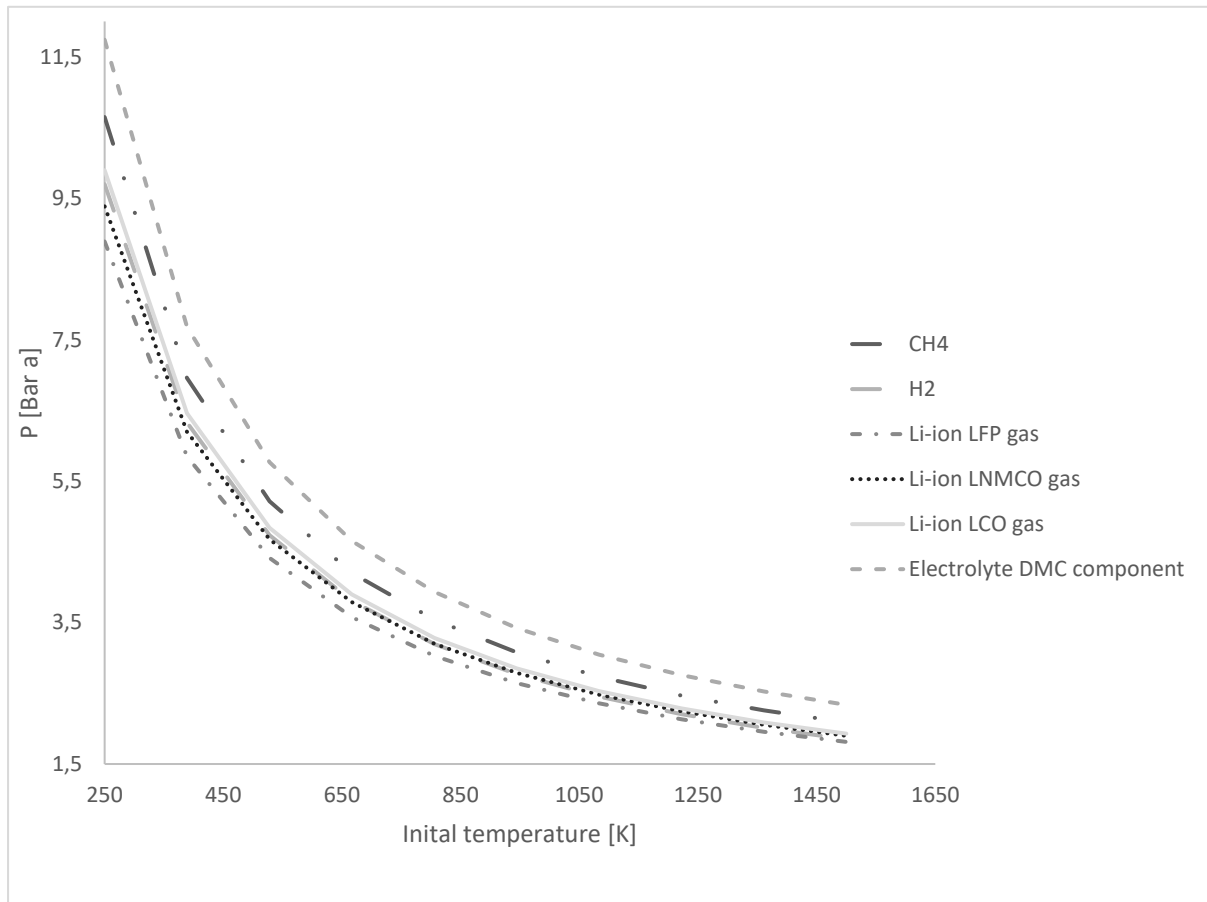
Figure 5-4: The figure depicts the relation between pressure and initial temperature of the reactants. The impact temperature has on pressure is the exact invers the temperature impacts the burning velocity.

A.3 Laminar Flame Speed Figure
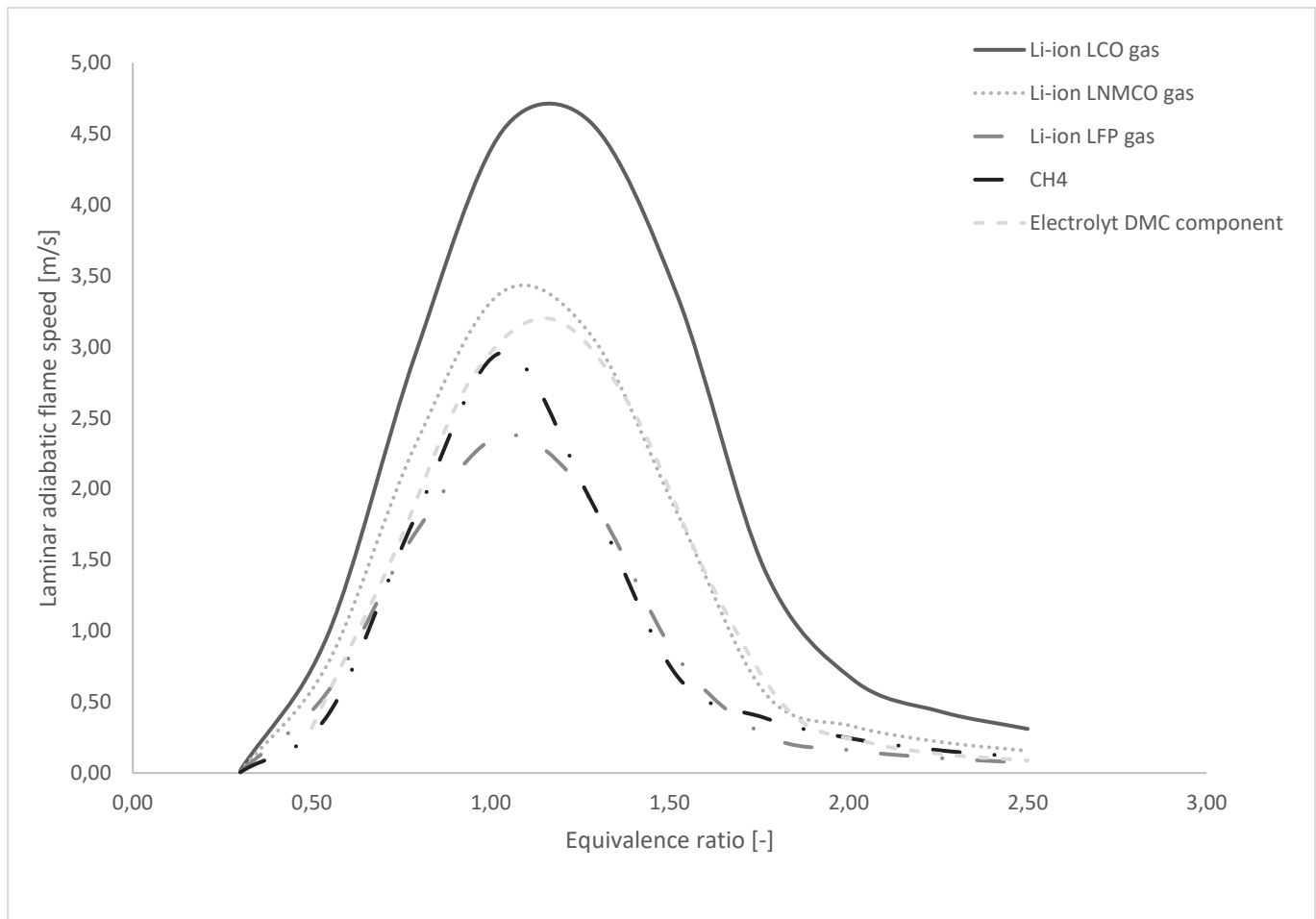
Figure 5-5: Laminar flame speed as a function of the equivalence ratio, at 298.15 K, and 1 atm. The dataset graphicly represented in this figure is derived from the dataset in Figure 3-5 and Figure 3-10. The dataset is computed in Cantera 2.3.0.
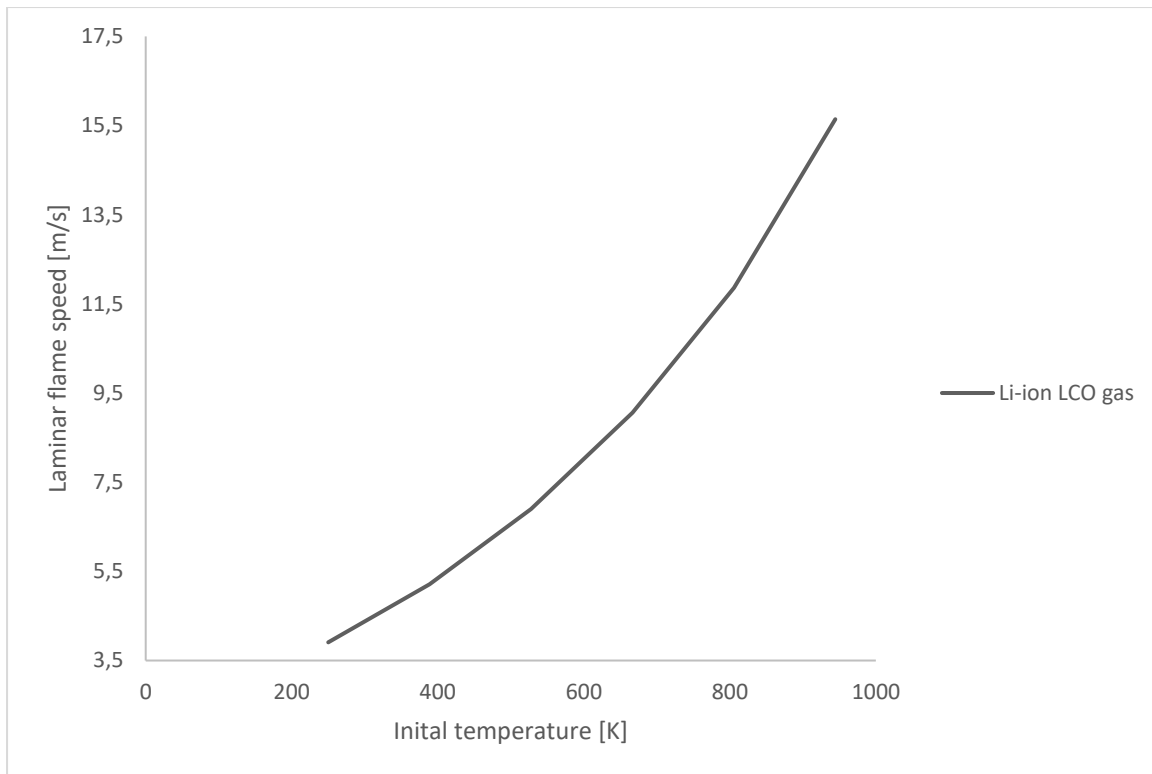
Figure 5-6: Laminar flame speed as a function of the initial temperature, fuel-air is stoichiometric, and pressure is 1 atm. The dataset is computed in Cantera 2.3.0, with GRI-3 MECH.

A.4 Additional Gulder -Alpha and Beta Coefficients Figures
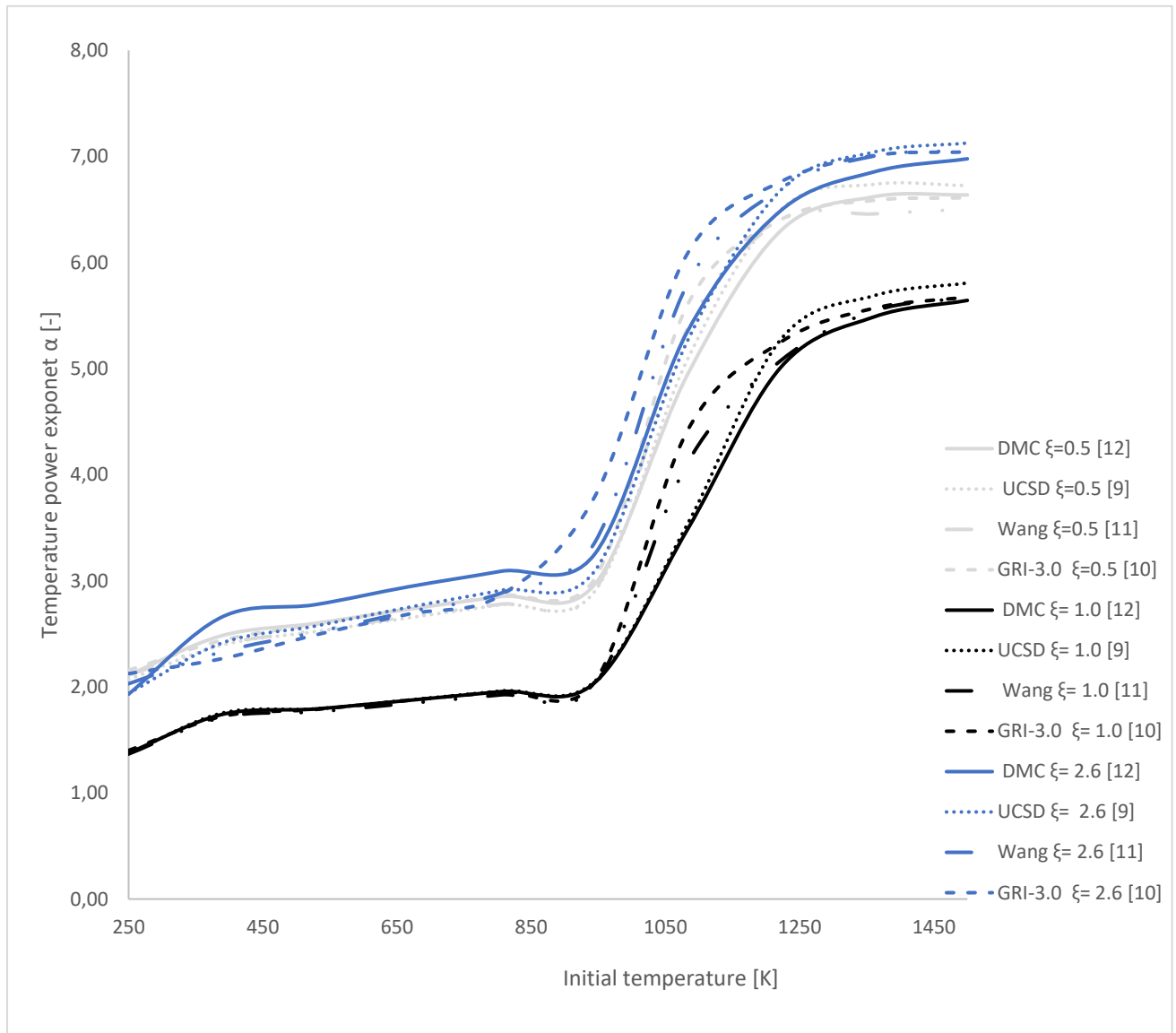
Figure 5-7: Power exponent coefficient, α, for the discharged gas emitted from an LCO battery premixed with air, and methane-air at initial conditions of 1 atm. The power exponent, α, is estimated with the GRI-3.0 mechanism on Cantera 2.3.0, the parameters have been fitted with the Python numerical optimization solver LMFIT. The solver where configured with multistart, central differencing, the population size and random seeding was set at 1000, and the specific tolerance were sat to 0.0001.
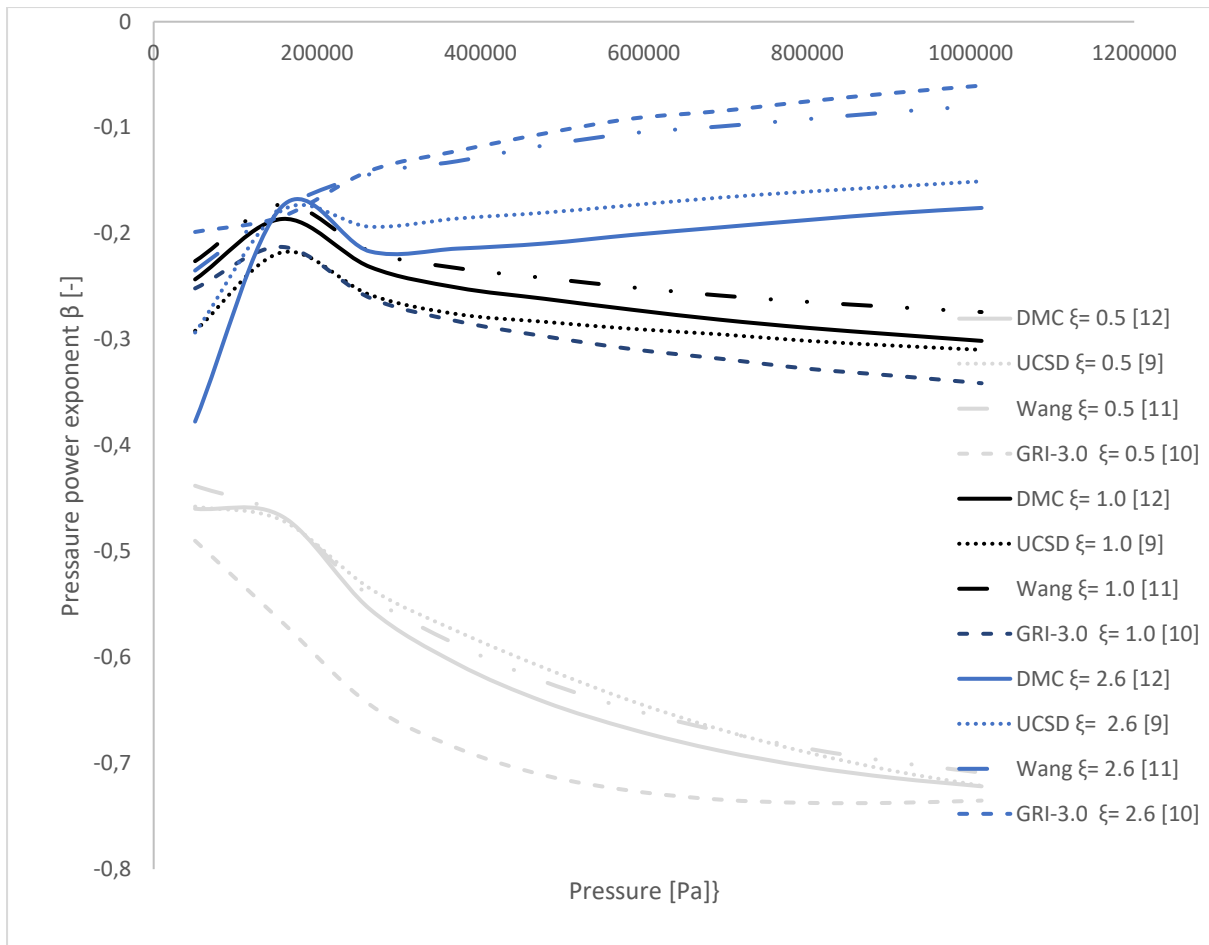
Figure 5-8: Power exponent coefficient, β, for the discharged gas emitted from an LCO battery premixed with air, and methane-air at initial conditions of 1 atm. The power exponent, β, is estimated with the GRI-3.0 mechanism on Cantera 2.3.0, the parameters have been fitted with the Python numerical optimization solver LMFIT. The solver where configured with multistart, central differencing, the population size and random seeding was set at 1000, and the specific tolerance were sat to 0.0001.

..

A.5 Temperature from Hioki Hilogger of the batteries F37 and F39 as seen and discussed in Chapter 4.
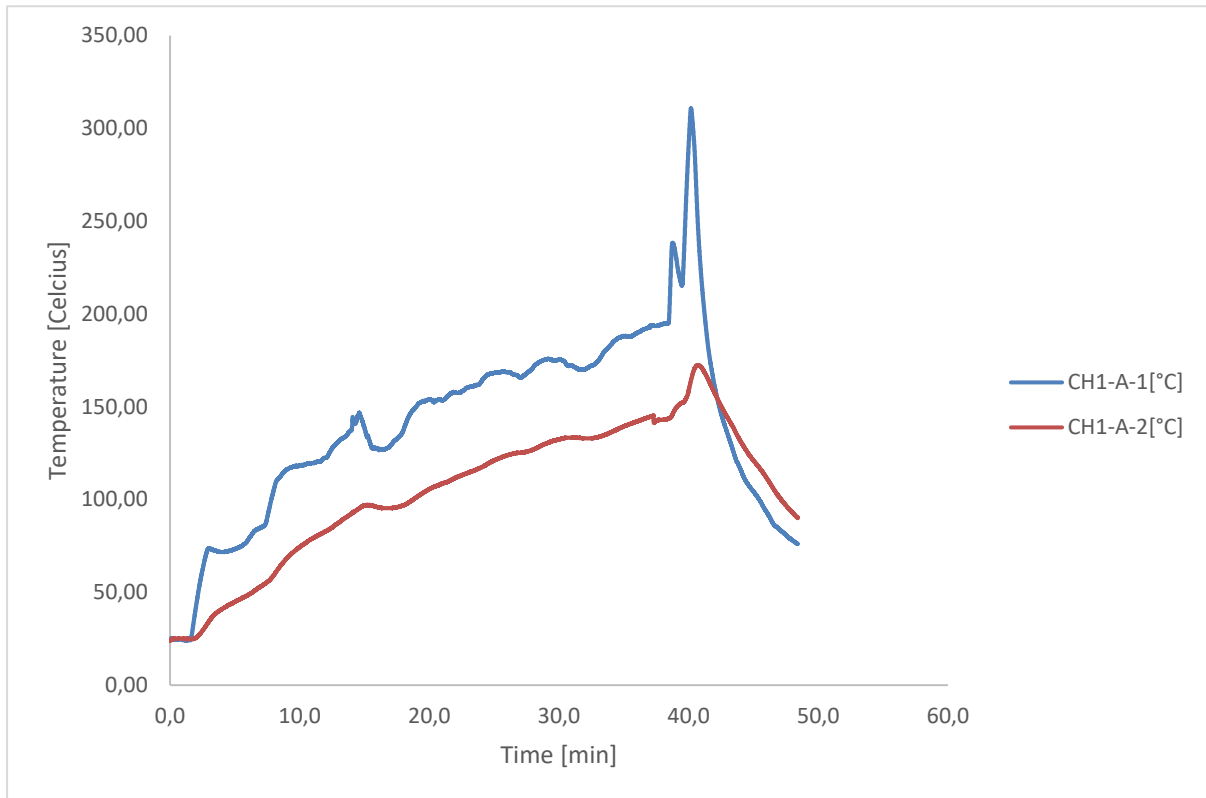
Figure 5-9: Surface-temperature of the F37 battery, as seen in chapter 4.
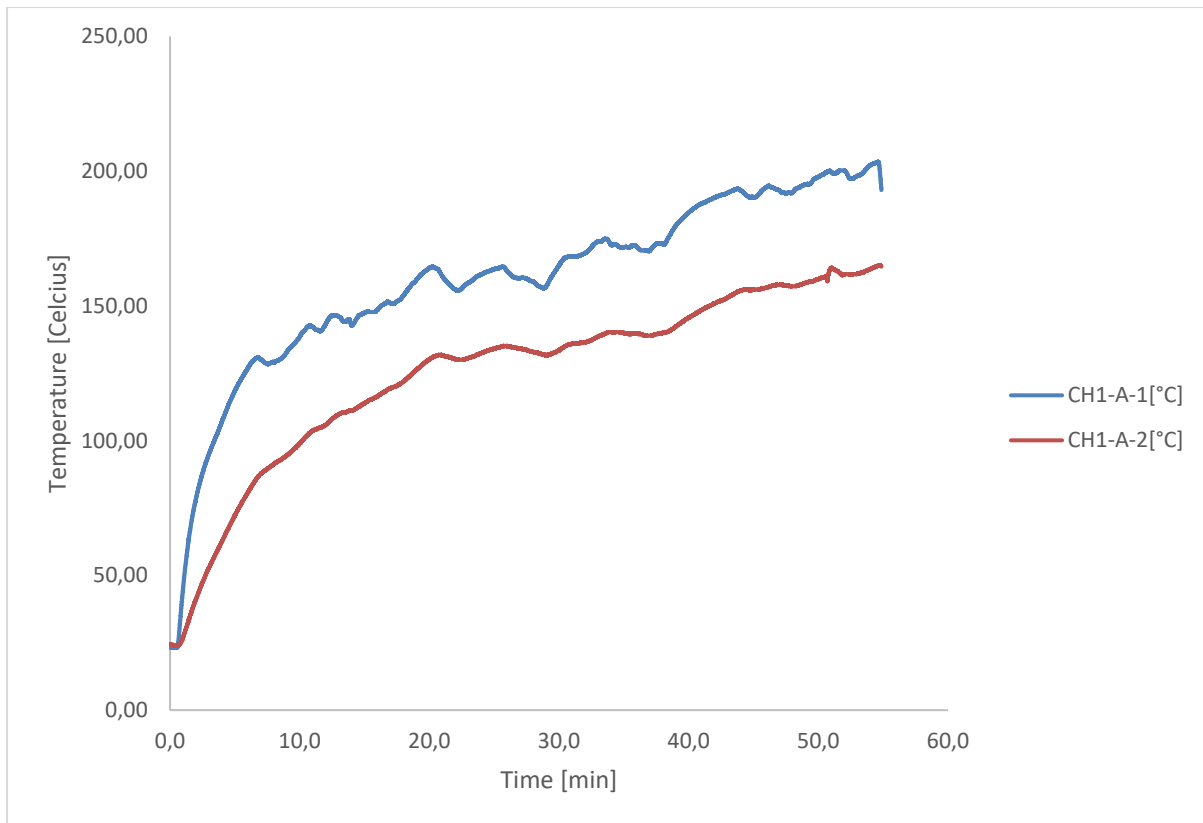
Figure 5-10: Surface-temperature of the F39 battery, as seen in chapter 4.

Appendix B
Cantera and LMFIT source code

B.1 Laminar burning Velocity Cantera 2.3.0 source code

"""

Adiabatic flame temperature and equilibrium composition for a fuel/air mixture

as a function of equivalence ratio, including formation of solid carbon.

"""

```python
import cantera as ct
import numpy as np
import sys
import csv


###################################################################################
###
# Edit these parameters to change the initial temperature, the pressure, and
# the phases in the mixture.


# Simulation parameters
Pi = ct.one_atm  # pressure [Pa]
Ti = 298.15  # unburned gas temperature [K]
width = 0.4  # m
loglevel = 1  # amount of diagnostic output (0 to 8)


# phases
gas = ct.Solution('gri30.xml')
mix_phases = [(gas, 1.0)]
mix = ct.Mixture(mix_phases)
# the phases that will be included in the calculation, and their initial moles




# gaseous fuel species
fuel_species = 'C3H8:1'#Propane
#fuel_species = 'coc*ooc:1'#Graphite
#fuel_species = 'CH4:0.068, CO2:0.412, H2:0.3, C2H6:0, C2H4:0.082, CO:0.13'#NMC
#fuel_species = 'CH4:0.041, CO2:0.53, H2:0.309, C2H6:0.003, C2H4:0.068, CO:0.049'//LFP
#fuel_species = 'H2:1'#H2
#fuel_species = 'CH4:1'#CH4




# equivalence ratio range
npoints = 10
phi = np.linspace(0.3, 2.5, npoints)
```

```
###############################################################################
###
```

```
# create some arrays to hold the data
sl = np.zeros(npoints)
T = np.zeros(npoints)
P = np.zeros(npoints)
xeq = np.zeros((mix.n_species,npoints))

for i in range(npoints):
    # set the gas state
    gas.set_equivalence_ratio(phi[i], fuel_species, 'O2:5, N2:18.8')#Propane
    #gas.set_equivalence_ratio(phi[i], fuel_species, 'O2:3, N2:11.28')#LCO
    #gas.set_equivalence_ratio(phi[i], fuel_species, 'O2:0.509, N2:1.91384')#NMC
    #gas.set_equivalence_ratio(phi[i], fuel_species, 'O2:0.4755, N2:1.78788')#LFP
    #gas.set_equivalence_ratio(phi[i], fuel_species, 'O2:0.5, N2:1.88')#H2
    #gas.set_equivalence_ratio(phi[i], fuel_species, 'O2:2, N2:7.52')#CH4
    mix = ct.Mixture(mix_phases)
    mix.T = Ti
    mix.P = Pi

    # equilibrate the mixture adiabatically at constant P
    f = ct.FreeFlame(gas, width=width)
    f.set_max_time_step(1000)
    f.set_refine_criteria(ratio=3, slope=0.06, curve=0.12)
    f.transport_model = 'Multi'
    f.solve(loglevel,auto=True,refine_grid=True)
    T[i] = mix.T
    P[i] = mix.P
    sl[i] = f.u[0]
    print('At phi = {0:12.4g}, Sl = {1:12.4g}, temperatur {2:12.4g}, pressure {3:12.4g}
pa'.format(phi[i], sl[i], T[i], P[i]))
    xeq[:,i] = mix.species_moles
```

```
# write output CSV file for importing into Excel
csv_file = 'Propane.GRI.flamespeed.Multi.csv'
with open(csv_file, 'w') as outfile:
    writer = csv.writer(outfile)
    writer.writerow(['phi','Sl (m/s)', 'T (k)', 'P(pa)'] + mix.species_names)
    for i in range(npoints):
        writer.writerow([phi[i], sl[i], T[i], P[i]] + list(xeq[:,i]))
print('Output written to {0}'.format(csv_file))



import matplotlib.pyplot as plt
plt.plot(phi, sl)
plt.xlabel('Equivalence ratio')
plt.ylabel('Adiabatic flame speed [m/s]')
plt.show()
```

B.2 Constant Volume Combustion Cantera 2.3.0 source code

```
"""
Adiabatic flame temperature and equilibrium composition for a fuel/air mixture
as a function of equivalence ratio, including formation of solid carbon.
"""
print('PHI-Multi-dmc')
import cantera as ct
import numpy as np
import sys
import csv
```

```
###############################################################################
###
# Edit these parameters to change the initial temperature, the pressure, and
# the phases in the mixture.

# Simulation parameters
Pi = ct.one_atm  # pressure [Pa]
Ti = 298.15  # unburned gas temperature [K]
width = 0.4  # m
loglevel = 1  # amount of diagnostic output (0 to 8)

# phases
gas = ct.Solution('sandiego_mechCK.cti')
mix_phases = [(gas, 1.0)]
mix = ct.Mixture(mix_phases)
# the phases that will be included in the calculation, and their initial moles



# gaseous fuel species
fuel_species = 'C3H8:1'#Propane
#fuel_species = 'coc*ooc:1'#DMC
#fuel_species = 'CH4:0.086, CO2:0.249, H2:0.3, C2H6:0.012, C2H4:0.086, CO:0.276'#LCO
#fuel_species = 'CH4:0.068, CO2:0.412, H2:0.3, C2H6:0, C2H4:0.082, CO:0.13'#NMC
#fuel_species = 'CH4:0.041, CO2:0.53, H2:0.309, C2H6:0.003, C2H4:0.068, CO:0.049'#LFP
#fuel_species = 'H2:1'#H2
#fuel_species = 'CH4:1'#CH4



# equivalence ratio range
npoints = 10
phi = np.linspace(0.5, 2.5, npoints)


###############################################################################
###
```

```python
# create some arrays to hold the data
P = np.zeros(npoints)
xeq = np.zeros((mix.n_species,npoints))

for i in range(npoints):
    # set the gas state
    gas.set_equivalence_ratio(phi[i], fuel_species, 'O2:5, N2:18.8')#Propane
    #gas.set_equivalence_ratio(phi[i], fuel_species, 'O2:0.76, N2:2.8759')#LCO
    #gas.set_equivalence_ratio(phi[i], fuel_species, 'O2:3.0, N2:11.28')#DMC
    #gas.set_equivalence_ratio(phi[i], fuel_species, 'O2:0.509, N2:1.91384')#NMC
    #gas.set_equivalence_ratio(phi[i], fuel_species, 'O2:0.4755, N2:1.78788')#LFP
    #gas.set_equivalence_ratio(phi[i], fuel_species, 'O2:0.5, N2:1.88')#H2
    #gas.set_equivalence_ratio(phi[i], fuel_species, 'O2:2, N2:7.52')#CH4
    #gas.set_equivalence_ratio(phi[i], fuel_species, 'O2:5, N2:18.8')#Propane
    mix = ct.Mixture(mix_phases)
    mix.T = Ti
    mix.P = Pi

    # equilibrate the mixture adiabatically at constant P
    gas.equilibrate('UV')
    P[i]=gas.P
    print('At phi = {0:12.4g}, Pressure {1:12.4g} pa'.format(phi[i], P[i]))
    xeq[:,i] = mix.species_moles

# write output CSV file for importing into Excel
csv_file = 'Propane.PRESSURE.csv'
with open(csv_file, 'w') as outfile:
    writer = csv.writer(outfile)
    writer.writerow(['phi','P(pa)'] + mix.species_names)
    for i in range(npoints):
        writer.writerow([phi[i], P[i]] + list(xeq[:,i]))
print('Output written to {0}'.format(csv_file))
```

B.3 Constant Pressure Combustion Cantera 2.3.0 source code

```
"""
Adiabatic flame temperature and equilibrium composition for a fuel/air mixture
as a function of equivalence ratio, including formation of solid carbon.
"""
print('PHI-Multi-graphite')
import cantera as ct
import numpy as np
import sys
import csv


###############################################################################
###
# Edit these parameters to change the initial temperature, the pressure, and
# the phases in the mixture.

# Simulation parameters
Pi = ct.one_atm  # pressure [Pa]
Ti = 293.15  # unburned gas temperature [K]
width = 0.4  # m
loglevel = 1  # amount of diagnostic output (0 to 8)


# phases
gas = ct.Solution('dmc_1i_dmm_24_mech.cti')
mix_phases = [(gas, 1.0)]
mix = ct.Mixture(mix_phases)
# the phases that will be included in the calculation, and their initial moles



# gaseous fuel species
#fuel_species = 'C3H8:1'#Propane
#fuel_species = 'CH4:0.086, CO2:0.249, H2:0.3, C2H6:0.012, C2H4:0.086, CO:0.276'#LCO
fuel_species = 'coc*ooc:1'#DMC
```

```
#fuel_species = 'CH4:0.068, CO2:0.412, H2:0.3, C2H6:0, C2H4:0.082, CO:0.13'#NMC
#fuel_species = 'CH4:0.041, CO2:0.53, H2:0.309, C2H6:0.003, C2H4:0.068, CO:0.049'#LFP
#fuel_species = 'H2:1'#H2
#fuel_species = 'CH4:1'#CH4


# equivalence ratio range
npoints = 10
phi = np.linspace(0.5, 2.5, npoints)


#################################################################################
###


# create some arrays to hold the data
T = np.zeros(npoints)
P = np.zeros(npoints)
xeq = np.zeros((mix.n_species,npoints))
density = np.zeros(npoints)
density0 = np.zeros(npoints)
C = np.zeros(npoints)

for i in range(npoints):
    # set the gas state
    #gas.set_equivalence_ratio(phi[i], fuel_species, 'O2:5, N2:18.8')#Propane
    #gas.set_equivalence_ratio(phi[i], fuel_species, 'O2:0.76, N2:2.8759')#LCO
    gas.set_equivalence_ratio(phi[i], fuel_species, 'O2:3, N2:11.28')#DMC
    #gas.set_equivalence_ratio(phi[i], fuel_species, 'O2:0.509, N2:1.91384')#NMC
    #gas.set_equivalence_ratio(phi[i], fuel_species, 'O2:0.4755, N2:1.78788')#LFP
    #gas.set_equivalence_ratio(phi[i], fuel_species, 'O2:0.5, N2:1.88')#H2
    #gas.set_equivalence_ratio(phi[i], fuel_species, 'O2:2, N2:7.52')#CH4
    mix = ct.Mixture(mix_phases)
    mix.T = Ti
    mix.P = Pi
```

```python
    T[i] = mix.T
    P[i] = mix.P
    xeq[:,i] = mix.species_moles
    density0[i] = gas.density_mass
    mix.equilibrate('HP')
    density[i] = gas.density_mass
    C[i] = density0[i]/density[i]
    print('Rel = {0:7f} , and Phi = {1:7f}'.format(C[i],phi[i]))
# write output CSV file for importing into Excel
csv_file = 'DMC.DMC.C.csv'
with open(csv_file, 'w') as outfile:
    writer = csv.writer(outfile)
    writer.writerow(['phi','C '])
    for i in range(npoints):
        writer.writerow([phi[i], C[i]])
print('Output written to {0}'.format(csv_file))
```

```python
import matplotlib.pyplot as plt
plt.plot(phi, C)
plt.xlabel('Equivalence ratio')
plt.ylabel('C')
plt.show()
```
##
###

B.4 Deflagration Index Cantera 2.3.0 source code

```python
"""
Adiabatic flame temperature and equilibrium composition for a fuel/air mixture
as a function of equivalence ratio, including formation of solid carbon.
"""
print('PHI-Multi-graphite')
import cantera as ct
import numpy as np
import sys
import csv
```

```
###############################################################################
###
# Edit these parameters to change the initial temperature, the pressure, and
# the phases in the mixture.

# Simulation parameters
Pi = ct.one_atm  # pressure [Pa]
Ti = 298.15  # unburned gas temperature [K]
width = 0.4  # m
loglevel = 1  # amount of diagnostic output (0 to 8)

# phases
gas = ct.Solution('dmc_1i_dmm_24_mech.cti')
mix_phases = [(gas, 1.0)]
mix = ct.Mixture(mix_phases)
# the phases that will be included in the calculation, and their initial moles


# gaseous fuel species
#fuel_species = 'C3H8:1'#Propane
fuel_species = 'CH4:0.086, CO2:0.249, H2:0.3, C2H6:0.012, C2H4:0.086, CO:0.276'#LCO
#fuel_species = 'coc*ooc:1'#DMC
#fuel_species = 'CH4:0.068, CO2:0.412, H2:0.3, C2H6:0, C2H4:0.082, CO:0.13'#NMC
#fuel_species = 'CH4:0.041, CO2:0.53, H2:0.309, C2H6:0.003, C2H4:0.068, CO:0.049'#LFP
#fuel_species = 'H2:1'#H2
#fuel_species = 'CH4:1'#CH4


# equivalence ratio range
npoints = 10
phi = np.linspace(0.3, 2.5, npoints)


###############################################################################
###
```

```python
# create some arrays to hold the data
sl = np.zeros(npoints)
T = np.zeros(npoints)
P = np.zeros(npoints)
xeq = np.zeros((mix.n_species,npoints))
Kg = np.zeros(npoints)
PMAX = np.zeros(npoints)
gammaU = np.zeros(npoints)


for i in range(npoints):
    # set the gas state
    gas.set_equivalence_ratio(phi[i], fuel_species, 'O2:5, N2:18.8')#Propane
    #gas.set_equivalence_ratio(phi[i], fuel_species, 'O2:0.76, N2:2.8759')#LCO
    #gas.set_equivalence_ratio(phi[i], fuel_species, 'O2:3, N2:11.28')#DMC
    #gas.set_equivalence_ratio(phi[i], fuel_species, 'O2:0.509, N2:1.91384')#NMC
    #gas.set_equivalence_ratio(phi[i], fuel_species, 'O2:0.4755, N2:1.78788')#LFP
    #gas.set_equivalence_ratio(phi[i], fuel_species, 'O2:0.5, N2:1.88')#H2
    #gas.set_equivalence_ratio(phi[i], fuel_species, 'O2:2, N2:7.52')#CH4
    mix = ct.Mixture(mix_phases)
    mix.T = Ti
    mix.P = Pi
    gammaU[i]=(gas.cp_mass)/(gas.cv_mass)
    # equilibrate the mixture adiabatically at constant P
    f = ct.FreeFlame(gas, width=width)
    f.set_max_time_step(1000)
    f.set_refine_criteria(ratio=3, slope=0.06, curve=0.12)
    f.transport_model = 'Mix'
    f.solve(loglevel,auto=True,refine_grid=True)
    T[i] = mix.T
    P[i] = mix.P
    sl[i] = f.u[0]
    xeq[:,i] = mix.species_moles
    mix.equilibrate('UV')
    PMAX[i]=(gas.P/100000)
```

```
    Kg[i]=((PMAX[i])-1.01325)*4.835975864*sl[i]*(((PMAX[i])/1.01325)**(1/gammaU[i]))
# write output CSV file for importing into Excel
csv_file = 'LCO.DMC.KG.csv'
with open(csv_file, 'w') as outfile:
    writer = csv.writer(outfile)
    writer.writerow(['phi','Kg (Bar*m*s^-1)'])
    for i in range(npoints):
        writer.writerow([phi[i], Kg[i]])
print('Output written to {0}'.format(csv_file))



import matplotlib.pyplot as plt
plt.plot(phi, Kg)
plt.xlabel('Equivalence ratio')
plt.ylabel('Deflagration index [Bar*m*s^-1]')
plt.show()
```

B. 5 Gulder Coefficients LMFIT 0.9.6, Cantera 2.3.0 source code

B. 5. 1 Omega, Eta and Xi

```
import cantera as ct
import numpy as np
import sys
import csv
from numpy import sqrt, pi, exp, linspace, loadtxt
from lmfit import  Model
import matplotlib.pyplot as plt
import copy


#################################################################################
###
# Edit these parameters to change the initial temperature, the pressure, and
# the phases in the mixture.

# Simulation parameters
```

```
Pi = ct.one_atm  # pressure [Pa]
Ti = 298.15  # unburned gas temperature [K]
width = 0.4  # m
loglevel = 1  # amount of diagnostic output (0 to 8)


# phases
gas = ct.Solution('gri30.xml')
mix_phases = [(gas, 1.0)]
mix = ct.Mixture(mix_phases)
# the phases that will be included in the calculation, and their initial moles



# gaseous fuel species
fuel_species = 'C3H8:1'#Propane
#fuel_species = 'coc*ooc:1'#Graphite
#fuel_species = 'CH4:0.068, CO2:0.412, H2:0.3, C2H6:0, C2H4:0.082, CO:0.13'#NMC
#fuel_species = 'CH4:0.041, CO2:0.53, H2:0.309, C2H6:0.003, C2H4:0.068, CO:0.049'//LFP
#fuel_species = 'H2:1'#H2
#fuel_species = 'CH4:1'#CH4



# equivalence ratio range
npoints = 10
phi = np.linspace(0.3, 2.5, npoints)


####################################################################################
###



# create some arrays to hold the data
sl = np.zeros(npoints)
T = np.zeros(npoints)
P = np.zeros(npoints)
xeq = np.zeros((mix.n_species,npoints))
```

```python
for i in range(npoints):
    # set the gas state
    gas.set_equivalence_ratio(phi[i], fuel_species, 'O2:5, N2:18.8')#Propane
    #gas.set_equivalence_ratio(phi[i], fuel_species, 'O2:3, N2:11.28')#LCO
    #gas.set_equivalence_ratio(phi[i], fuel_species, 'O2:0.509, N2:1.91384')#NMC
    #gas.set_equivalence_ratio(phi[i], fuel_species, 'O2:0.4755, N2:1.78788')#LFP
    #gas.set_equivalence_ratio(phi[i], fuel_species, 'O2:0.5, N2:1.88')#H2
    #gas.set_equivalence_ratio(phi[i], fuel_species, 'O2:2, N2:7.52')#CH4
    mix = ct.Mixture(mix_phases)
    mix.T = Ti
    mix.P = Pi


    # equilibrate the mixture adiabatically at constant P
    f = ct.FreeFlame(gas, width=width)
    f.set_max_time_step(1000)
    f.set_refine_criteria(ratio=3, slope=0.06, curve=0.12)
    f.transport_model = 'Mix'
    f.solve(loglevel,auto=True,refine_grid=True)
    T[i] = mix.T
    P[i] = mix.P
    sl[i] = f.u[0]
    xeq[:,i] = mix.species_moles



from lmfit import minimize, Minimizer, Parameters
data = np.genfromtxt('flamespeed-LCO-gri30.Multi.csv',delimiter=',')
x = phi
y = sl



def Gulder1(x, omega, eta, xi):
    "1-d gaussian: gaussian(x, amp, cen, wid)"
    return (omega*(x**eta) * exp(-xi*(x-1.075)**2))


gmodel = Model(Gulder1)
```

```
result = gmodel.fit(y, x=x, omega=1, eta=1, xi=1)


print(result.fit_report())


plt.plot(x, y,        'bo')
plt.plot(x, result.best_fit, 'r-')
plt.show()
```

B. 5. 2 Alpha

```
from numpy import sqrt, pi, exp, linspace, loadtxt
from lmfit import  Model
from lmfit import minimize, Minimizer, Parameters
import cantera as ct
import numpy as np
import sys
import csv
import matplotlib.pyplot as plt
import copy


# Simulation parameters
npoints = 10
p = ct.one_atm  # pressure [Pa]
Tin = np.linspace(250, 1000, npoints)  # unburned gas temperature [K]
reactants = 'c3h8:1, O2:5, N2:18.8'#Propane
width = 0.4  # m
loglevel = 1  # amount of diagnostic output (0 to 8)
sl = np.zeros(npoints)



#Burning velocity for corresponding temperature interval
for i in range(npoints):
    gas = ct.Solution('gri30.xml')
    gas.TPX = Tin[i], p, reactants##
```

```
    # Set up flame object
    f = ct.FreeFlame(gas, width=width)
    f.set_refine_criteria(ratio=3, slope=0.06, curve=0.12)
    f.set_max_time_step(1000)
    f.transport_model = 'Multi'
    f.solve(loglevel,auto=True,refine_grid=True)
    print('multicomponent flamespeed = {0:7f} m/s, and temperature = {1:7f} K
'.format(f.u[0], Tin[i]))
    sl[i] = f.u[0]


#Burning velocity at NTP
TNTP=293.15
gas = ct.Solution('gri30.xml')
gas.TPX = TNTP, p, reactants##
# Set up flame object
f = ct.FreeFlame(gas, width=width)
f.set_refine_criteria(ratio=3, slope=0.06, curve=0.12)
f.set_max_time_step(1000)
f.transport_model = 'Multi'
f.solve(loglevel,auto=True,refine_grid=True)
slf = f.u[0]


from lmfit import minimize, Minimizer, Parameters
x = Tin
y = sl
print(y)


def Gulder2(x, alpha):
    "1-d gaussian: gaussian(x, amp, cen, wid)"
    return (slf*(x/298.15)**alpha)


gmodel = Model(Gulder2)


result = gmodel.fit(y, x=x, alpha=1)
```

```python
print(result.fit_report())


plt.plot(x, y,        'bo')
plt.plot(x, result.best_fit, 'r-')
plt.show()
```

B. 5. 3 Beta

```python
"""
A freely-propagating, premixed hydrogen flat flame with multicomponent
transport properties.
"""


from numpy import sqrt, pi, exp, linspace, loadtxt
from lmfit import  Model
from lmfit import minimize, Minimizer, Parameters
import cantera as ct
import numpy as np
import sys
import csv
import matplotlib.pyplot as plt
import copy



# Simulation parameters
npoints = 10
p = np.linspace(0.5*ct.one_atm, 10*ct.one_atm, npoints) # pressure [Pa]
Tin = 298.15  # unburned gas temperature [K]
reactants = 'c3h8:1, O2:5, N2:18.8'#Propane
width = 0.4  # m
loglevel = 1  # amount of diagnostic output (0 to 8)
sl = np.zeros(npoints)


#Burning velocity for corresponding pressure interval
for i in range(npoints):
    gas = ct.Solution('gri30.xml')
    gas.TPX = Tin, p[i], reactants
```

```python
    # Set up flame object
    f = ct.FreeFlame(gas, width=width)
    f.set_refine_criteria(ratio=3, slope=0.06, curve=0.12)



    # Solve with multi-component transport properties
    f.transport_model = 'Multi'
    f.solve(loglevel) # don't use 'auto' on subsequent solves
    sl[i] = f.u[0]

#Burning velocity at NTP
PNTP=101325
gas = ct.Solution('gri30.xml')
gas.TPX = Tin, PNTP, reactants##
# Set up flame object
f = ct.FreeFlame(gas, width=width)
f.set_refine_criteria(ratio=3, slope=0.06, curve=0.12)
f.set_max_time_step(1000)
f.transport_model = 'Multi'
f.solve(loglevel,auto=True,refine_grid=True)
slf = f.u[0]

from lmfit import minimize, Minimizer, Parameters
x = p
y = sl
print(y)

def Gulder2(x, beta):
    "1-d gaussian: gaussian(x, amp, cen, wid)"
    return (slf*(x/101325)**beta)

gmodel = Model(Gulder2)

result = gmodel.fit(y, x=x, beta=1)
```

```
print(result.fit_report())


plt.plot(x, y,        'bo')
plt.plot(x, result.best_fit, 'r-')
plt.show()
```

B. 6 NASA Polynomials LMFIT 0.9.6, Cantera 2.3.0 source code

```
from numpy import sqrt, pi, exp, linspace, loadtxt
from lmfit import  Model
from lmfit import minimize, Minimizer, Parameters
import cantera as ct
import numpy as np
import sys
import csv
import matplotlib.pyplot as plt
import copy
import math


# Simulation parameters
npoints = 100
Tin = np.linspace(300, 1000 , npoints)  # unburned gas temperature [K]
p=101325.0

reactants = 'h2:1, o2:0.5, n2:1.78'  # premixed gas composition

gas = ct.Solution('dmc_1i_dmm_24_mech.cti')
S = np.zeros(npoints)
Cp = np.zeros(npoints)
H = np.zeros(npoints)
for i in range(npoints):

    gas.TPX = Tin[i], p, reactants
```

```
    S[i]=gas.entropy_mole
    Cp[i]=gas.cp_mole
    H[i]=gas.enthalpy_mole


from lmfit import minimize, Minimizer, Parameters
x = Tin
y = Cp
def NASA2a123(x, a1, a2, a3):
    return (((a1)+(a2*x**1)+(a3*x**2))*8314)
gmodel = Model(NASA2a123)
resulta1a123 = gmodel.fit(y, x=x, a1=10, a2=0.001, a3=0.001)


a1 = resulta1a123.best_values["a1"]
a2 = resulta1a123.best_values["a2"]
a3 = resulta1a123.best_values["a3"]


x = Tin
y = (Cp[npoints-1])
def NASAa345(x, a4, a5):
    return (((a1)+(a2*x**1)+(a3*x**2)+(a4*x**3)+(a5*x**4))*8314)
gmodel = Model(NASAa345)
resulta1a45 = gmodel.fit(y, x=x,a4=0.000001 ,a5=0.000000001)



a4 = resulta1a45.best_values["a4"]
a5 = resulta1a45.best_values["a5"]


x = 1000
y = (H[npoints-1])
def NASA2a6(x, a6):
    return ((a1+((a2*x)/2)+((a3*x**2)/3)+((a4*x**3)/4)+((a5*x**4)/5)+((a6)/x))*8314*1000)
gmodel = Model(NASA2a6)
resulta1a6 = gmodel.fit(y, x=x, a6=-1300)
```

```python
x = 1000
y = (S[npoints-1])
print(y)
def NASA2a7(x, a7):
    return (((a1*np.log(x)+(a2*x)+((a3*x**2)/2)+((a4*x**3)/3)+((a5*x**4)/4)+a7))*8314)
gmodel = Model(NASA2a7)
resulta1a7 = gmodel.fit(y, x=x, a7=0.01)



print(resulta1a123.fit_report())
print(resulta1a45.fit_report())
print(resulta1a6.fit_report())
print(resulta1a7.fit_report())
```

Appendix C
XiFoam Source Code

C.1. blockMeshDict

```
/*--------------------------------*- C++ -*----------------------------
------*\
| =========                 |
|
| \\      /  F ield         | OpenFOAM: The Open Source CFD Toolbox
|
```

```
|  \\    /   O peration     | Version:  2.1.1
|
|   \\  /    A nd           | Web:       www.OpenFOAM.org
|
|     \\/     M anipulation  |
|
\*-----------------------------------------------------------------------
------*/
FoamFile
{
    version     2.0;
    format      ascii;
    class       dictionary;
    object      blockMeshDict;
}
// * * * * * * * * * * * * * * * * * * * * * * * * * * * * * * * * * *
* * * //

convertToMeters 0.01;

vertices
(
    (0 0 0)
    (0 0 10)
    (45 0 10)
    (45 0 0)
    (0 10 0)
    (0 10 10)
    (45 10 10)
    (45 10 0)
);

blocks
(
    hex (0 3 7 4 1 2 6 5) (90 20 1) simpleGrading (1 1 1)
);

edges
(
);

boundary
(
    inlet
    {
        type patch;
        faces
        (
            (0 1 5 4)
        );
    }
    outlet
    {
        type patch;
        faces
        (
            (3 2 6 7)
        );
```

```
    }
    upperWall
    {
        type wall;
        faces
        (
            (4 5 6 7)
        );
    }
    lowerWall
    {
        type wall;
        faces
        (
            (0 1 2 3)

        );
    }
    front
    {
        type cyclic;
        neighbourPatch back;
        faces
        (
            (0 3 7 4)
        );
    }
    back
    {
        type cyclic;
        neighbourPatch front;
        faces
        (
            (1 2 6 5)
        );
    }
);

mergePatchPairs
(
);


//
********************************************************************
** //
```

C. 2 combustionProperties

```
/*--------------------------------*- C++ -*----------------------------
------*\

| =========                 |
|

| \\      /  F ield         | OpenFOAM: The Open Source CFD Toolbox
|
```

```
| \\    /   O peration     | Version:  2.1.1
|
| \\  /    A nd            | Web:        www.OpenFOAM.org
|
|   \\/     M anipulation  |
|
\*-------------------------------------------------------------------------
------*/
FoamFile
{
    version     2.0;
    format      ascii;
    class       dictionary;
    location    "constant";
    object      combustionProperties;
}
// * * * * * * * * * * * * * * * * * * * * * * * * * * * * * * * * * * * *
* * * //


laminarFlameSpeedCorrelation Gulders;


fuel            LCO;


Su              Su [0 1 -1 0 0 0 0] 0.67;


SuModel         transport;


equivalenceRatio equivalenceRatio [0 0 0 0 0 0 0] 1;


sigmaExt        sigmaExt [0 0 -1 0 0 0 0] 338;
```

```
XiModel          fixed;


XiCoef           XiCoef [0 0 0 0 0 0 0] 0.62;


XiShapeCoef      XiShapeCoef [0 0 0 0 0 0 0] 1;


uPrimeCoef       uPrimeCoef [0 0 0 0 0 0 0] 1;


GuldersCoeffs

{

    Methane

    {

        W                0.422;

        eta              0.15;

        xi               5.18;

        alpha            2;

        beta             -0.5;

        f                2.3;

    }


    Propane

    {

        W                0.446;

        eta              0.12;

        xi               4.95;

        alpha            1.77;

        beta             -0.2;

        f                2.3;

    }
```

```
IsoOctane

{

    W               0.4658;

    eta             -0.326;

    xi              4.48;

    alpha           1.56;

    beta            -0.22;

    f               2.3;

}

LCO

{

    W               0.612;

    eta             0.758;

    xi              2.555;

    alpha           1.99;

    beta            -0.24;

    f               2.3;

}
DMC

{

    W               0.364;

    eta             0.51;

    xi              3.592;

    alpha           2.9;

    beta            -0.25;

    f               2.3;

}
H2

{
```

```
        W                 2.094;

        eta               1.068;

        xi                0.424;

        alpha             2.9;

        beta              0.71;

        f                 2.3;

    }

}


ignite      yes;


ignitionSites

(

    {

        location (0.03 0.05 0.05);

        diameter 0.003;

        start 0;

        duration 0.1;

        strength 300;

    }

);


ignitionSphereFraction 1;


ignitionThickness ignitionThickness [0 1 0 0 0 0 0] 0;


ignitionCircleFraction 0;


ignitionKernelArea ignitionKernelArea [0 2 0 0 0 0 0] 0;
```

```
//
************************************************************************
** //
```

C. 3 thermophysicalProperties

```
/*--------------------------------*- C++ -*----------------------------------*\
| =========                 |
|
| \\      /   F ield         | OpenFOAM: The Open Source CFD Toolbox
|
|  \\    /    O peration      | Version:  2.1.1
|
|   \\  /     A nd            | Web:       www.OpenFOAM.org
|
|    \\/      M anipulation   |
|
\*---------------------------------------------------------------------------*/
FoamFile
{
    version     2.0;
    format      ascii;
    class       dictionary;
    location    "constant";
    object      thermophysicalProperties;
}
// * * * * * * * * * * * * * * * * * * * * * * * * * * * * * * * * * * * //

thermoType
hhuMixtureThermo<homogeneousMixture<sutherlandTransport<specieThermo<ja
nafThermo<perfectGas>>>>>;

stoichiometricAirFuelMassRatio stoichiometricAirFuelMassRatio [ 0 0 0 0
0 0 0 ] 4.56;

reactants
{
    specie
    {
        nMoles          1;
        molWeight       27.6282;
    }
    thermodynamics
    {
        Tlow            250;
        Thigh           5000;
        Tcommon         1000;
        highCpCoeffs    (3.28 1.00e-3 0 0 0 -4.43e3 5.31);
```

```
        lowCpCoeffs       (4.75 2.00e-4 -5.81e-10 -1.41e-13 2.47e-17 -
5.13e3 -1.65);
    }
    transport
    {
        As                1.67212e-06;
        Ts                170.672;
    }
}

products
{
    specie
    {
        nMoles            1;
        molWeight         29.414;
    }
    thermodynamics
    {
        Tlow              250;
        Thigh             5000;
        Tcommon           1000;
        highCpCoeffs      (3.41 1.00e-3 -2.7e-10 -5.92e-13 0 -1.44e4
4.56);
        lowCpCoeffs       (4.69 2.0e-4 -6.96e-10 -2.99e-13 0 -1.52e4 -
3.28);
    }
    transport
    {
        As                1.67212e-06;
        Ts                170.672;
    }
}


//
*****************************************************************
** //
```

Appendix D

Theoretic Method To Approximate The Burning Velocity of Gaseous Carbonate

The electrolyte solutions in the LCO, LFP, and LCO/NMC batteries are mixtures of several carbonate species, i.e. dimethyl carbonate, ethylene carbonate, polypropylene carbonate and diethyl carbonate. But it is only possible to estimate the burning velocity for the dimethyl carbonate. Due to this limitation of a theoretic method to approximate the burning velocity of the other components in the electrolyte solution has been developed in the following appendix.

To approximate the laminar burning velocity for the for the carbonates ethylene carbonate, polypropylene carbonate and diethyl carbonate the following assumption has been made:

$$\omega_{DMC} \approx \omega_i, i = \{EC, PC \text{ and } DE\} \tag{5-1}$$

Formula 5-2 states that the reaction rates between dimethyl carbonate, ethylene carbonate, polypropylene carbonate and diethyl carbonate are equal. This assumption is not validated, by any sources and therefor can impact the result significantly.

Based on this assumption, a correction factor has been derived from the first approximation of the laminar burning velocity which has the form:

$$S_l = \frac{1}{\rho_0} \sqrt{\frac{\omega k}{c_p}} \tag{5-3}$$

The correction factor can be expressed as following:

$$F = \frac{\rho_{0,DMC}}{\rho_{0,i}} \frac{\sqrt{c_{p.DMC}}}{\sqrt{c_{p.i}}} \frac{\sqrt{k_i}}{\sqrt{k_{DMC}}}, i = EC, PC, DE \tag{5-4}$$

There is currently only available thermal conductivity data for carbonates in liquid phase. This data is published in [14]. It is in this regard necessary to readjust the correction factor and exclude the thermal conductivity correction:

$$F^* = \frac{\rho_{0,DMC}}{\rho_{0,i}} \frac{\sqrt{c_{p.DMC}}}{\sqrt{c_{p.i}}}, i = EC, PC, DE \tag{5-5}$$

This correction factor can be implemented to give a rough approximation for

$$S_{l,i} = FS_{l,DMC}, i = EC, PC, DE \tag{5-6}$$

Table 5-1: The chemical properties of the carbonate species in the battery-electrolytes [13]

Solvent	MW [g/mol]	C_p (25°C) [J/Kg*K]	$P_{o (Liqui)}$(25 °C) [kg/m³]	$P_{o (gas)}$(25 °C) [kg/m³]
Ethylene carbonate (EC)	88	1.90 (40 °C)	1321	3.6
Propylene carbonate(PC)	102	2.53	1200	4.17
Dimethyl carbonate (DMC)	90	0.59 (40 °C)	1063	3.68
Diethyl carbonate (DEC)	118	0.75|	969	4.82

The Cp, and density values must be evaluated as mixtures of fuel and air. These correction factors will be based on a mixture of stochiometric equivalence ratio of fuel and air.

$$y_i = \frac{1}{\left(\alpha + \frac{\beta}{2} - \frac{\gamma}{4}\right) \cdot 4.76 + 1}$$

$$x_i = \frac{M_i}{\left(\alpha + \frac{\beta}{2} - \frac{\gamma}{4}\right) \cdot 4.76 M_{air} + M_i} \tag{5-7}$$

$$\rho_{i,mix} = x_i \cdot \rho_i + (1 - x_i) \cdot \rho_{air}$$

$$c_{p,i,mix} = x_i \cdot c_{p,i} + (1 - x_i) \cdot c_{p,air}$$

Table 5-2: Correction factors to approximate the burning velocity for ethylene carbonate, propylene carbonate and dimethyl carbonate.

Solvent	α		β	γ	y_i	x_i	$C_{p,mix}$ (25°C) [kJ/kg·k]	$P_{o,mix (gas)}$(25 °C) [kg/m³]	F^* [-]

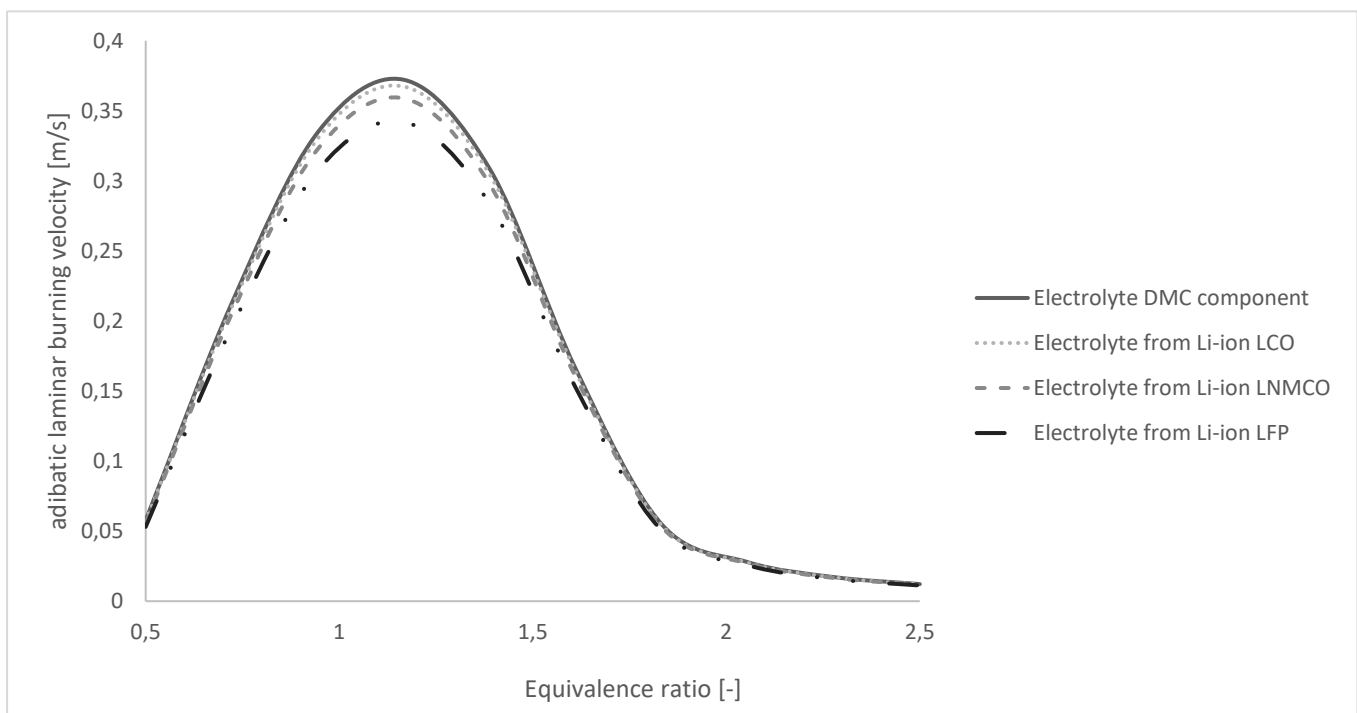|								
Ethylene carbonate (EC)	3		4	3	0.05	0.13	1.12	1.52	0.88
Propylene carbonate(PC)	4		6	3	0.03	0.11	1.14	1.49	0.89
Dimethyl carbonate (DMC)	3		6	3	0.04	0.11	0.94	1.45	1.0
Diethyl carbonate (DEC)	5		10	3	0.02	0.08	0.94	1.46	1.0
LCO	-		-	-	-	-	0.96	1.458	0.987
NMC	-		-	-	-	-	0.978	1.461	0.977
LFP	-		-	-	-	-	1.014	1.475	0.953

Figure 5-8: Comparison of the laminar burning velocity of the electrolyte in three lithium-ion batteries premixed with air, at initial conditions of 1 atm, and 298.15 K, were the burning velocity is a function of equivalence ratio. All the data are estimated based on the burning velocity of dimethyl carbonate -air and the correction factor approximated in formula (5-5).